Master's thesis

NTNU
Norwegian University of Science and Technology
Faculty of Information Technology and Electrical Engineering
Department of Electric Power Engineering

Lars Thaulow Bremnes

PSCAD Simulations of Distance Protection Performance in a Grid with high Wind Power Penetration

Master's thesis in Electric Power Engineering
Supervisor: Hans Kristian Høidalen
June 2022

NTNU
Norwegian University of
Science and Technology

Lars Thaulow Bremnes

PSCAD Simulations of Distance Protection Performance in a Grid with high Wind Power Penetration

Master's thesis in Electric Power Engineering
Supervisor: Hans Kristian Høidalen
June 2022

Norwegian University of Science and Technology
Faculty of Information Technology and Electrical Engineering
Department of Electric Power Engineering

NTNU
Norwegian University of
Science and Technology

Preface

This master thesis concludes my work in the master's program in Electrical Power Engineering at the Norwegian University of Science and Technology (NTNU). It has been a rewarding journey to work with this project and participate in the preparations for the renewable energy transition.

I want to thank my supervisor Pr. Hans Kristian Høidalen for his guidance throughout my final year at NTNU. It has been informative being part of the ProDig project and rewarding getting the opportunity to present my work to all the participants.

In addition, I would like to thank Andrzej Holdyk, Research Scientist at SINTEF, for his continuous guidance on PSCAD modeling and for sharing key parameters on the system model in PSCAD, Jon Are Suul, Research Scientist at SINTEF, for sharing his knowledge on the wind turbine model used in this thesis, Jorun Irene Marvik, senior engineer at Statnett, for providing key parameters for the system model in PSCAD, Pr. Olimpo Anaya-Lara, professor at the University of Strathclyde (Visiting professor at NTNU), for his quick response on questions, Md. Aamir Rahmani, Ph.D. student at Michigan Technological University, for being a good discussion partner and for comparing my PSCAD model to his Simulink model.

Trondheim, June 2022
Lars Thaulow Bremnes

Abstract

Distance relays are considered to be the most reliable protection for transmission lines. This may not be the case anymore, as the share of renewable energy sources (RES) becomes a more substantial part of the power system. By introducing a large amount of RES there are expected problems to arise for distance relays ability to measure the correct fault impedance, which will lead to faulty operations.

This master thesis uses PSCAD to simulate the performance of the distance protection function in distance relays, for high penetration of wind power. It is developed a system model in cooperation with Statnett and SINTEF, to make a representable model of a system at Fosen, where there are wind farms connected to the 420kV grid. Statnett has raised concerns that their distance relays in Fosen may experience faulty operations, where multiple wind farms were finalized in 2020.

To investigate this, there are performed multiple simulations where different parameters are used to observe their impact on distance protection performance. There are used five changeable parameters, fault type, fault resistance, fault distance, wind farm control strategy, and wind power penetration level, bringing out a total of 1080 simulations. The main objectives for this thesis has been formulated into three questions which is going to be answered.

1. How does fault resistance impact distance relays fault detection capability?
2. How does the increased penetration level of wind power influence protection performance?
3. What wind farm control strategies are the most reliable, and which has the most negative impact on protection performance?

Question 1: The increase in fault resistance has a great impact on distance relays fault detection capability. This is due to the unpredictable current from wind farms compared to the main grid which is dominated by synchronous generators. This will lead to an under-or overreach situation for the relay. It is especially the relay closest to the wind farm that suffers the most, the other relays have either none or very few misoperations.

Question 2: With increasing wind power penetration levels, distance relay performance is greatly impacted. There have been performed simulations for extreme future scenarios, with penetration levels of 50% - 100%, where it is a clear indication, that the higher the penetration level, the more misoperations the relays encounter.

Question 3: The three wind farm control strategies tested in the thesis are; Constant active power, Constant reactive power, and Balanced currents. It is concluded that the Constant reactive power strategy is the most reliable for distance performance, and the Balanced currents strategy has the most negative impact.

Sammendrag

Distansevern anses å være det mest pålitelige vernet når det kommer til å beskytte høyspentlinjer. Dette er kanskje ikke tilfelle lenger, da andelen av fornybare energikilder blir en vesentlig større del av kraftsystemet. Ved å introdusere store mengder av fornybare energikilder, forventes det at distansevern vil få problemer med impedansmålingene, som vil føre til uønskede situasjoner.

I denne masteravhandlingen brukes PSCAD for å simulere hvordan distansevern takler en høy andel fornybar energikilde koblet til høyspentnettet. Det er utviklet en modell i samarbeid med Statnett og SINTEF, som skal representere et system på Fosen, hvor det er vindparker tilkoblet 420kV-nettet. Statnett har uttrykt bekymring for at deres distansevern i Fosen kan oppleve feil, hvor flere vindparker ble ferdigstilt i 2020.

For å undersøke dette er det utført flere simuleringer der forskjellige parametere brukes for å observere deres innvirkning på distansevernene. Det er totalt fem parametere som endres, feiltype, feilmotstand, feilavstand, vindpark kontroll-strategi og andel vindkraft ifh. vanlig synkrongenerator-kraft. Dette har gitt totalt 1080 simuleringer. Det er tre spørsmål som utgjør hovedmålet med denne masteravhandlingen;

1. Hvordan påvirker feilmotstand feildeteksjonen til distansevern?
2. Hvordan påvirker vindparkens økte effektnivå distansevernets pålitelighet?
3. Hvilken vindpark kontroll-strategi er den mest pålitelige, og hvilken har mest negativ innvirkning?

Spørsmål 1: Økningen i feilmotstand har stor innvirkning på distansevernenes evne til å oppdage feil. Dette skyldes den uforutsigbare strømmen fra vindparker sammenlignet med sentralnettet som er dominert av synkrongeneratorer. Dette vil føre til at distansevern måler en unøyaktig impedans og feiltolker hvilken sone feilen ligger i. Det er spesielt vernet nærmest vindparken som blir påvirket, mens de andre vernene observerer enten ingen eller veldig få feilsituasjoner.

Spørsmål 2: For høyere andel av vindkraft tilknyttet sentralnettet, påvirkes distansevernene i økende grad. Det er hovedsakelig utført simuleringer for ekstrem tilfeller av vindkraft (mulige fremtidige scenarioer), 50% - 100%. Resultatene viser til at det er en klar indikasjon på at jo høyere nivået er, jo flere feiloperasjoner har vernet.

Spørsmål 3: De tre vindpark kontroll-strategiene som er testet i dette prosjektet er; konstant aktiv effekt, konstant reaktiv effekt og balanserte strømmer. Det konkluderes med at strategien for konstant reaktiv kraft er den mest pålitelige for distansevern, og Balanserte strømmer strategien har den mest negative påvirkningen på vernene.

Table of Contents

List of Figures

List of Tables

1 Introduction

1.1 Background and motivation

Renewable energy sources like wind and solar power are becoming a more significant part of today's power system. As they are an unstable power source where the power is not constantly available, a converter model must be used to synchronize with the main grid. This procedure needs careful controlling and more complex fault handling than conventional energy sources such as hydro or coal, which use synchronous generators. In a power system where the amount of renewable energy is becoming more significant, grid protection is expected to be greatly influenced with its performance and security[8][9]. If the EU's climate goals for 2050[10] are realizable, i.e., to be the first carbon-neutral continent, the increase in renewable energy integration will be exponential over the next 28 years. This means that renewable energy sources will become a more considerable part of today's power systems and may even be the most significant part. This will make grid synchronization, fault handling, and protection more crucial than ever.

Distance relays are commonly used in transmission lines as primary or backup protection. They deliver high reliability, excellent backup properties, and selectivity for meshed power systems dominated by synchronous generators. When large amounts of renewable energy sources are connected to the main grid, the distance protection function in distance relays might experience incorrect operations. This issue has been highlighted in several papers [11][12][13], where concern about the relays ability to measure the correct fault impedance due to the short circuit current contribution from converters being limited and unpredictable compared to synchronous generators. This may lead to undesired operations where the relay may under- or overreach, or not trip at all, which is unacceptable.

This thesis's main objective will be to answer the questions below.

- How does fault resistance impact distance relays fault detection capability?
- How does the increased penetration level of wind power influence protection performance?
- What wind farm control strategies are the most reliable, and which has the most negative impact on protection performance?

1.2 Approach

As this is a continuation of previous theses[14][15], it is evident to continue using the same program as before, i.e., the EMTDC-based simulation program, PSCAD. PSCAD is a graphical simulation program chosen for previous theses as it is considered the most reliable program for power electronic simulations. Since the model from earlier theses was not passed on, a model needed to be made from scratch.

The earlier thesis [14] used a PWM model to simulate ABCG faults, as that model was designed to only handle symmetrical faults. The model used in this thesis is principally intended to address unsymmetrical faults but will include results for all types of faults. Both the prior and this thesis exclusively focus on Type 4 wind turbines, which use full-size converters.

The system model developed and the parameters given by Statnett are relatively comparable to a wind farm at Fosen. This is because Statnett had expressed concerns that they would encounter problems on distance relays, as mentioned in the previous thesis [14]. The Fosen system has multiple wind farms connected to the 420kV main grid. This thesis focuses solely on one wind farm, which produces roughly 440MW. To observe how the distance relay performs for different wind power penetration levels, it is introduced a parallel infeed Thevenin equivalent, representing a background grid with synchronous generators.

1.3 Scope

The objective of this thesis is to try and answer the questions given in chapter 1.1. Therefore, a model needs to be made in PSCAD with the ability to observe the distance relays performance, especially the trip times. There are in total five changeable parameters included in this thesis. Fault type, where AG, ABG, AB, ABCG, and ABC are included. Fault resistance, which is set to range from 0.1Ω to 10Ω to monitor the impact of increasing fault resistance. Fault distance, set to 10%, 50%, and 90% of the line closest to the wind farm, to watch for possible under- or overreaching made by the relays. Control strategy, where there are included three different types, Constant P, Constant Q, and Balanced I. Lastly, the wind power penetration level which is set to range from 50% up to 100% to observe the most extreme cases and possible future scenarios.

2 Theory

The state of art and related work for this thesis is was carried out in the pre-project preceding this thesis[16], and is included for overall readability. However, there is supplied additional relevant information in some of the chapters.

2.1 Short circuits

In a power system, there are several types of short circuits with different impacts on the system. The most common fault is a single line to ground fault (L-G), which is responsible for about 70% of all faults in a power system[1]. Other types of faults are; two-phase (L-L), three-phase (L-L-L), two-phase-to-ground (L-L-G), and three-phase-to-ground (L-L-L-G). Since L-L-L and L-L-L-G short circuits are involving all phases, these are called balanced faults, or symmetrical faults. This means that the current and voltage vectors are arranged with a 120°phase shift and have the same magnitude. Unbalanced faults, or unsymmetrical faults, are faults that only impact one or two of the phases, L-G, L-L, and L-L-G. Here the phase shift and magnitude can vary. In figure 1 the different fault types are shown, where the unbalanced faults are presented in a, b and c and balanced faults in d and e.

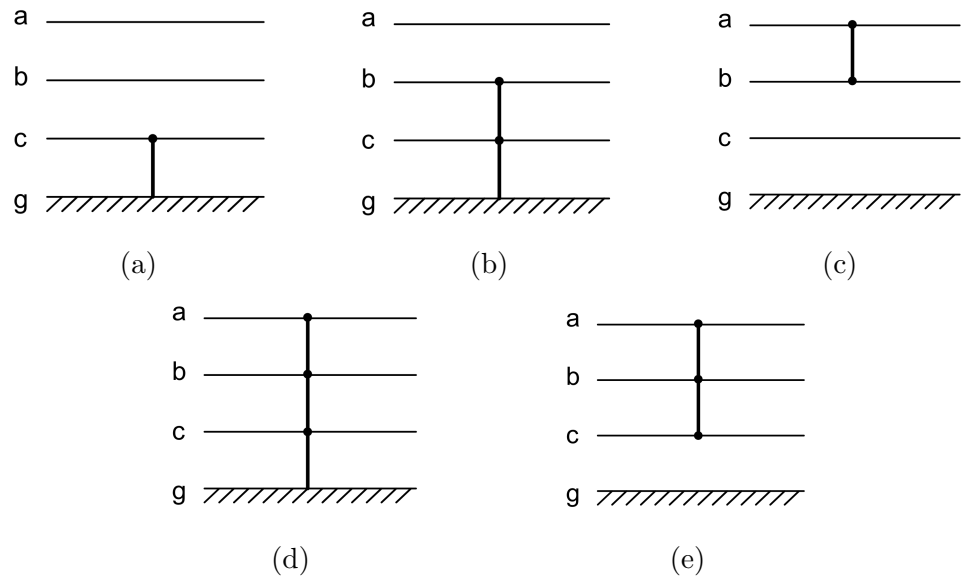

Figure 1: Different types of short circuits, a) L-G, b) L-L-G, c) L-L, d) L-L-L-G, e) L-L-L

In general, a short circuit current has two different components, one steady-state AC component, and one DC component. These components can be expressed by solving the differential equation for an R-L circuit, with an applied sinusoidal voltage shown

in equation 2.1 and 2.2. Here I_m is the magnitude of the steady-state current, U_m is the magnitude of the source voltage with an angle θ, and $\phi = tan^{-1}(\frac{\omega L}{R})$. In a synchronous generator (SG) dominated power system it can be assumed that the ratio between reactance and resistance is very high ($\omega L >> R$), the ratio can typically be 110[1]. By assuming a high X/R ratio, then $\phi = 90°$, which means that the DC current component is zero if the fault is occurring at a time where the voltage is at its peak $\theta = 90°$. On the other hand, if the fault occurs when the voltage angle is 0°, the DC current component will be at its maximum. This can be seen from figure 2.

$$L\frac{di}{dt} + Ri = U_m sin(\omega t + \theta) \tag{2.1}$$

$$i = I_m sin(\omega t + \theta - \phi) - I_m sin(\theta - \phi)e^{-Rt/L} \tag{2.2}$$

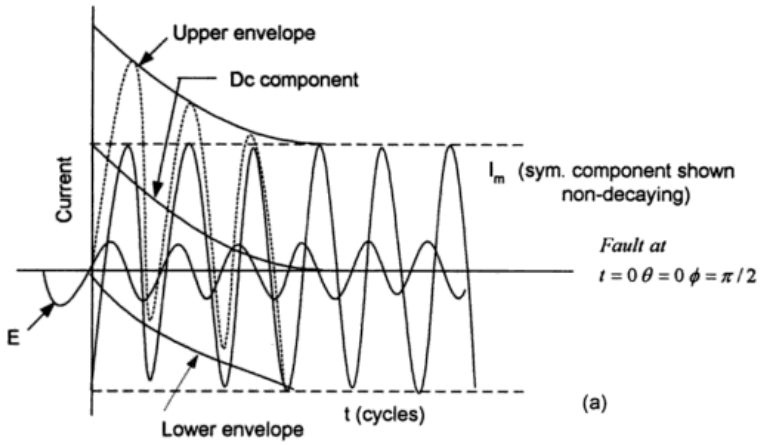

Figure 2: Transient current component[1]

2.1.1 Symmetrical components

In the early 20th century, Fortescue[17] described a way of representing an unsymmetrical system with three symmetrical components, which are the positive-, negative- and zero sequence. When a three-phase system is operating in normal conditions, the system is in balance or in symmetry. This means that the voltages and currents vectors are phase-shifted with 120°and have the same magnitude. The vectors can be broken down into positive-, negative- and zero-sequence components, which are shown in figure 3. These components can be used to represent a system that is in unbalance or asymmetry, as shown in figure 4.

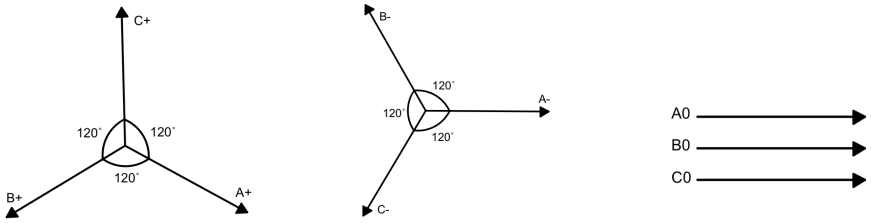

(a) (b) (c)

Figure 3: Vector representation of a) positive-, b) negative- and c) zero-sequence

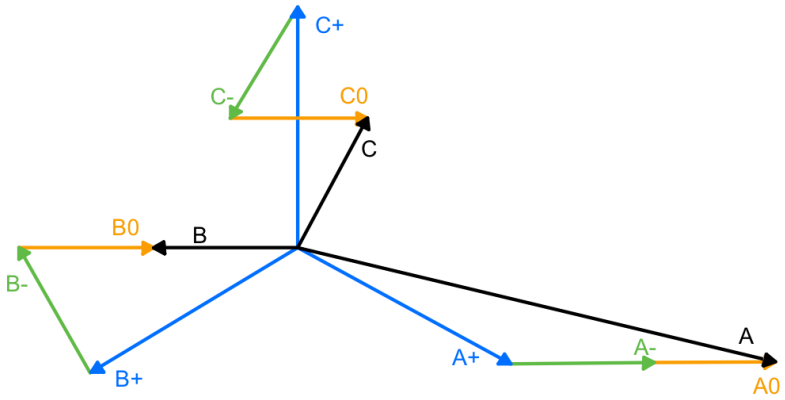

Figure 4: Vector diagram, showing how the asymmetrical system can be represented by positive-, negative- and zero-sequence components

These components are also represented in equations 2.3, where V_a, V_b, and V_c, are the voltages for each phase[1][18]. There are only shown equations for voltages, but the same applies for currents.

$$\begin{aligned} \vec{V_a} &= \vec{V_a^+} + \vec{V_a^-} + \vec{V_a^0} \\ \vec{V_b} &= \vec{V_b^+} + \vec{V_b^-} + \vec{V_b^0} \\ \vec{V_c} &= \vec{V_c^+} + \vec{V_c^-} + \vec{V_c^0} \end{aligned} \tag{2.3}$$

The phase voltages are build up by the positive- (V_a^+, V_b^+, V_c^+), negative- (V_a^-, V_b^-, V_c^-), and zero-sequence (V_a^0, V_b^0, V_c^0) components. Each of these are given by equations 2.4 - 2.6[19].

$$\begin{aligned} \vec{V_a^+} &= \hat{V}^+ \angle \phi^+ \\ \vec{V_b^+} &= \hat{V}^+ \angle -\frac{2\pi}{3} + \phi^+ \\ \vec{V_c^+} &= \hat{V}^+ \angle \frac{2\pi}{3} + \phi^+ \end{aligned} \tag{2.4}$$

$$\begin{aligned} \vec{V_a^-} &= \hat{V}^- \angle \phi^- \\ \vec{V_b^-} &= \hat{V}^- \angle \frac{2\pi}{3} + \phi^- \\ \vec{V_c^-} &= \hat{V}^- \angle -\frac{2\pi}{3} + \phi^- \end{aligned} \tag{2.5}$$

$$\vec{V_a^0} = \vec{V_b^0} = \vec{V_c^0} = \hat{V}^0 \angle \phi^0 \tag{2.6}$$

In matrix form, the equations can be represented as equation 2.7, where $a = 1e^{j\frac{2\pi}{3}}$

$$\begin{bmatrix} \vec{V_a} \\ \vec{V_b} \\ \vec{V_c} \end{bmatrix} = \begin{bmatrix} 1 & 1 & 1 \\ 1 & a^2 & a \\ 1 & a & a^2 \end{bmatrix} \begin{bmatrix} \vec{V^0} \\ \vec{V^+} \\ \vec{V^-} \end{bmatrix} \tag{2.7}$$

2.1.2 Ground fault

Ground faults as mentioned earlier, are the most common fault type in a power system. It is therefore important to know the principle behind the calculation of these types of fault. When a fault appears on a line, the current travels from the fault point, through the ground, and back to the generator or transformer's neutral point. The grounding of such components is also evident in the ground fault current calculation. If the generator or transformer is isolated from the ground, the fault current is relatively small[1]. Otherwise, directly grounded and low inductance- or resistance grounded systems may have higher ground fault currents.

In the rest of this chapter, a three phase system that is directly grounded will be assumed. When a fault appears on phase a, the sequence current components can be found as shown in equation 2.8, where $a = 1e^{-j\frac{2\pi}{3}}$

$$\begin{bmatrix} I_0 \\ I_+ \\ I_- \end{bmatrix} = \frac{1}{3} \begin{bmatrix} 1 & 1 & 1 \\ 1 & a & a^2 \\ 1 & a^2 & a \end{bmatrix} \begin{bmatrix} I_a \\ 0 \\ 0 \end{bmatrix} = \frac{1}{3} \begin{bmatrix} I_a \\ I_b \\ I_c \end{bmatrix} \tag{2.8}$$

When calculating this we get, $I_0 = I_+ = I_- = \frac{1}{3} I_a$, where I_a is the fault current in phase a. By including $I_a = \frac{V_a}{Z_f}$, it can be written as in equations 2.9.

$$\begin{aligned} 3I_0 Z_f &= V_a \\ 3I_0 Z_f &= V_+ + V_- + V_0 \\ 3I_0 Z_f &= -I_0 Z_0 + (V_a - I_+ Z_+) - I_- Z_- \end{aligned} \tag{2.9}$$

Which can be formulated to give the final equation for the fault current in phase a.

$$I_a = 3I_0 = \frac{3V_a}{(Z_+ + Z_- + Z_0) + 3Z_f} \tag{2.10}$$

2.2 Distance Relay

2.2.1 Distance protection fundamentals

Distance relays are one of the most used relays on transmission lines in a SG dominated power system. They deliver a high level of operational security, excellent backup properties, and exemplary selectivity. If correctly coordinated, distance relays can detect faults in very complex meshed systems. Distance relays use multiple zones to get a wide range of protection. The zones cover different parts of the transmission line, where usually zone 1 covers 80% of the line and zone 2 covers 120%[20]. The different zone coverage is due to uncertainties in parameters when the relay performs its measurements. If zone 1 was set to cover 100% of the line, the relay could measure the wrong impedance and lead to faulty operations. Each zone is also set with a time delay, which usually is in the range of 0.2-0.3s[20]. The time delays are set between each zone, to provide selectivity, so only the closest relay to the fault will trip. The other zones are meant for backup, for other relays that are further down the line. It can also be possible to use one of the zones, 3 or 4, as backward protection. This helps the system increase its selectivity. In figure 5, there is a simple example of a system, where relay R1 protects 80% of the line between bus A and B, zone 2 protects 120%, reaching over bus B, and lastly zone 3 protects

the rest of the line between bus B and C. It can also be seen from the figure that the time delay is increasing for each zone. For example, zone 1 time delay is set to 0.2s, zone 2 is 0.4, while zone 3 is 0.6.

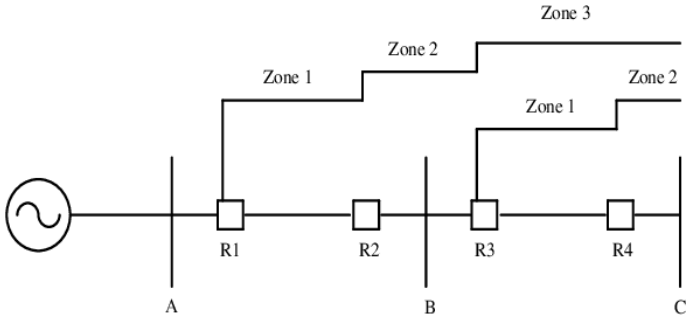

Figure 5: Single line diagram with distance relay zones

The distance relay measures the impedance (Z) of the protected line to indicate if there is a fault present or not. More specifically, it measures the voltage (V) and current (I) and calculates the impedance. It can also calculate the distance to the fault because the reactance per unit length in the transmission line is known.

To illustrate how the fault enters the different zones of the distance relay, an RX-diagram can be used. In such a diagram the real and imaginary parts of the calculated impedance are plotted to show the trajectory of the fault impedance and can be tracked into one zone. An RX-diagram is presented in figure 6, where the x-axis represents the resistance (R) and the y-axis the reactance (X). The angle α can be adjusted to suit the protected line, usually set to 20-30%. θ is the line impedance angle and is usually used as a resistive reach angle as shown to the right in figure 6. The total resistive reach is dependent on load impedance and power swings. The load impedance at normal load is usually much greater than the resistive reach.

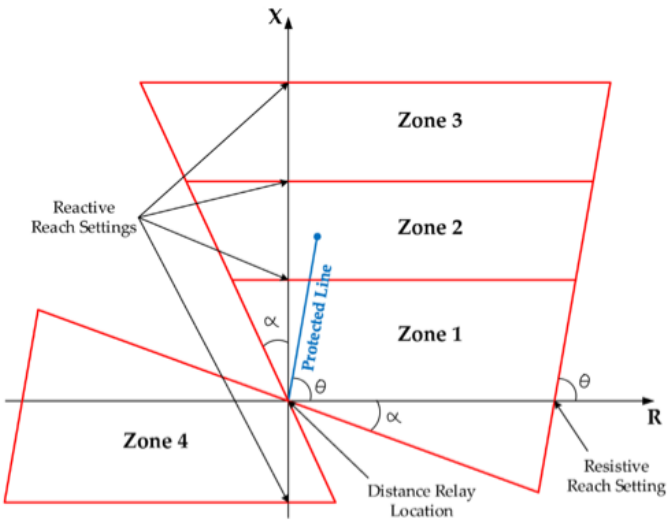

Figure 6: RX-diagram, showing zones for a distance relay[2]

In a three phase system, it is important to know about the different loops the fault current can travel through. There are in total six different current paths, which are L1-G, L2-G, L3-G, L1-L2, L2-L3, and L3-L1. The distance relay has to calculate the impedance for each of these loops. The equations for the six pathways are shown in equations 2.11 and 2.12. Here $U_{L(1-3)}$ are the phase voltages, $I_{L(1-3)}$ are the phase currents, I_0 is the zero-sequence current and K_0 is the zero-sequence compensation factor.

$$\begin{aligned} Z_{L1-G} &= \frac{U_{L1}}{I_{L1} + K_0 I_0} \\ Z_{L2-G} &= \frac{U_{L2}}{I_{L2} + K_0 I_0} \\ Z_{L3-G} &= \frac{U_{L3}}{I_{L3} + K_0 I_0} \end{aligned} \tag{2.11}$$

$$\begin{aligned} Z_{L1-L2} &= \frac{U_{L1} - U_{L2}}{I_{L1} - I_{L2}} \\ Z_{L2-L3} &= \frac{U_{L2} - U_{L3}}{I_{L2} - I_{L3}} \\ Z_{L3-L1} &= \frac{U_{L3} - U_{L1}}{I_{L3} - I_{L1}} \end{aligned} \tag{2.12}$$

Since the distance relay calculates the impedance based on positive-sequence quantities, K_0 is used to compensate for the zero-sequence currents which flow through the ground. K_0 represents a constant factor for a line, and can be calculated us-

ing equation 2.13, where Z_0 and Z_1 are the zero- and positive-sequence impedance respectively, and K is set to either 1 or 3, depending on relay design[21].

$$K_0 = \frac{Z_0 - Z_1}{K \cdot Z_1} \tag{2.13}$$

2.2.2 Influence of fault resistance

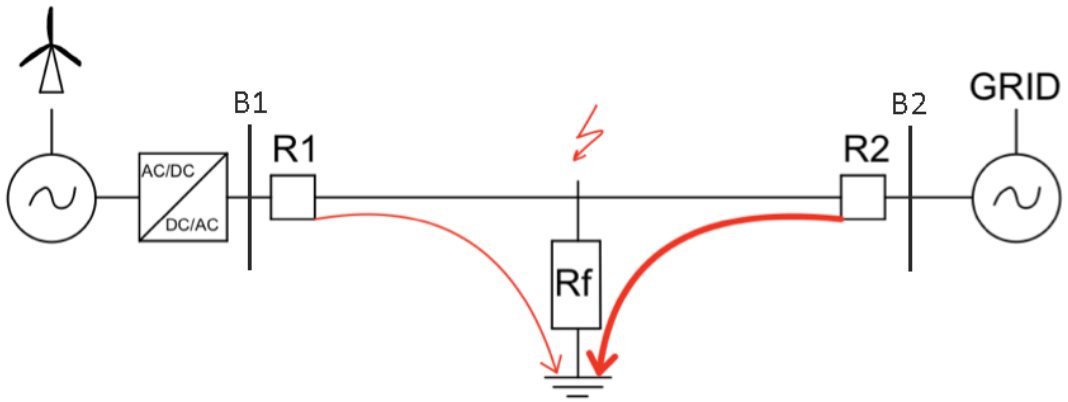

Figure 7: One line diagram, showing the current contribution from both the wind farm and main grid. The size of the red lines represents the size of the current

When considering a transmission line where one bus is connected to renewable energy sources (RES), and the other one is connected to the main grid (as in figure 7), it is important to know the difference in current contribution. Since the converter on the RES side has an upper limit for current output, the contribution is therefore limited. For the main grid, the contribution can be many times the current from the converter. This can be challenging for distance relay measurements and can lead to inaccurate operations of the relay. The apparent impedance seen by R1 is given in equation 2.14. Where I_1 and I_2 are the phase currents from B1 and B2 respectively, Z_{1-f} is the line impedance to the fault, and Z_{ad} is the additional part including the fault resistance R_f [12]. This additional part to the impedance is dependent on what type of fault is present. E.g., for an L-L-L fault, the impedance for each phase seen by the two relays R1 and R2 are shown in equations 2.15 and 2.16 respectively.

$$Z_{app-R1} = \frac{U_1}{I_1} = \frac{I_1 Z_{R1-f} + (I_1 + I_2) R_f}{I_1} = Z_{R1-f} + Z_{ad} \tag{2.14}$$

By inspecting these equations, the ratio between current I_1 and I_2 is impacting the

impedance measurement, particularly when R_f is large[12][22]. When increasing the current ratio $\frac{I_2}{I_1}$ the impedance measurement for relay 1 is increasing, and for relay 2 it is decreasing. In figure 7 the difference in current contribution is shown by the size of the arrows through the fault resistance, for visualization.

$$Z_{app-R1} = Z_{R1-f} + (1 + \frac{I_2}{I_1}) \cdot R_f \tag{2.15}$$

$$Z_{app-R2} = Z_{R2-f} + (1 + \frac{I_1}{I_2}) \cdot R_f \tag{2.16}$$

For ground faults, the apparent impedance for each phase seen by R1 and R2 are shown in equations 2.17 and 2.18 respectively.

$$Z_{app-R1} = Z_{R1-f} + \frac{I_1 + I_2}{I_1 + K_0 3I_0} \cdot R_f \tag{2.17}$$

$$Z_{app-R2} = Z_{R2-f} + \frac{I_2 + I_1}{I_2 + K_0 3I_0} \cdot R_f \tag{2.18}$$

Lastly in equations 2.19 and 2.20, the impedance measurements for L-L fault (AB) is shown for the two relays.

$$Z_{app-R1} = Z_{R1-f} + \frac{I_{1A} + I_{2A}}{I_{1A} - I_{1B}} \cdot R_f \tag{2.19}$$

$$Z_{app-R2} = Z_{R2-f} + \frac{I_{2A} + I_{1A}}{I_{2A} - I_{2B}} \cdot R_f \tag{2.20}$$

The ratio between $\frac{I_2}{I_1}$ impacts not only the magnitude of the fault impedance but also the angle. The angle changes due to the difference in frequencies of the two currents[3]. E.g., if the frequency of the current I_1 is 50.25Hz and I_2 is 50.00Hz, the fault impedance angle will rotate with 90° per second. If the fault does not disconnect after a certain amount of time, e.g., 0.5 seconds, the angle would have rotated 45° clockwise. On the other hand, if the frequency of the current I_2 is larger than I_1, it will rotate counterclockwise. The angle difference can be calculated with equation 2.21. As seen in figure 8, the fault impedance components are shown in an RX-diagram, with the impact of both the fault resistance (R_f) and the different current contribution (K_{XY}). The higher the frequency differences are between the two currents, the faster it will lead to either overreaching or underreaching[3].

$$\frac{I_2}{I_1} = K_{XY} \cdot 1\angle(360° \cdot \Delta f \cdot \Delta t) \tag{2.21}$$

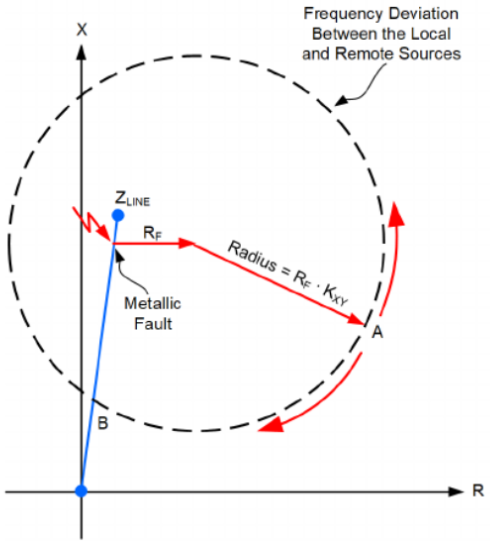

Figure 8: Impact of fault resistance on impedance measurement. Due to the difference in frequencies, the fault impedance may rotate along the dotted circle. Point "A" represents where the static impedance for the high inertia (SG) system is located[3].

Overreaching is the term used for when the distance relay measures the fault impedance to be smaller than it really is. This leads to unnecessary disconnections of lines, which is not optimal to maintain selectivity. Underreaching, on the other hand, is when the relay measures a higher fault impedance, which will leave the measured fault impedance outside the correct zone. It will therefore not detect the fault as it should and lead to an unnecessarily long time before disconnecting, which can harm vulnerable equipment.

2.3 Converter and Control

2.3.1 Converter Basics

Converters are a key component in systems where RES are present since the power from such sources, like wind and solar, is more unpredictable and the power is not always available. A converter is a common name for both inverter and rectifier, where an inverter is when a DC signal is inverted to an AC signal, and a rectifier is the opposite, AC to DC. There are several different converter technologies, with different applications. Voltage source converter (VSC) and current source converter (CSC)

are the most commonly used in wind power systems[19]. These types of converters often use insulated-gate bipolar transistors (IGBT), which are preferred in high voltage applications. These converters can also produce an AC signal without having any AC-signal as input[23]. By using pulse width modulation (PWM), making an AC signal is done by switching on and off the IGBTs to make the sinusoidal signal. Here the on and off time ratio is called duty cycle, meaning if the duty cycle is 70%, the IGBT is on 70% and off 30% of the time.

The main difference between VSC and CSC is that VSC keeps the polarity of the DC voltage constant, meaning it can change the power flow by changing the polarity of the current[23]. CSC, on the other hand, keeps the polarity of current constant and changes the power flow by changing the polarity of the voltage. The different converter technologies can use different typologies, such as two-level, three-level, or multi-level configurations. The deciding factor when choosing such a topology often comes down to cost and losses[24]. A two-level VSC is depicted in figure 9, where six IGBTs are used, and the constant DC voltage is shown to the right in the figure. This is an example of a rectifier, but by mirroring the system, it can be changed to an inverter, delivering AC voltage.

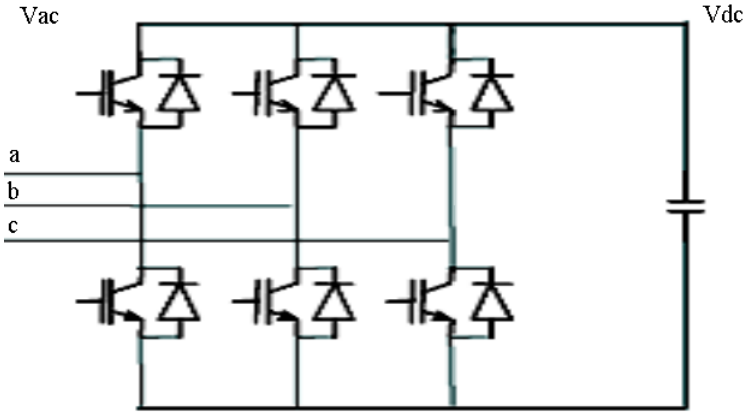

Figure 9: Two-level VSC

2.3.2 Grid Synchronization

When having converters connected to the main grid, a reliable control structure for the synchronization process is important. The control system has to control the frequency, voltage, current, and active- and reactive power, or just one of them. Synchronization to the grid is a process that can be done in different ways, depending on the practical use of the system. For grid synchronization, there are three categories that are mainly used; grid-forming, grid-feeding, and grid-supporting[5].

Grid-forming acts as an ideal AC voltage source with low output impedance and it requires the voltage amplitude and frequency as reference. Grid-feeding acts as an ideal AC current source in parallel with a high impedance, where the references are the active and reactive powers. Lastly, grid-supporting can use both configurations above and use all the parameters above as a reference, where also a droop control is needed.[5]

The control system for a converter needs to have a reference frame to more easily control the system. There are often two types of reference frames that are used; $\alpha\beta$, which is also called the stationary reference frame, and dq, the synchronous reference frame[5]. Each of these reference frames has a two-axis system, where $\alpha\beta$ refers to the real and imaginary axis and dq refers to the direct and quadratic axis, respectively. The two axis in each of the reference frames are orthogonal to each other, and the difference between them is how they operate. The $\alpha\beta$-axis is fixed, and since the sinusoidal signals from the grid are rotating counterclockwise, it is called a "stationary reference frame". On the other hand, the dq-axis is rotating counterclockwise with the angular speed ω, which means that the dq-axis and the sinusoidal signals rotate together, therefore the name "synchronous reference frame". The different reference frames are shown in figure 10.

The dq reference frame has some drawbacks when it comes to unbalanced faults, but it is easier to operate than the $\alpha\beta$ reference frame. There are some solutions to improve the dq reference frame and make it more suitable for unbalanced faults [25][26], but they will not be presented.

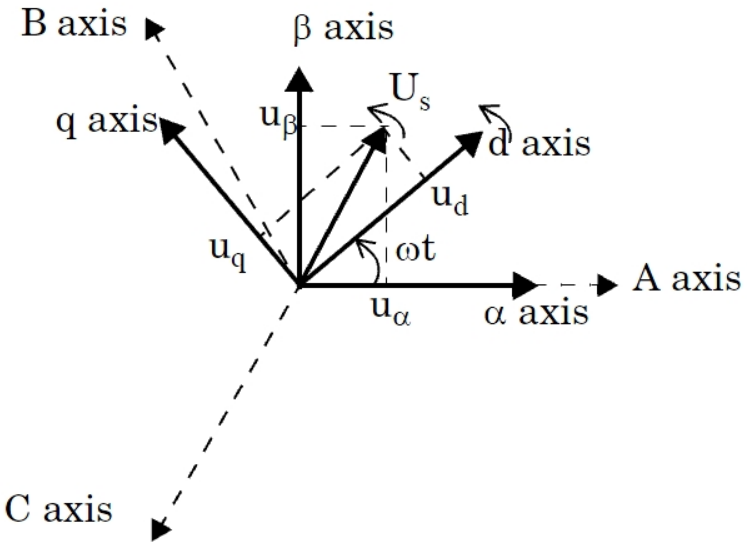

Figure 10: Vector representation of the $\alpha\beta$-axis and dq-axis, also including ABC-axis and voltage vector U_s, where the voltage is decomposed to both $\alpha\beta$ frame (u_α, u_β) and dq frame (u_d, u_q)[4]

The synchronous reference frame uses a technology called phase-locked loop (PLL) to synchronize with the main grid, where the main goal is to estimate the phase angle. The method starts with transforming the three phase voltage signals to dq frame using the Park transformation, where a feedback loop from the estimated phase angle is used. By taking the rated frequency as a feedforward loop, it can better estimate the phase angle[5]. A block diagram of this configuration is shown in figure 11 a).

The stationary reference frame often use a technology called frequency-locked loop (FLL) together with a second-order generalized integrator (SOGI). This transforms the three phase voltage to $\alpha\beta$ frame using the Clark transformation, where a feedback loop returns from the estimated $\alpha\beta$ voltage. It uses the FLL to estimate the grid frequency, and since the SOGI is implemented in both the $\alpha\beta$ frame (Dual-SOGI, or DSOGI), it can estimate the quadrature voltage (the voltage which is orthogonal to the current). A block diagram of this configuration is shown in figure 11 b).

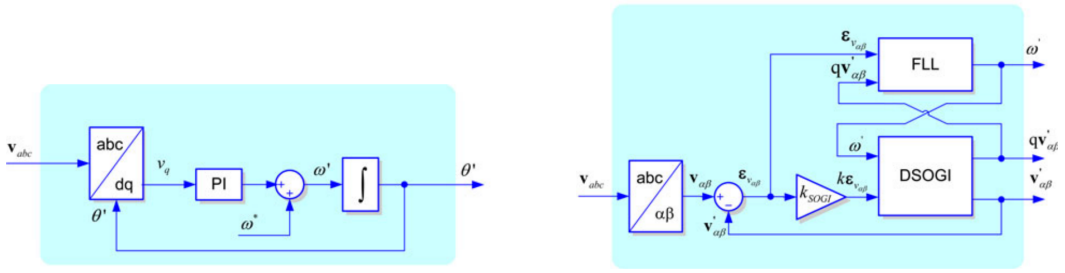

(a) (b)

Figure 11: a) Synchronous reference frame with PLL, and b) Stationary reference frame with DSOGI and FLL[5]

2.3.3 Virtual Flux Estimation

Another technology is the voltage-sensor-less virtual flux estimation[27], which is used for VSCs. This method is a type of grid-supporting control with current source, where the voltage and frequency are measured from the grid. The advantages of this method are reduced costs due to fewer sensors, increased flexibility, and improved performance of the converter control system[27].

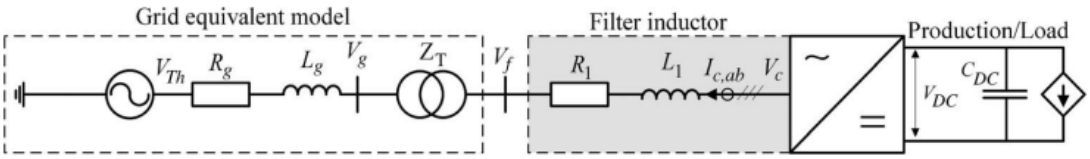

Figure 12: Basic system that is considered in this chapter[6].

The following is based on the ideal virtual flux estimation where the system in figure 12 is used[27][6]. The definition of flux is the integral of the voltage and is shown in equation 2.22.

$$\Psi = \int V \cdot \mathrm{d}t + \Psi_0 \tag{2.22}$$

$$V_{f,\alpha\beta} = V_{c,\alpha\beta} - R_1 \cdot I_{c,\alpha\beta} - L_1 \cdot \frac{\mathrm{d}I_{c,\alpha\beta}}{\mathrm{d}t} \tag{2.23}$$

$$I_{c,\alpha\beta} = v_{ref,\alpha\beta} \cdot \frac{1}{2} V_{DC} \tag{2.24}$$

When combining the standard equation for flux 2.22 with the voltage equation for the filter inductor (equation 2.23), the flux on the grid-side can be calculated. In equation 2.23, V_f is the grid-side voltage, V_c and I_c is the converter side voltage and current, where all variables are represented in $\alpha\beta$-quantities, lastly, R_1 and L_1 are the filters internal resistance and inductance. $I_{c,\alpha\beta}$ is given in equation 2.24. The resulting grid-side flux in $\alpha\beta$ reference frame, uses the voltage references $v_{ref,\alpha\beta}$, but in the case of PWM operation, the DC voltage signal, and the voltage over the filter to calculate the flux, which is shown in equation 2.25.

$$\Psi_{f,\alpha\beta} = \int \left(v_{ref,\alpha\beta} \cdot \frac{1}{2} V_{DC} - R_1 \cdot I_{c,\alpha\beta} \right) \mathrm{d}t - L_1 \cdot I_{c,\alpha\beta} \tag{2.25}$$

By transforming equation 2.25 into per unit values, where

$$V_{base} = \hat{V}_{phase} \qquad V_{b,\alpha\beta} = 2 \cdot V_b \qquad \Psi_b = \frac{V_b}{\omega_b} \tag{2.26}$$

we get:

$$\psi_{f,\alpha\beta} = \omega_b \int \Big(v_{ref,\alpha\beta} \cdot v_{DC} - r_1 \cdot i_{c,\alpha\beta} \Big) \mathrm{dt} - l_1 \cdot i_{c,\alpha\beta} \tag{2.27}$$

A block diagram can also be used to depict how this works, as shown in figure 13. Now the phase angle for the voltage at the grid-side (θ_f) can be estimated by taking the phase angle for the flux (γ_f) and adding 90°. This is because the flux lags the voltage by 90°. The equations for calculating these angles are shown in equation 2.28.

$$\gamma_f = \arctan\left(\frac{\psi_{f,\beta}}{\psi_{f,\alpha}}\right) \qquad \theta_f = \gamma_f + 90^\circ \tag{2.28}$$

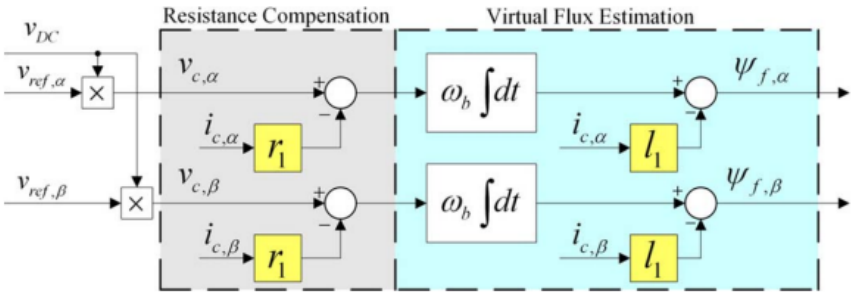

Figure 13: Ideal virtual flux estimation[6]

2.3.4 Control strategies

In this section, three different control strategies for power control are presented. BPSC (balanced positive sequence control), PNSC (positive-negative sequence compensation), and AARC (average active-reactive control) [27]. These three strategies calculate the current reference for the active and reactive current components and can be combined to vary between the three strategies. The combined current reference equation 2.29, includes two factors that decide what strategy is used, or if there is a combination of them. These factors are K_p and K_q, and can alter between -1 and 1. The other parameters in equation 2.29 are i_p^* and i_q^* which are the active and reactive current reference components, $\bar{p}^*$ and $\bar{q}^*$ which are the average active and reactive power reference, and χ^+ and χ^- which are the positive -and negative-sequence frequency-scaled virtual flux components. The subscript $\perp$ represents 90°lagging.

$$i^* = i_p^* + i_q^* = \frac{\bar{p}^*}{|\chi^+|^2 + k_p|\chi^-|^2} \cdot (-\chi_\perp^+ + k_p\chi_\perp^-) + \frac{\bar{q}^*}{|\chi^+|^2 + k_q|\chi^-|^2} \cdot (-\chi_\perp^+ + k_q\chi_\perp^-) \quad (2.29)$$

The BPSC strategy has the task of keeping the currents balanced (Balanced I), which will result in the lowest current magnitudes for a certain average power transfer. The drawback of this strategy is that it will also produce second harmonic oscillations in both active and reactive power flow. To eliminate the power oscillations that occur with BPSC, the PNSC or AARC strategies can be used. As described in [27], the power oscillations can be eliminated by setting the factors to -1 or 1. To achieve a constant active power strategy (Constant P), K_p needs to be equal to -1 to eliminate the reactive components in the PNSC, and K_q needs to be 1 to eliminate the reactive components in the AARC. Opposite, for constant reactive power strategy (Constant Q), $K_p = 1$ and $K_q = -1$. Later in this thesis, the names constant P, Constant Q, and Balanced I will be used to describe the three different control strategies.

2.4 Grid Codes

Grid codes are important specifications to ensure that the power system is operated correctly. These specifications are set by the country's transmission system operator (TSO). The grid codes are therefore not always the same for each country. EU[28] has however developed such specifications where each country can adjust the parameters individually within a certain limit.

Due to the rapid increase in RES, the Fault Ride Through (FRT) requirement is considered to be one of the most important specifications for such resources. Regular SG delivers reactive power when a voltage dip is present, but in wind turbines, this is not possible so it has to be managed differently. The wind park is required to remain connected to the grid for a certain amount of time during a voltage dip, so transient faults may have the time to ride through, therefore the name FRT.

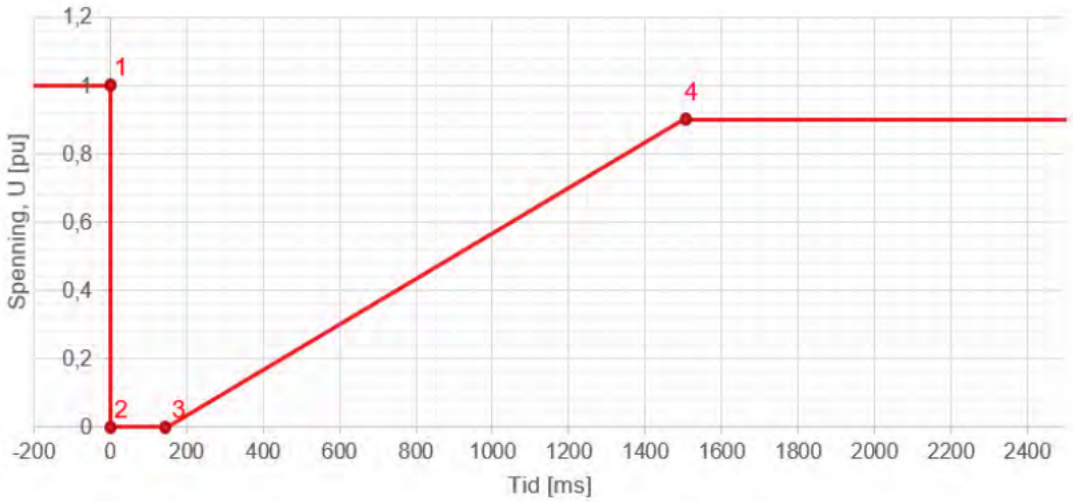

Figure 14: Norwegian grid code FRT, above 110kV[7]

Norway's TSO is Statnett, which sets the grid codes and specifies the FRT requirements for Norway [7]. The FRT curve in figure 14, shows at what level the voltage can not cross during a fault. The time delays are also set by Statnett, and they have used two different models, one for voltage levels over 110kV and one for under 110kV. Figure 14 depicts only the one for voltage levels over 110kV. Here the voltage can drop to zero during a fault, and remain zero for 150ms. After 150ms, the voltage can not cross the linear line between points 3 and 4 for the next 1350ms. Lastly after 1500ms, the voltage has to be higher than 0.9pu[7].

3 Method

Most of this chapter is also based on the pre-project[16], but is introducing a new system model. This thesis is a continuation of two previous theses, it shares the same intent, which is to investigate the functionality of distance relays by simulation in PSCAD. The procedure for the first thesis was to use a PWM-model, which the student made from scratch[14], and then simulate symmetrical faults, as the model only included controls for symmetrical faults. The second thesis compared the PWM-model with a wind turbine model provided by SINTEF[15]. In this thesis, solely the model from SINTEF has been used. The wind turbine model, which includes all the necessary parameters to simulate a wind turbine or wind farm, will be presented in detail, as well as a system model. The system model has been developed with support from both SINTEF and Statnett and includes transformers, transmission lines, and distance relays.

3.1 EMTDC-PSCAD

The EMTDC-based program PSCAD is a powerful and advanced graphical simulation tool for electrical purposes. It lets the user create complex circuits with the ability to analyze results and manage data completely integrated within the system. PSCAD also comes with many premade test setups, which can be a good starting point for new users. It is also considered to be the most reliable program dealing with power electronics. The program is to some degree difficult to start using, which was experienced, but after many hours of modeling, testing, and simulating the program became easier to manage. It was essential to use PSCAD as both prior theses were made in it, and SINTEF's wind turbine model is modeled in PSCAD.

3.2 SINTEF wind turbine model

The wind turbine model provided by SINTEF was initially made to focus on unsymmetrical faults, limiting its capability to manage symmetrical faults. However, it is presumably more realistic than the previous model [14]. The model does not use a PWM but instead simplifies the power electronics, which may have some drawbacks. Overall the model from SINTEF is considered to be a representable model and can be adjusted to deliver power from a single wind turbine, or from a whole wind farm.

SINTEF has modeled an average voltage source converter (VSC), which is done instead of a PWM model to minimize the complexity and to keep it more simple.

As seen from figure 15, the average VSC is illustrated, where there is used a fixed DC voltage to simplify the calculations, and the output voltage of the converter is based on the PR-Current control (PR as in proportional resonant), which again takes the calculated current reference, based on the control strategies described in chapter 2.3.4[6][29]. The virtual flux estimation described in chapter 2.3.3 is used to synchronize to the grid, where the phase angle is estimated by equation 2.28.

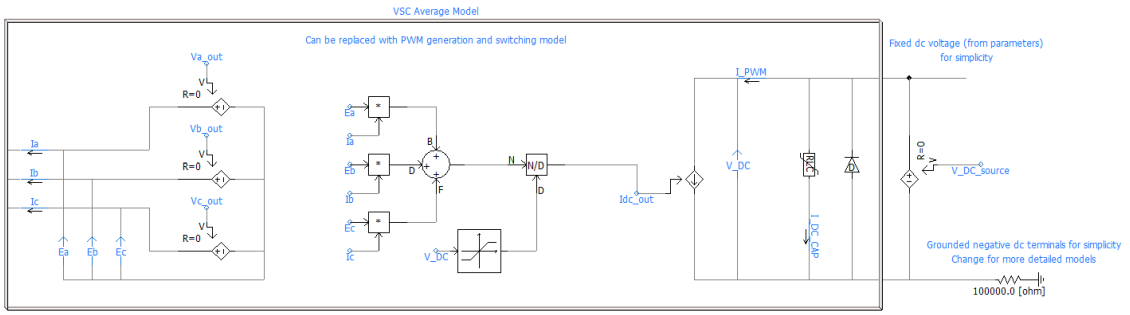

Figure 15: Average VSC, from SINTEF-Model

There are many components in the SINTEF model that does not need mentioning due to its complexity. Overall the model consists of the average VSC, which goes through an LC-filter, then through a Y-Δ transformer to the point of common coupling (PCC). The measurements are done both before and after the LC-filter, to measure the current reference. There are also some measurements on the high voltage side of the transformer for active and reactive power calculations. The model has a initialization sequence, which purpose is to "start" the system and wait for PSCAD to finish with its own initialization sequence. The whole start-up sequence takes about 1 second, of which PSCAD's start-up sequence takes normally 0.2-0.3 seconds. After this initialization sequence, the system is in steady-state and delivers the required power.

3.3 System model overview

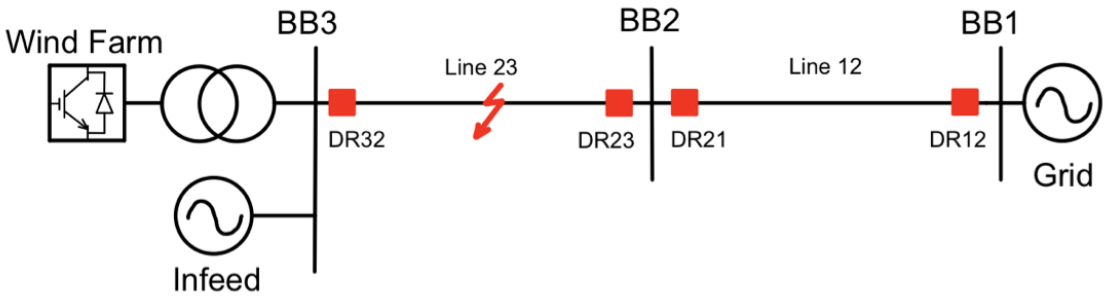

Figure 16: A simplified system model.

A simplified system model is presented in figure 16, to better understand the system. The system is developed to imitate the system at Fosen, where multiple wind farms are connected to the main grid at both BB2 and BB3. This thesis solely focus on the connection at BB3, where also an parallel thevenin equivalent infeed is used to regulate the penetration level from BB3. The infeed is intended to be depicting the backward grid dominated by synchronous generators. There are in total four relays connected to the system, two on each line, where the fault is only placed at line 23. The line length of line 12 is 70km, and for line 23 it is 50km. The transformers are simplified, not showing the parallel setup which is used, this will be presented in detail in chapter 4. The main grid equivalent is shown to the right in figure 16.

4 System Modeling

This chapter will give a more thorough description of how the different components and modules are designed. Firstly, presenting the various parts of the system, then how the simulations were performed. This is presented to more easily replicate the model and be able to compare results in future projects.

4.1 System model

The system model has been developed in PSCAD in cooperation with both SINTEF and Statnett on key parameters. The whole system is shown in figure 17, with a description in table 1 of the different components marked with numbers. The system is to some degree similar to the previous theses, but there are used some different modules and parameters. One draft of the system model was built in the pre-project[16], but this semester there were made changes to some parameters on the transmission line, transformers, and distance relay impedance calculations, which will be explained in the next chapters.

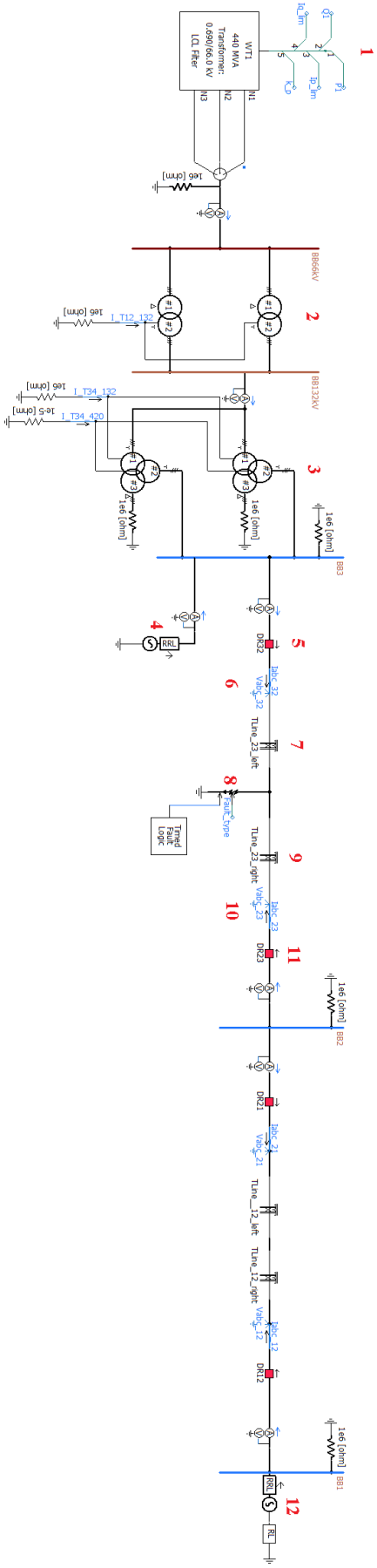

Figure 17: System model overview

System Model Description	
Number in figure 17	Description of the component
1	Wind turbine model, with five inputs. P1 and Q1 are power factor references, Ip_lim and Iq_lim are the current limiting factors, and lastly k_p is the control element which is set between -1 and 1 (-1 = Constant active power — 0 = Balanced currents — 1 = Constant reactive power)
2	Two winding transformers in parallel, T1 and T2.
3	Three winding transformers in parallel, T3 and T4.
4	This source represents the infeed which is connected when the penetration level of wind power is set to 90%-50%. When simulating 100% wind power the infeed is disconnected.
5	The distance relay connected to the wind farm side, and sees towards bus 2 (DR32). In PSCAD, it is only a breaker which gets a trip signal.
6	Here the measurements for DR32 are taken and sent to the DR32 logic.
7	First half of the transmission line
8	This is where the fault is located, and where the fault type and time of fault are inputs.
9	Second half of the transmission line
10	Measurements for DR23, which is sent to DR23 logic.
11	The distance relay which sees towards the wind farm (DR23), connected at bus 2.
12	This is the representation of the main grid equivalent.

Table 1: System model description

The second half of the line model is not described as it uses the same components as in the first half. The only difference is the names of the components, where the relays are named DR12 (connected to bus 1) and DR21 (connected to bus 2).

4.2 Transformer and Transmission line

From the system model in figure 17, it can be seen that there are used a total of four transformers. This transformer setup was used as it is comparable with the Fosen system. The first two are two winding transformers, while the other two are three winding transformers. They are put in parallel due to the high power flow from the wind farm, which was set to 440MW as it is relatively close to the production at this station. The transformer data for all transformers are shown in table 2.

Transformer values		
	T1 and T2	T3 and T4
Block name	3 phase 2 winding transformer	3 phase 3 winding transformer
Power rating [MVA]	220	300
Voltage #1/#2/#3 [kV]	66/132	132/420/22
Winding #1-#2-#3	$\Delta - Y$	$Y - Y - \Delta$
Positive sequence leakage reactance [pu]	0.13	(#1-#2) = 0.144 (#1-#3) = 0.132 (#2-#3) = 0.092
Copper loss [pu]	0.004	0.0029 (All windings)

Table 2: Transformer values for all transformers used in the system model

In both the earlier theses and the pre-project, an average transmission line model called Bergeron Model was used. This is the simplest model to use when modeling a transmission line, but for this thesis, it was decided to go for the Frequency-Dependent Phase Model, which SINTEF was using in their model. A tower model had to be included to use this model, whereas SINTEF used the "3 Conductor Flat Tower" model, as shown in figure 18. This model uses the conductor and ground wire data, which can be seen in table 3. Otherwise, the tower is configured as shown in figure 18, with different parameters on distances and lengths. This model setup calculates the parameters for the transmission line, which is given in table 3 (pr km values).

Since the system should be comparable to the system at Fosen, it was modeled with three different busbars BB1, BB2, and BB3. The line lengths between each bus were 70km for line 12, and 50km for line 23. In the Fosen system, there are wind farms connected to both BB2 and BB3, but for simplicity, there was only included one wind farm in this thesis connected to BB3.

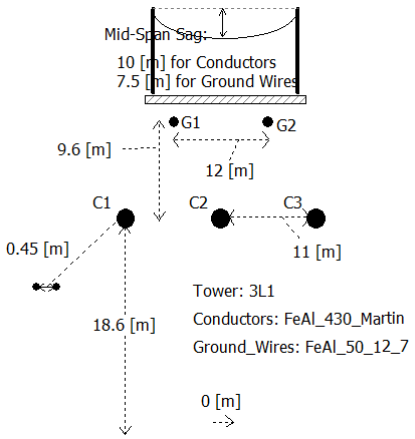

Figure 18: 3 conductor flat tower model used together with the Frequency Dependent Phase Model

Transmission Line Data			
	Line Type	Outer Radius [mm]	DC Resistance [ohm/km
Conductor Wire	FeAl_430_Martin	36.17	0.0414
Ground Wire	FeAl_50_12_7	14.5	0.3643
	Resistance [mΩ/km]	Inductance [mH/km]	Capacitance [nF/km]
Positive Sequence	22.1219	0.9589	12.3468
Zero Sequence	210.1408	2.3472	9.0825

Table 3: Transmission Line parameters

4.3 Main source and Infeed

The main grid source was developed with parameters delivered by Statnett, which can be found in table 4. Here the positive- and zero-sequence impedances are different from each other, and the source acts like a slack bus with 0°phase angle.

Main source		
Voltage [kV]	Positive Sequence Impedance [Ω]	Zero Sequence Impedance [Ω]
420∠0°	32∠86°	33∠84°

Table 4: Main Grid parameters

As mentioned earlier, it was decided to set the power from the wind farm to 440MW, as this was close to the actual production of this substation. For the ability to observe how the distance relay operate for different penetration levels of the wind power, there was introduced an infeed source at BB3. The infeed was chosen to

act as a 44MW SG, i.e., 10% of the total power, so the penetration level could change by 10% for each iteration. For a 44MW SG with an ideal transformer, the current can be calculated to the 420kV bus as $I = \frac{S}{U\sqrt{3}} = \frac{44MVA}{420kV\sqrt{3}} = 60.48A$. This was done by inspecting the current magnitude while simulating for different positive sequence impedance, to get close to 60.48A. The delivered power from the infeed source should also be as close to 44MW as possible. This was achieved by changing the phase angle of the voltage, and inspecting the power output. It was managed to get relatively close by using phase angle of 23°. The parameters used to simulate different penetration levels are shown in table 5. The power flow for all different penetration levels are shown in appendix A, tables 10-15.

Infeed			
Wind power	Infeed	Positive sequence impedance	Source voltage
100%	0%	940∠86°	420∠23°
90%	10%	470∠86°	420∠23°
80%	20%	313.33∠86°	420∠23°
70%	30%	235∠86°	420∠23°
60%	40%	188∠86°	420∠23°
50%	50%	156.67∠86°	420∠23°

Table 5: Parameters for the infeed, showing the different positive sequence impedance used for different penetration level of wind power.

4.4 Power Flow

As mentioned in the previous chapter, the wind farm was set to deliver 440MW, thus only active power. This is controlled by changing the inputs on the wind turbine model in PSCAD, by setting P1=1 and Q1=0. The current limits, Ip_lim and Iq_lim were set to 1.2pu, since this was done in previous theses. The K_p control factor was set to either -1, 0, or 1, Constant P, Balanced I, or Constant Q respectively, as described in chapter 2.3.4. This was done to observe how the relays operate during different control strategies and how it affects them.

For different penetration levels of wind power, the power flow changed gradually from the wind farm to the infeed. The power flow for all the different penetration levels can be seen in appendix A, where the power flow direction is from the wind farm towards the main grid. In these tables, there are 5 different measurements, on the 66kV bus, 132kV bus, BB3(wind farm bus), BB2 and BB1(main grid).

4.5 Distance Relay Algorithm

The distance relay algorithm was developed using the "cookbook" from PSCAD[30]. This is the same method that was used in previous theses. In figure 19 the distance relay algorithm is presented with numbering, which is described in table 6. This is a simple way of modeling a distance relay function, where the impedance is measured and the algorithm sends a trip signal if the measured impedance is within one of the given zones.

The zone settings are done as described in chapter 2.2.1, with zone 1 covering 80% of the line, and zone 2 covering 120% of the line. The α angle is chosen to be 20°, and the line impedance angle, θ, is used as the resistive reach angle. The resistive reach length for relays along line 23 was set to 15Ω and 20Ω for zone 1 and zone 2 respectively, and for relays on line 12 was set to 25Ω and 30Ω for zone 1 and zone 2 respectively. The zero sequence compensation factor K_0 was calculated using equation 2.13, but due to a misunderstanding of the impedance measurement block for ground faults, the K_0 factor from SINTEF's model was used (explained later in the discussion chapter 6.1.2).

The breakers on the line were set to "relay operation" which means that a breaker will open if a trip command from the distance relay is received. This was decided in cooperation with supervisor, to get a genuine behavior of the power system when one breaker trips, and to observe how the wind farm side relay (DR32) would operate during this situation.

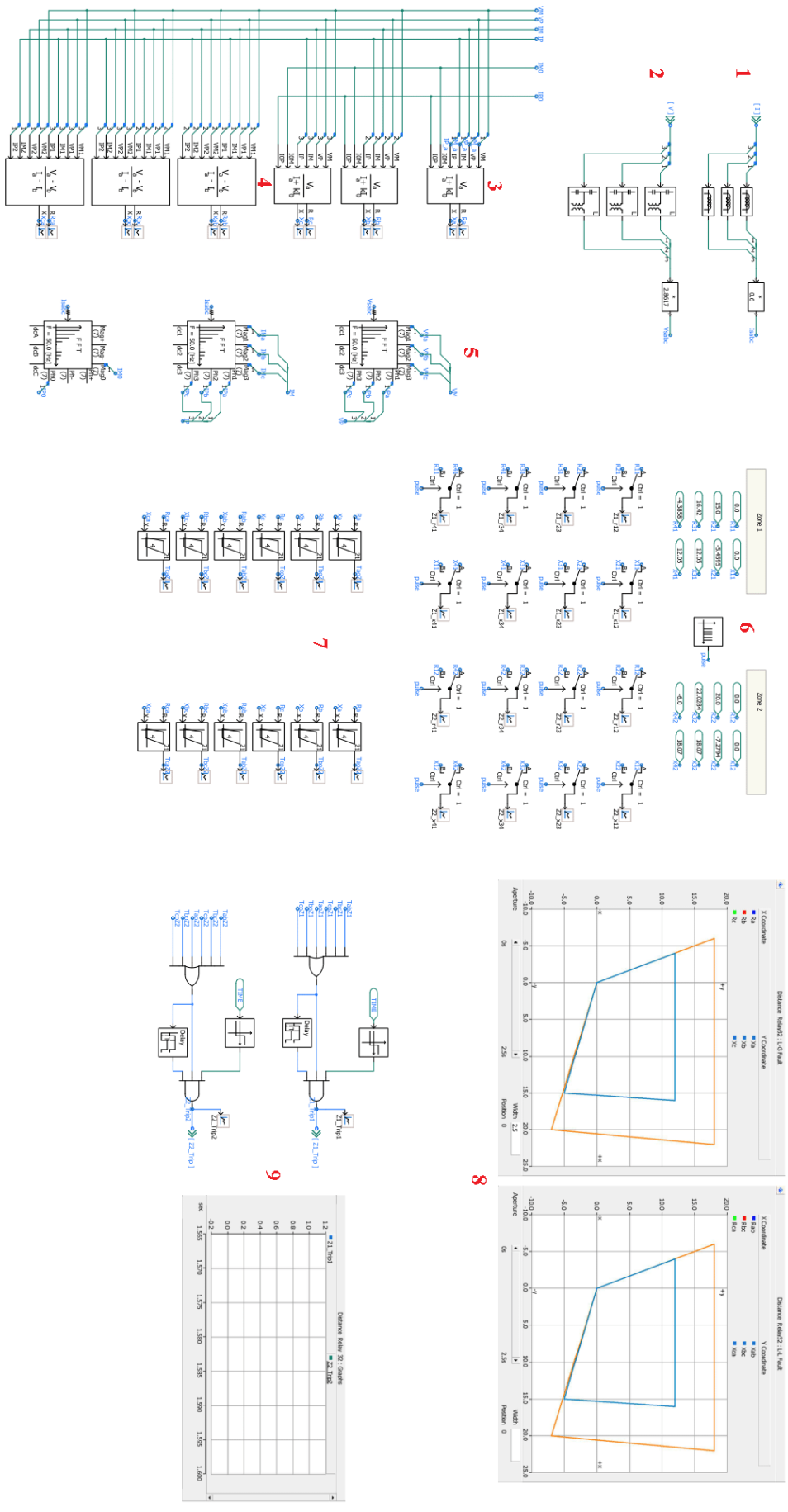

Figure 19: Distance protection relay model

Distance Protection Relay - Model Description	
Number in figure 19	Component Description
1	The current transformer imitates the influence of non-ideal measurements, with a correction factor of 0.6 to scale it back to original values. The current transformer uses PSCAD standard values, except the primary/secondary turn ratio which was changed to 1/600.
2	The voltage transformer imitates the influence of non-ideal measurements, with a correction factor of 2.8617 to scale it back to original values. The voltage transformer uses PSCAD standard values, except capacitor 1 which was changed to 1996.834 [pF].
3	The three blocks below the number is the impedance measurements for single line to ground faults. It uses PSCAD standard values, except K_0, which is changed to $1.650628\angle -17.770889°$, a number delivered from SINTEF, calculated as in equation 2.13 .
4	The three blocks below the number is the impedance measurements for line to line faults.
5	The voltage and current signals from the CT and VT are split into magnitude and phase angle, by using the FFT block (Fast Fourier Transformation). The third FFT block extracts the zero sequence current magnitude and phase angle.
6	This shows the coordinates for the resistive and reactive reach for zone 1 and 2 There are also shown how the zones are plotted, using a pulse and a control signal switch.
7	There are used quadrilateral settings for the distance relays, where the inputs Ra and Xa represent the real and imaginary parts of the measured impedance for A-G faults and Rab and Xab for A-B faults. The output signal gives a trip signal for the specific zone.
8	This shows the graphical representation of the relay zones. There are two plots, one for L-G faults and the other for L-L faults. Zone 1 has blue color while zone 2 has orange.
9	Lastly, the logic for the trip signal is presented. All the trip signals from the quadrilateral blocks pass through an OR block to give a signal if one of the zone detects the fault. There are two delays, the first ensures no trip in the initialization process, and the second represents the delay for the zones. Zone 1 has a delay of 40ms, and zone 2 has a delay of 350ms. These three signals then go through an AND block

Table 6: Distance protection relay model description

4.5.1 Simulation setup

As the goal of this thesis is to observe distance relays, and how they operate for different fault resistances, penetration levels, and control strategies, a considerable amount of simulations had to be performed. It requires a significant amount of computational power to perform many simulations simultaneously. To do this efficiently, it was decided to use a block called "multiple run", which can output up to 6 variables and records up to 6 variables. As shown in the figure 20, there are used three different outputs, which circulate between the variables given in table 7. The recorded values are stored as trip times for the given zones of different relays, and exported to Excel for further management.

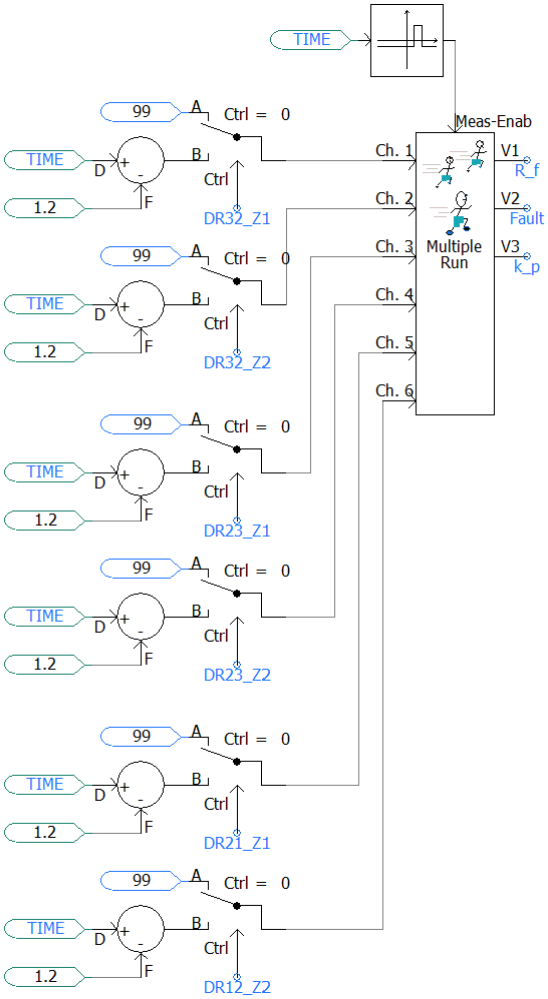

Figure 20: Multiple run block, which goes through the given values in the table 7

In figure 20, DR12 zone 1 or DR21 zone 2 are not included. The simulations for these zones were also performed but had to be done separately, as the block only had 6 inputs. As the positive sequence impedance parameter of the infeed source

and the MVA rating of the wind turbine model is changing against each other as shown in table 8, these had to be changed manually. With the use of "Simulation sets", i.e., run simulations in parallel, this was done more efficiently than if each simulation had to run independently. The simulation sets could include up to 8 sets. By making three different "projects files", one for each fault distance (10%, 50%, and 90% of the line), and by repeating this for different penetration levels (50%-100%), there were made a total of 18 project files. Now by putting all these files in to three different simulation sets, it was possible to simulate the projects simultaneously, decreasing manual workload of simulating.

Multiple Run					
Fault type	AG	ABG	AB	ABCG	ABC
Rf [Ω]	0.1	1	5	10	
Kp	-1	0	1		

Table 7: Multiple run parameters for the output variables

Simulation Setup			
Penetration Level	Wind turbine [MW]	Infeed [MVA]	Infeed Z^{+}[Ω]
100%	440	0	Disconnected
90%	396	44	940
80%	352	88	470
70%	308	132	313.33
60%	264	176	235
50%	220	220	188

Table 8: Parameters changed for different simulation sets.

5 Results

In this chapter the main results of the thesis will be presented. Additional results, showing the complete list of trip times for all different parameters are included appendix E. The simulations are performed as described in chapter 4.5.1, where all different parameters are circled through. In total there were performed 1080 simulations, where the trip times for all the relays were recorded.

The results only contain trip times for DR32 and DR23, as for DR12 and DR21 there was only observed one irregularity for all the 1080 simulations. This was for an AB fault, 90% out on the line, with a fault resistance of 10Ω, 90% penetration level, and the wind farm was controlled with Constant Q ($K_p = 1$). On this occasion, DR21 tripped in zone 1, 5ms after DR23 tripped in zone 1. Since there was only one false trip for all 1080 simulations, these relays are not included in the results, but this one occasion will be discussed later in chapter 6.2.

The following chapters are presenting results regarding the questions asked in the introduction. Firstly, results of different fault resistance will be presented, then different penetration levels of wind power with different control strategies. Each penetration level is divided into separate chapters, to more easily study the results. The reason for setting the penetration level from 50% to 100% was to observe the most extreme cases of wind power penetration.

The diagrams in this chapter are presented with colors indicating how the relay behaved during different faults. See table 9 for a description of the different colors.

Trip Color Description			
	Name	Trip Zone 1	Trip Zone 2
Green	Healthy Trip	<100ms	<500ms
Yellow	Delayed Trip	>100ms	>500ms
Red	No Trip	-	-
Purple	Trip In False Zone	-	-

Table 9: Description of colors and trip times

5.1 Fault Resistance

In the following diagrams, results of DR32 and DR23 performance during increasing fault resistance are presented. The diagrams in this chapter include results for unsymmetrical faults only, as the wind turbine model is most suitable for this purpose, and symmetrical faults can lead to inaccurate results. The diagrams include results for all control strategies, but is divided between all penetration levels of wind power to see the impact of fault resistance on each level.

DR32 is experiencing most misoperations as seen from the diagrams in figure 21. There is observed an increase in misoperations for higher fault resistance for each penetration level, especially for the highest levels. It is also observed that for increasing fault resistance the relay under-or overreaches more often.

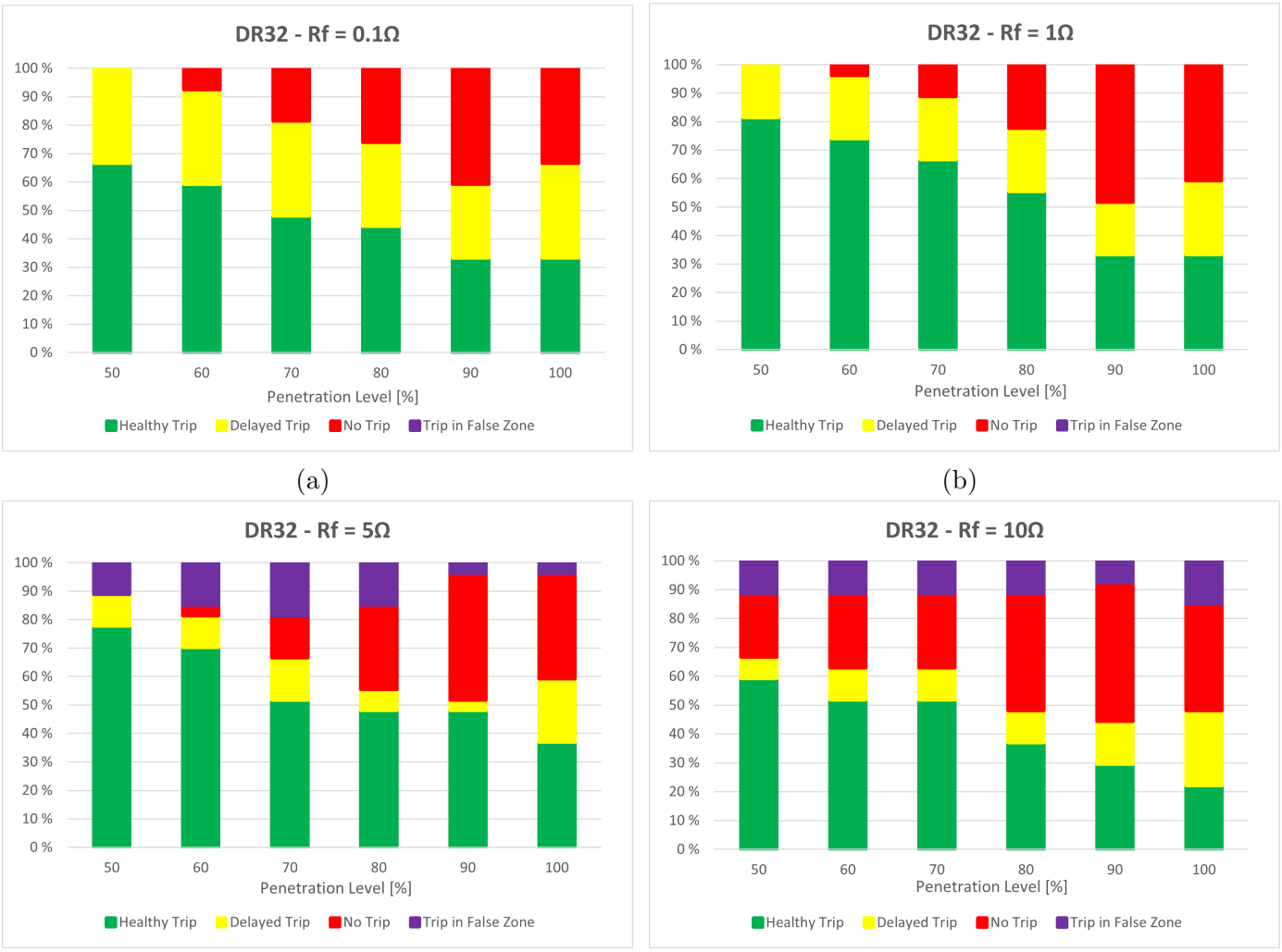

(a) (b)

(c) (d)

Figure 21: Impact of fault resistance on DR32, including simulations for unsymmetrical faults only, all control strategies, and divided between all penetration levels. a) $Rf = 0.1\Omega$, b) $Rf = 1\Omega$, c) $Rf = 5\Omega$ and d) $Rf = 10\Omega$.

DR23 does not get affected as much as DR32, as seen from the diagrams in figure 22, but there are also observed that for a fault resistance of 10Ω, there are some trips in false zone. Otherwise, there are some delayed trips in the lower fault resistances.

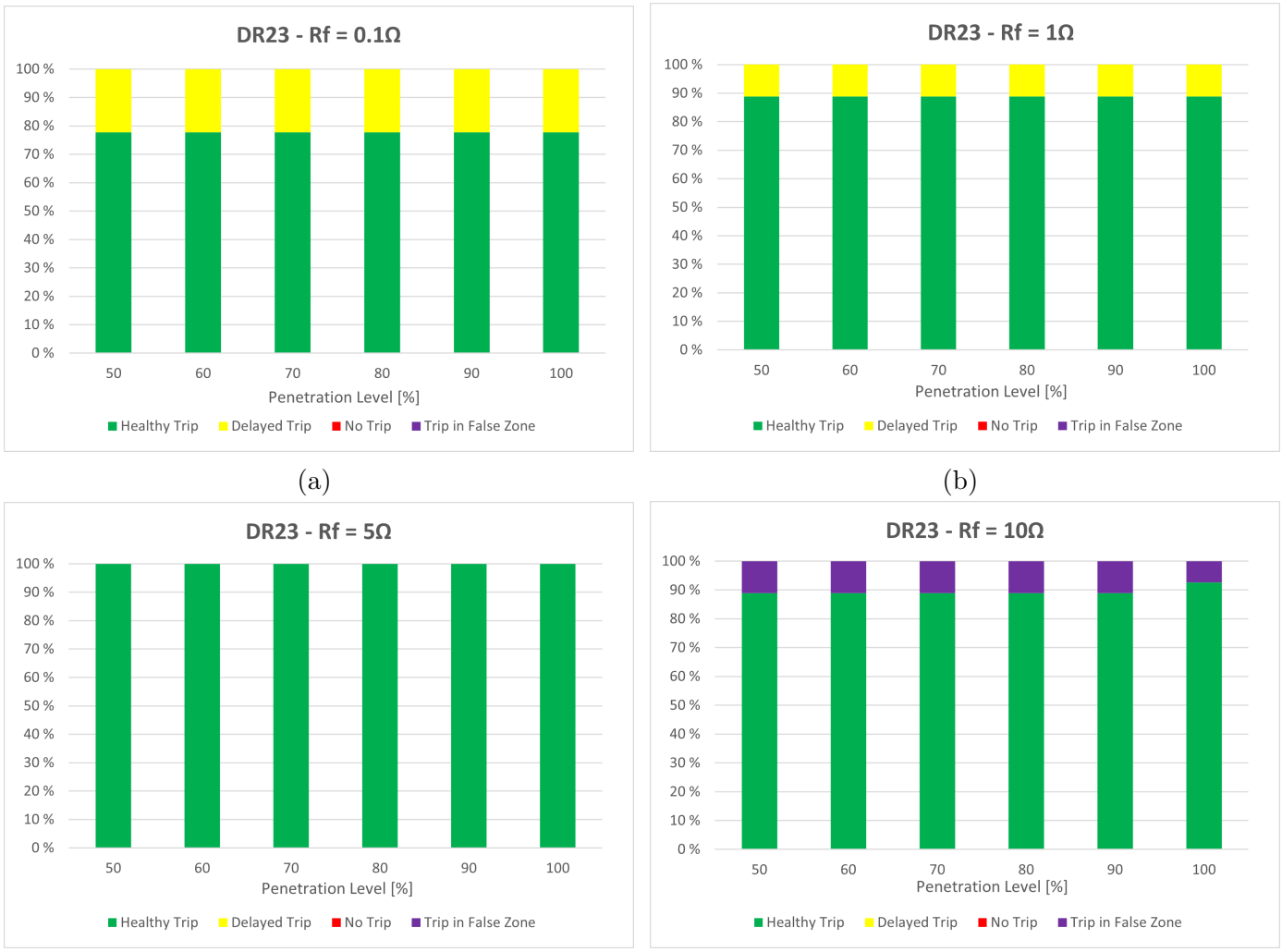

(a) (b)

(c) (d)

Figure 22: Impact of fault resistance on DR23, including simulations for unsymmetrical faults only, all control strategies, and divided between all penetration levels. a) $Rf = 0.1\Omega$, b) $Rf = 1\Omega$, c) $Rf = 5\Omega$ and d) $Rf = 10\Omega$.

For comparison, there are added diagrams for symmetrical faults in appendix D figure 35. It is clear from these diagrams that the wind farm model is not suited for symmetrical faults.

5.2 Wind Power Penetration Level and Control Strategy

The diagrams in this chapter are sorted to depict the impact of different penetration levels of wind power. They include simulations for all fault types, distances, and fault resistances, and are divided between penetration levels and control strategies.

5.2.1 Penetration level = 100%

For a penetration level of 100%, as can be seen from figure 23a, the DR32 has a significant percentage of "no trip", "delayed trip", and a low percentage of "healthy trip". It can also be observed that the Constant P control strategy, has the highest amount of faulty operations, while Constant Q has the lowest. The Balanced I control strategy is performing somewhere between the other two strategies. For DR23 at the grid-side, figure 23b, there are a minimal amount of misoperations, without "no trip", and very few "delayed trip" and "trip in false zone".

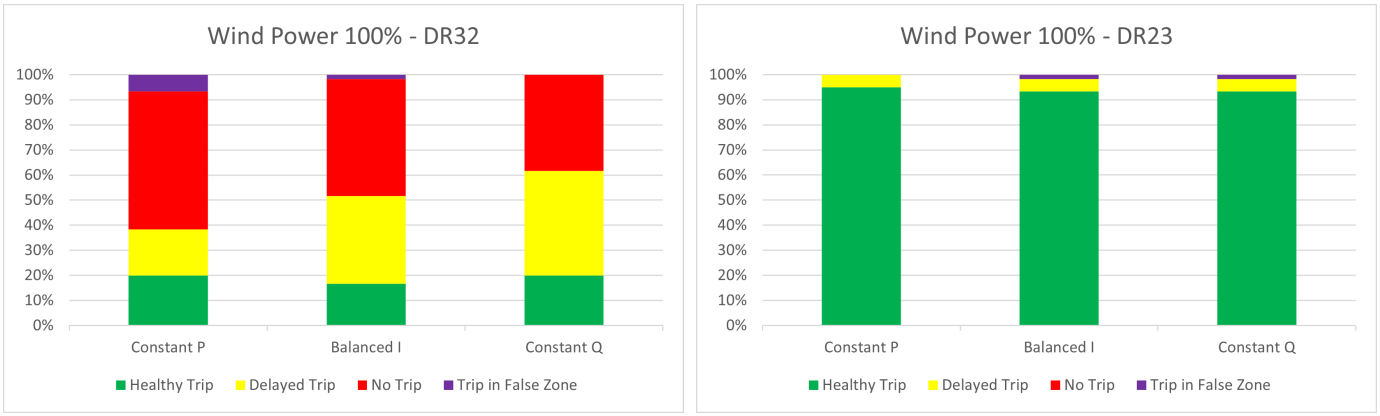

(a) (b)

Figure 23: Results for 100% penetration level, divided for the different control strategies, a) DR32 and b) DR23.

5.2.2 Penetration level = 90%

When decreasing the penetration level to 90%, the Constant Q strategy increases its amount of "no trip" by 15% for DR32 (figure 24a), while the amount of "healthy trip" barely increases. Otherwise, there is observed a slight increase in the "healthy trip" region for Balanced I. When comparing the results for DR23, at 100% penetration level to figure 24b, it is seen that Constant P is detecting one "trip in false zone". Apart from that, it remains the same.

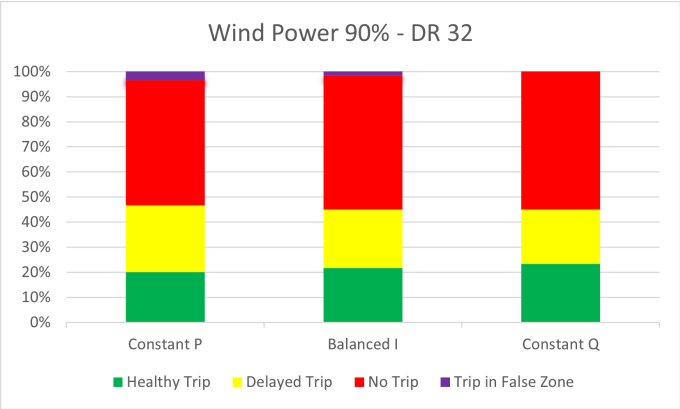

(a)

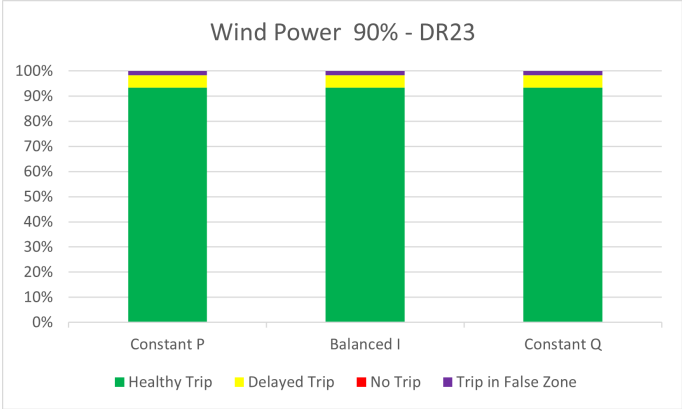

(b)

Figure 24: Results for 90% penetration level, divided for the different control strategies, a) DR32 and b) DR23.

5.2.3 Penetration level = 80%

At this penetration level, DR32 (figure 25a) doubles its "healthy trip" for Constant P strategy as from 90%, while for the two other strategies, a slight increase is observed. DR23 experience no difference from the last change (figure 25b).

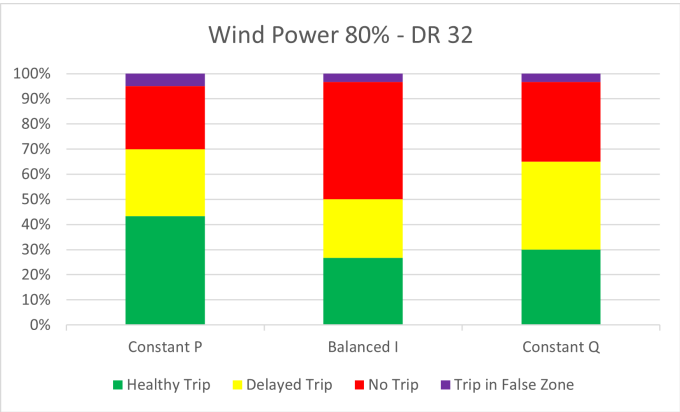

(a)

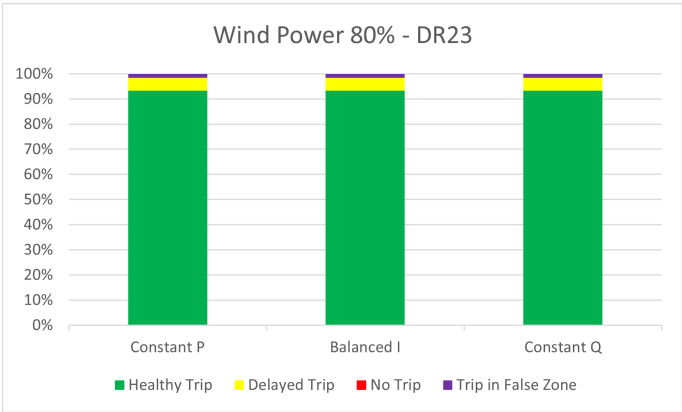

(b)

Figure 25: Results for 80% penetration level, divided for the different control strategies, a) DR32 and b) DR23.

5.2.4 Penetration level = 70%

With even more synchronous generation present, DR32 starts experiencing fewer faulty operations, as observed in figure 26a. It is thus, observed an increase in "trip in false zone" for all control strategies. Still, DR23 remains the same as earlier (figure 26b).

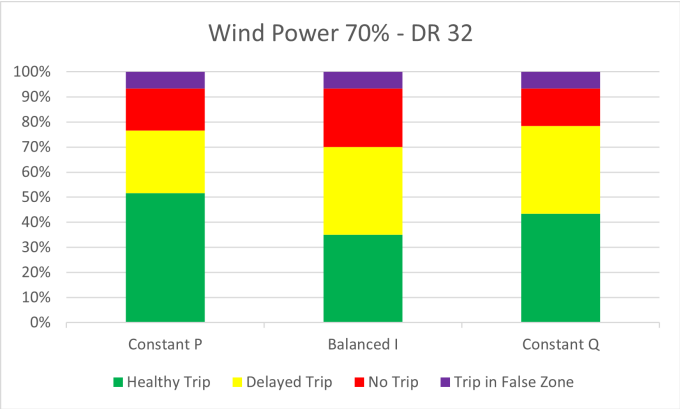

(a)

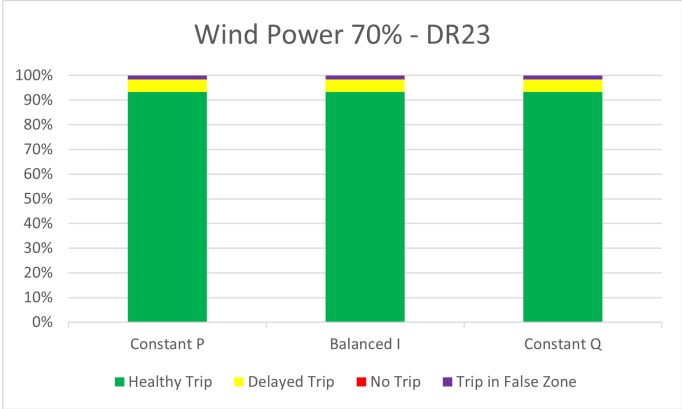

(b)

Figure 26: Results for 70% penetration level, divided for the different control strategies, a) DR32 and b) DR23.

5.2.5 Penetration level = 60%

With 60% penetration level, both Balanced I and Constant Q increased the "healthy trip" region by 20% (figure 27a). There is also observed that DR32 detects the most "trip in false zone". DR23 has no change (figure 27b).

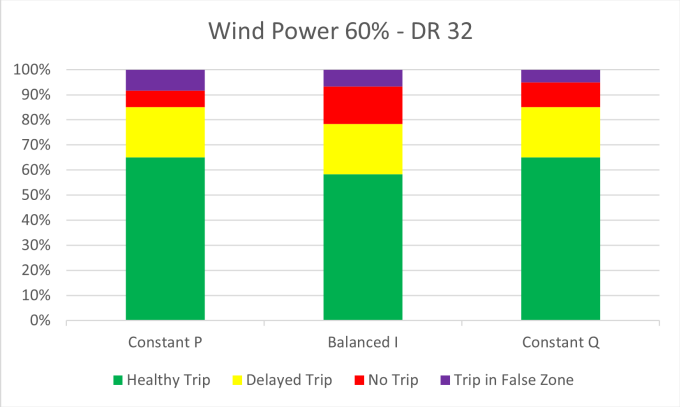

(a)

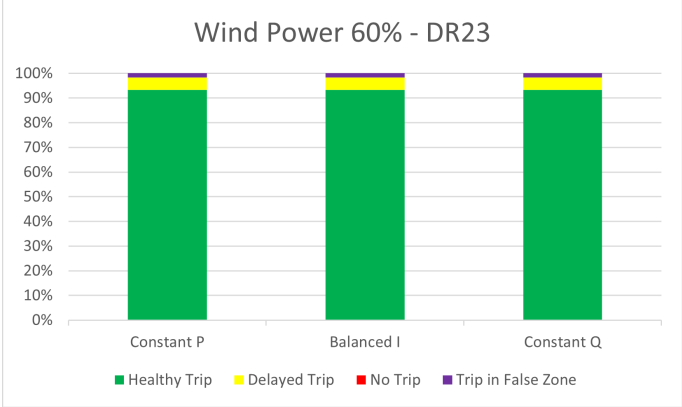

(b)

Figure 27: Results for 60% penetration level, divided for the different control strategies, a) DR32 and b) DR23.

5.2.6 Penetration level = 50%

Lastly for a penetration level of 50%, DR32 experiences most "healthy trip" as seen from figure 28a. "Trip in false zone" almost remain the same. Otherwise, it has the lowest "no trip" and "delayed trip". DR23 remains the same as for 90% penetration level (figure 28b).

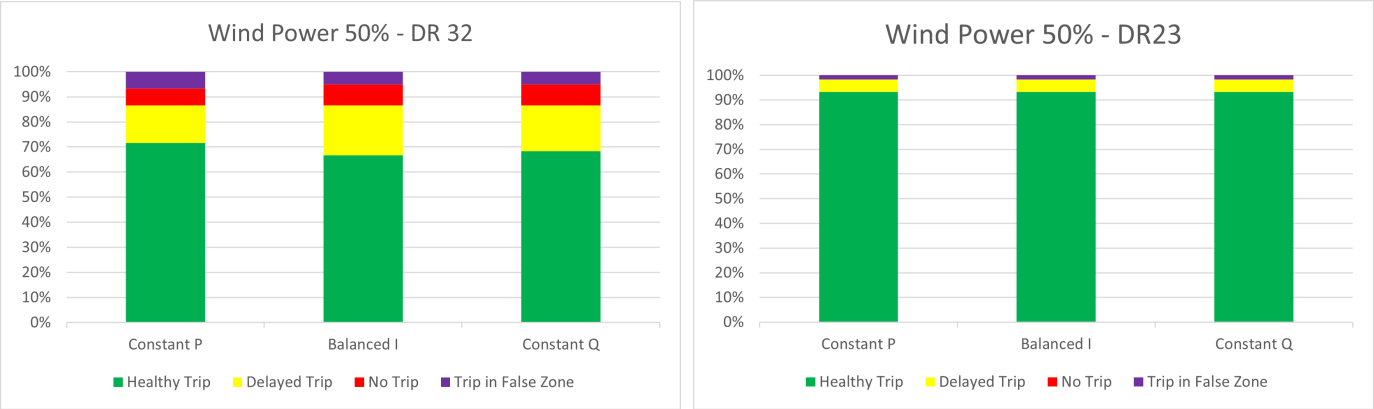

(a) (b)

Figure 28: Results for 50% penetration level, divided for the different control strategies, a) DR32 and b) DR23.

6 Discussion

This chapter discusses the model and modeling process and the results. The questions presented in the introduction chapter 1.1, will be discussed in detail with references to other comparable results.

6.1 System model and the modeling process

The system model is developed in collaboration with both SINTEF and Statnett. The parameters are comparable to the real system at Fosen, but the model does not include other sources or loads at the different busses other than the wind farm and the main grid equivalent. This makes the model less genuine than the real system, but it is adequate for this thesis. Otherwise, it makes the model more simple, which could be a good starting point for further work, making it more practical to extend the model.

6.1.1 SINTEF Wind Turbine Model

The SINTEF wind turbine model was initially made to manage unsymmetrical faults. Therefore it is not a representable model for symmetrical faults, even though it was used for all faults in this thesis. The thing that makes the model not suitable for this purpose is that it can not synchronize to the grid when the voltage drops to zero (or close to zero). This has to do with the PLL structure which is used, which does not have a method to manage the loss of synchronization (LOS) situations. The model is believed to be more precise than the previous model, considering that the established model can have different control strategies. Thus, this is a simulation that has ideal conditions, i.e., rated wind speed, which is not reasonable in reality. If the wind speed should be included as a variable, then the DC voltage at the converter DC-link may drop during low wind speeds, leading to lower power output and lower short circuit currents during faults.

Since the breakers in the model were set to "relay mode", i.e., act as real breakers (not remain connected during the fault as in the previous thesis), the fault situation changes as one breaker trips. In doing so, it was desired to see how the wind farm side relay would observe the new situation. In such events, the wind farm experienced LOS, where the voltage dropped to zero (or close to zero). The result was that the wind farm control tried to synchronize to the grid but could not, and the voltage and frequency increased until the simulation was over. This issue was not fixed

during this thesis but is something that should be investigated in future projects. This issue occurred mainly at a fault distance of 90%, for all types of faults, but also symmetrical faults on 10% and 50% fault distances. The list with all results combined in appendix E shows this, especially for the 100% penetration level.

6.1.2 Distance Relay Algorithm

The algorithm for the distance relays was modeled as described in chapter 2.2.1, with the use of "Cookbook" from PSCAD[30]. This is the simplest way of setting up distance relays, as it only contains the distance protection function (21). The distance protection function only calculates the impedance for each fault loop and sends a trip signal if the measured impedance is in one of the zones. Alternatively, the distance relay algorithm could include more advanced relay functions, e.g., directional phase/ground overcurrent protection, over-or under-voltage protection, weak-infeed protection, or faulted phase-selector. These functions would increase the algorithms protection reliability, but it requires a great deal of modeling. Therefore, it was decided to solely focus on the distance protection function.

As described in chapter 4.5 table 6, numbers 1 and 2, the current- and voltage-transformers were scaled back to original values. This was done by inspecting the magnitude and changing the correction factor. In retrospect, it could have been made even more accurate, especially the voltage transformer correction factor, as the voltage output was slightly different from the input voltage, about 2kV.

Another factor that could be more precise is the zero sequence compensation factor K_0, which was used for impedance calculations for ground faults. This factor was taken from SINTEF's model, as there was a misunderstanding due to missing input angle information, whether in degree or radians. When this problem was detected, SINTEF's correction factor was used instead of calculating a new for this thesis system model (a mistake). The value of K_0 used was $1.650628\angle - 17.770889°$, but the correct one for this thesis was $1.572337\angle - 19.120988°$. Due to the small difference in both magnitude and angle, it is reasonable to assume that the error did not contribute to large false calculations.

6.1.3 Infeed source

The infeed is almost modeled as an ideal voltage source, except for the positive sequence impedance and phase shift relative to the main grid. This simplification is made due to the complexity of modeling a representative synchronous generator.

This process would take much longer to simulate, as the ramp-up time for such a source is many times longer than for the source used, and the module is somewhat challenging to design. For this thesis, it was enough to use the source described earlier. However, the infeed could be modeled more accurately than it was. As seen from the power flow tables in appendix A, there are some deviations in how much power was set to deliver and what actually was produced. For modeling the infeed, the same method as in previous thesis[14] was used, but since the power from the wind farm was larger, the power from the infeed was also increased. As shown in table 11 in appendix A, the active power from the infeed is 41.496MW, not 44MW as intended. The deviation can also be seen for the other penetration level as well. To get a more accurate value, the positive sequence impedance and the phase shift has to be changed.

6.2 Results

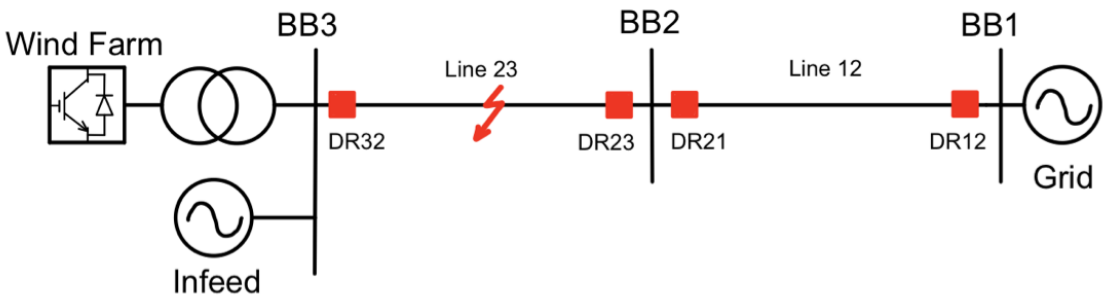

Figure 29: A simplified system model.

The simulations are performed to answer the questions given in the introduction. Investigate the impact of fault resistance, penetration level, and control strategies on distance relay performance. In this thesis, a total of 1080 simulations have been carried out, where trip times for all distance relays in the system model are recorded. In figure 29, a simplified model of the system under investigation is presented, with names of the different components discussed in this chapter. The fault is only placed on line 23, and the infeed adjusts the penetration level. The power flow out from BB3 is predetermined to 440MW for all penetration levels.

As mentioned in chapter 5, there was only recorded one incident where the relays on line 12 encountered a misoperation. For this specific occasion, DR21, which shares the same bus as DR23, experienced a trip in zone 1. This was for an AB fault with $R_f = 10\Omega$, and the distance to fault was 90% of line 23 (10% behind DR21). The wind farm was controlled with the Constant Q strategy. This clearly indicates an

overreach, which is described in chapter 2.2.2, where the relay "thinks" the fault is in its protective zone. When inspecting this instance closer, as seen from figure 33 in appendix C, it is actually the impedance measurement for a BG fault that enters the zone, not the measurement for an AB fault. It is uncertain why this happened. Besides this incident, the relays on line 12 did not encounter other faulty operations.

Of all the 1080 simulations, DR23 only experienced 71 misoperations, where 51 of these were delayed trips. The delayed trips were not that much delayed either, only between 0.10625s and 0.11s for zone 1. The other 17 misoperations were "trip in false zone", where the relay overreached. All the 17 overreaches were for ABG faults with 10Ω fault resistance and located 10% out on the line (90% from DR23).

Considering the results presented in chapter 5.1, DR32 encounters a significant part of misoperations for all penetration levels as the fault resistance increases. Especially the results for 5Ω and 10Ω, seen from figure 31c and 31d, there is a noteworthy part of "trip in false zone". These trips are for when the relay underreaches and trips in zone 2 instead of zone 1, and overreaches and trips in zone 1 when it should trip in zone 2. It is also seen from appendix E, where all the trip times are shown, that for lower penetration levels at a fault distance of 90%, these misoperations occur more often. This is because of the different current contributions from the two sides when the infeed is introduced at BB3. The difference in current contribution, as described in chapter 2.2.2, shifts the fault resistance angle, triggering misoperations such as under-or overreach. For DR23, there is minimal change due to changing fault resistance, but there is observed an increase in trips in false zone for 10Ω.

When comparing the results from this thesis to other similar studies, there are similarities as the relays are experiencing more incorrect performances due to increased fault resistance[31][32]. This is not only because of the magnitude of the fault resistance, but also the different current contributions from the wind farm end (including the infeed) and the main grid. This results in unwanted operations.

For the performance of DR32 in chapter 5.2, there is a substantial difference in the three control strategies. For 100% penetration level, constant P control has the most negative impact on distance relay performance, while constant Q has the least impact. This does not relate to the paper [33], where constant Q has the highest impact on the performance. In the paper [33], there are only simulations for AG and AB faults, but the results from chapter 5.2 include simulations for all fault types, so the results are not entirely comparable. Regardless, as the penetration level decreases, especially for 80% and 70%, constant P has a significant improvement, while the two other strategies have less improvement. It is also observed that for

lower penetration levels, an increase to "trip in false zone". This is described in [31] as an issue due to infeed variations, which will influence the fault impedance angle, as described in chapter 2.2.2 (equation 2.21), resulting in under-or overreach for the relays.

The deciding factor when choosing such a control strategy is the grid codes given by the TSO (Transmission System Operator). It is, however, not the TSO that is determining what strategy is used, but the wind farm operator (WFO). The WFO must meet the grid code requirements and set the desired control strategy to suit this purpose. Nevertheless, it is greatly influenced by the TSO, which sets the rules (Grid codes), where the most important one is presumably FRT (Fault-Ride Through).

As mentioned earlier in the chapter 6.1.1, since the breakers operate in relay mode, the situation becomes unstable after one breaker trip. From the list of all trip times (appendix E), it is seen that for a fault distance of 90% and penetration level of 100% wind power, DR32 does not have any healthy trips, and for a penetration level of 90%, there is only one healthy trip. This is the result of the wind turbine model not having the structure to handle LOS (loss of synchronization). This should be fixed or be made more optimal in the future for a more reliable wind farm configuration.

The unsymmetrical fault AB does also experience problems due to this issue, as can be seen from the lists in appendix E. By further inspection of AB faults, it shows that DR32 starts to calculate the impedance inside the correct zone, but after the breaker at DR23 trips, DR32 can no longer detect the fault in any zone. This instance can be seen in appendix D figure 34a and 34b. Consequently, there are some inaccuracies in the results regarding fault resistance where AB faults are included.

Since the system model only includes the distance protection function for the relays, this thesis has some limitations. For more advanced testing, as done in [33], where an RTDS (real-time digital simulator) has been used, together with an actual physical relay, the results are more authentic. However, this model is believed to be substantial enough for this thesis and is a good starting point for further work.

7 Conclusion

In this thesis, simulations are performed to better understand how distance relays operate during different fault situations. The system model developed in PSCAD is relatively comparable to the system at Fosen, where Statnett has expected problems related to distance relays. Therefore, the result in this thesis could be of some use. The main objectives of the thesis have been to answer the following questions:

- How does fault resistance impact distance relays fault detection capability?
- How does the increased penetration level of wind power influence protection performance?
- What wind farm control strategies are the most reliable, and which has the most negative impact on protection performance?

To answer these questions, a system model was developed, with one wind farm, one infeed (to control the penetration level), transmission lines, and a main grid equivalent. The focus has been to record trip times for all relays connected to the transmission lines and observe how they perform during different fault situations. A total of 1080 simulations were conducted, where the changing parameters have been fault type, fault distance, fault resistance, wind power penetration level, and control strategies. Due to the issues regarding the wind turbine model not being suitable enough for managing the loss of synchronization situations, as experienced with "real" breaker operations and for symmetrical faults, some results were inaccurate. Especially the results with a fault distance of 90% and for symmetrical faults.

For the results regarding the fault resistance, there were presented diagrams including only unsymmetrical faults due to the wind turbine issue. A significant increase in misoperations of the relay closest to the wind farm was observed for higher fault resistances. There were just a few misoperations for the relay on the opposite side, some delayed trips, and trips in false zone. On the second line, there was only one incident where the relay seeing towards the main grid overreached, detecting a fault in forward-direction when it was in backward-direction. The main reason for these misoperations is the wind farm side's unpredictable current contribution compared with the current from the main grid. Both the wind farm current and infeed current is participating in influencing the angle, which leads to under-or overreach. This impacts the distance relays ability to detect faults in the correct zone, which concludes the answer to the question on fault resistance influence.

Considering the penetration level, it was also a substantial increase in misoperations for each increment. The issue regarding the wind park did influence the results for fault distance of 90%, but otherwise, it mainly operated as intended. To answer the question mentioned earlier about penetration level, the performance of traditional distance relays set to protect SG-dominated systems will expect many complications for extreme cases of wind power penetration level. Therefore, it is essential to use more capable relay functions suited for the increased share of renewable energy sources, which is expected.

Regarding the control strategies, all three presented performed differently for each penetration level. As shown in the results, there was no specific control strategy that was the most reliable in general. However, when assembling all penetration levels, as seen from the diagrams in figure 30, Constant P has the highest number of "healthy trip" but also the highest level of "trip in false zone", which is undesired. Balanced I have the least amount of "healthy trips" and the highest "no trip" making it the strategy with the most negative impact on protection performance. The overall most reliable strategy is Constant Q, which correlates to the findings in [33], and concludes the answer to the question about control strategies. These results are by no means acceptable for a relay, but they show the massive impact of renewable energy sources on the traditional distance protection function.

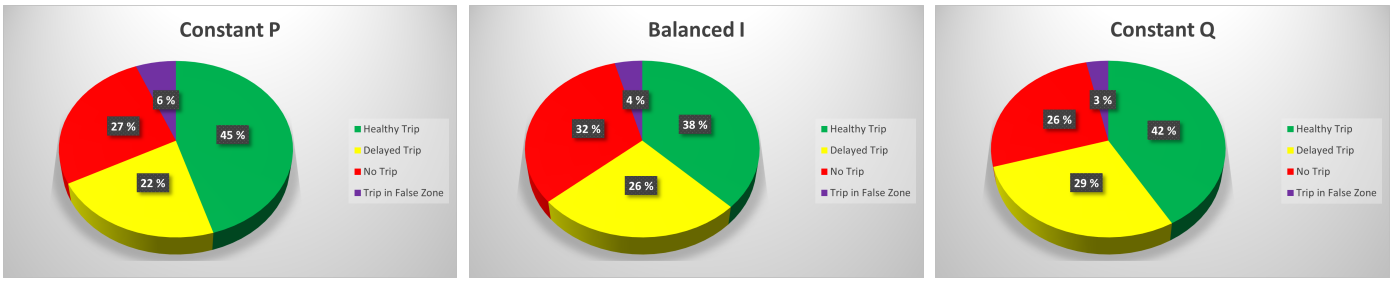

(a) (b) (c)

Figure 30: Concluded results of the three different control strategies, a) Constant P, b) Balanced I, and c) Constant Q.

8 Further Work

For further work, an improved wind turbine model should be included, where an upgrade of the PLL structure is added. This will make the model handle the situation when the grid-side breaker trips and even symmetrical faults. This was experienced to have a meaningful impact on the results in this thesis, so the results will be more representable by overcoming this issue. The simplest way of solving the problem is to "freeze" the PLL, as described in [34][35][36]. This method uses the pre-fault frequency and voltage angle to synchronize to the grid when detecting a LOS (loss of synchronization). This method has some drawbacks, but as a starting point for further work, it might be sufficient. There are also other methods to overcome this issue presented in [36].

Another element that also should be included is additional relay functions, as this thesis had only the distance protection function (21). It was experienced in this thesis that a backward fault tripped in the forward direction, which could be avoided if there was a directional overcurrent function. It is also expected problems with this function when connected to renewable energy sources[37][38]. Still, it could be acceptable if correctly set up by including the solutions made in German grid codes [39][37].

Another solution could be to use more modern strategies to overcome this issue, by using "pilot protection". Pilot protection uses a source of communication between the relays protecting a line to more efficiently disconnect the line. There are however tested this on mainly synchronous generator dominated systems, so for systems dominated by renewable energy sources, a new method "non-pilot protection" is under investigation[40]. This could be more suitable for protecting such transmission line tested in this thesis.

The most advantageous way would be to test on an RTDS (real-time digital simulator) with a physical relay, as done in [33]. By doing this, other relay functions would also be included and could be investigated. There should also be included simulations for several fault resistances and fault distances, as there were only four different fault resistances and three fault locations included in this thesis. This would give a more comprehensive understanding of the impact of both fault resistance and fault distance.

Bibliography

[1] J.C Das. *Power System Analysis: Short-Circuit Load Flow and Harmonics*. Marcel Dekker, Inc, 2002.

[2] José Serna and Jesús López-Lezama. Calculation of distance protection settings in mutually coupled transmission lines: A comparative analysis. *Energies*, 12:1290, 04 2019.

[3] Bogdan Kasztenny. Distance elements for line protection applications near unconventional sources. 06 2021.

[4] MathWorks. Alpha-beta-zero to dq0, dq0 to alpha-beta-zero. https://www.mathworks.com/help/physmod/sps/powersys/ref/alphabetazerotodq0dq0toalphabetazero.html.

[5] Joan Rocabert, Alvaro Luna, Frede Blaabjerg, and Pedro Rodríguez. Control of power converters in ac microgrids. *IEEE Transactions on Power Electronics*, 27(11):4734–4749, 2012.

[6] Jon Are Suul, Alvaro Luna, Pedro Rodriguez, and Tore Undeland. Voltage-sensor-less synchronization to unbalanced grids by frequency-adaptive virtual flux estimation. *IEEE Transactions on Industrial Electronics*, 59(7):2910–2923, 2012.

[7] Statnett. Nvf 2020, nasjonal veileder for funksjonskrav i kraftsystemet, 2020.

[8] Pan european sub group on protection equipment. Short circuit contribution of new generating units connected with power electronics and protection behaviour. April 2019. ENTSO-E.

[9] Yulei Feng, Zhe Zhang, Qinghua Lai, Xianggen Yin, and Huiyuan Liu. Impact of inverter interfaced generators on distance protection. In *2019 4th International Conference on Intelligent Green Building and Smart Grid (IGBSG)*, pages 512–515, 2019.

[10] Wind Europe. Getting fit for 55 and set for 2050, electrifying europe with wind energy. June 2021.

[11] Aboutaleb Haddadi, Evangelos Farantatos, Ilhan Kocar, and Ulas Karaagac. Impact of inverter based resources on system protection. *Energies*, 14(4), 2021.

[12] Yu Fang, Ke Jia, Zhe Yang, Yanbin Li, and Tianshu Bi. Impact of inverter-interfaced renewable energy generators on distance protection and an improved scheme. *IEEE Transactions on Industrial Electronics*, 66(9):7078–7088, 2019.

[13] Moumita Sarkar, Jundi Jia, and Guangya Yang. Distance relay performance in future converter dominated power systems. pages 1–6, 06 2017.

[14] Nicolay Anker Kavli. PSCAD Simulation of Distance Protection Performance in a Grid with Inverter Interfaced Generation. Master's thesis, NTNU, Norway, 2020.

[15] Andreas Breivik. Analysis of fault current contributions from inverter interfaced wind parks. Master's thesis, NTNU, Norway, 2021.

[16] Lars Thaulow Bremnes. Pscad simulations of inverter interfaced generation. Project report in TET5500, Department of Electric Power Engineering, NTNU – Norwegian University of Science and Technology, Dec. 2021.

[17] G Chicco and A Mazza. 100 years of symmetrical components. 01 2019.

[18] R.E. Betz and T. Summers. Introduction to symmetrical components and their use in statcom applications. 03 2005.

[19] Pedro Rodríguez Remus Teodorescu, Marco Liserre. *Grid Converters for Photovoltaic and Wind Power Systems*. John Wiley & Sons, Ltd, 2011.

[20] ALSTOM. *Network protection & automation guide*. Levallois-Perret, 2002.

[21] Aristotelis Tsimtsios and Vassilis Nikolaidis. Setting zero-sequence compensation factor in distance relays protecting distribution systems. *IEEE Transactions on Power Delivery*, 33:1236–1246, 06 2018.

[22] Amin Banaiemoqadam, Ali Hooshyar, and Maher A. Azzouz. A control-based solution for distance protection of lines connected to converter-interfaced sources during asymmetrical faults. *IEEE Transactions on Power Delivery*, 35(3):1455–1466, 2020.

[23] ENTSOE. Voltage source converters. https://www.entsoe.eu/Technopedia/techsheets/voltage-source-converters.

[24] Mika Ikonen, Ossi Laakkonen, and Marko Kettunen. Two-level and three-level converter comparison in wind power application. 01 2005.

[25] Pedro Rodriguez, Josep Pou, Joan Bergas, J. Ignacio Candela, Rolando P. Burgos, and Dushan Boroyevich. Decoupled double synchronous reference frame pll for power converters control. *IEEE Transactions on Power Electronics*, 22(2):584–592, 2007.

[26] Shinji Shinnaka. A robust single-phase pll system with stable and fast tracking. *IEEE Transactions on Industry Applications*, 44(2):624–633, 2008.

[27] Jon Are Suul. *Control of Grid Integrated Voltage Source Converters under Unbalanced Conditions : Development of an On-line Frequency-adaptive Virtual Flux-based Approach*. PhD thesis, NTNU, 2012.

[28] European-Union. Commission regulation (eu) 2016/631, April 2016.

[29] Jon Suul, A. Luna, Pedro Rodriguez, and Tore Undeland. Virtual-flux-based voltage-sensor-less power control for unbalanced grid conditions. *IEEE Transactions on Power Electronics - IEEE TRANS POWER ELECT*, 27:4071–4087, 09 2012.

[30] PSCAD. *PSCAD Cookbook Protection Studies*. 2018. Written for PSCAD v4.5.

[31] Subhadeep Paladhi, Qiteng Hong, and Campbell D. Booth. Adaptive distance protection for multi-terminal lines connecting converter-interfaced renewable energy sources. pages 1–5, March 2022. IET 16th International Conference on Developments in Power System Protection, IET 16th DPSP ; Conference date: 07-03-2022 Through 10-03-2022.

[32] Seghir Samira, Tahar Bouthiba, Dadda Samia, and Abdelhakim Bouricha. Fault resistance effect on distance protection in high voltage transmission lines. 12 2017.

[33] Di Liu, Qiteng Hong, Adam Dysko, Dimitrios Tzelepis, Guangya Yang, Campbell Booth, Ian Cowan, and Bharath Ponnalagan. Evaluation of hvdc system's impact and quantification of synchronous compensation for distance protection. *IET Renewable Power Generation*, March 2022.

[34] Bernd Weise. Impact of k-factor and active current reduction during fault-ride-through of generating units connected via voltage-sourced converters on power system stability. *IET Renewable Power Generation*, 9(1):25–36, 2015.

[35] Heng Wu and Xiongfei Wang. Design-oriented transient stability analysis of pll-synchronized voltage-source converters. *IEEE Transactions on Power Electronics*, 35(4):3573–3589, 2020.

[36] Xiuqiang He and Hua Geng. Synchronization stability analysis and enhancement of grid-tied multi-converter systems. In *2020 IEEE Industry Applications Society Annual Meeting*. IEEE, oct 2020.

[37] Aboutaleb Haddadi, Mingxuan Zhao, Ilhan Kocar, Ulas Karaagac, Ka Wing Chan, and Evangelos Farantatos. Impact of inverter-based resources on negative sequence quantities-based protection elements. *IEEE Transactions on Power Delivery*, 36(1):289–298, 2021.

[38] Aboutaleb Haddadi, Ilhan Kocar, Jean Mahseredjian, Ulas Karaagac, and Evangelos Farantatos. Negative sequence quantities-based protection under inverter-based resources challenges and impact of the german grid code. *Electric Power Systems Research*, 188:106573, 2020.

[39] István Erlich, Tobias Neumann, Fekadu Shewarega, Peter Schegner, and Jörg Meyer. Wind turbine negative sequence current control and its effect on power system protection. In *2013 IEEE Power Energy Society General Meeting*, pages 1–5, 2013.

[40] Houman Lahiji, Firouz Badrkhani Ajaei, and Ryan E. Boudreau. Non-pilot protection of the inverter- dominated microgrid. *IEEE Access*, 7:142190–142202, 2019.

Appendix

A Power flow with different penetration level of infeed

Power Flow - 100% Wind Power, 0% Infeed						
Measuring point	BB66	BB132	BB3	BB2	BB1	Infeed
P [MW]	439.13	437.133	435.893	433.376	431.214	0
Q [MVAr]	-0.315	-72.981	-131.404	-117.556	-96.188	0
S [MVA]	439.130	443.183	455.269	449.037	441.812	0

Table 10: Power flow for system with 100% wind power connected

Power Flow - 90% Wind Power, 10% Infeed						
Measuring point	BB66	BB132	BB3	BB2	BB1	Infeed
P [MW]	395.207	393.643	434.133	431.672	429.594	41.496
Q [MVAr]	-0.295	-59.111	-109.801	-94.475	-71.492	-3.632
S [MVA]	395.207	398.056	447.803	441.889	435.502	41.655

Table 11: Power flow for 90% wind power and 10% infeed.

Power Flow - 80% Wind Power, 20% Infeed						
Measuring point	BB66	BB132	BB3	BB2	BB1	Infeed
P [MW]	351.286	350.079	433.304	431.048	428.845	84.044
Q [MVAr]	-0.269	-47.659	-95.199	-78.978	-55.047	-9.857
S [MVA]	351.286	353.308	443.639	438.224	432.364	84.620

Table 12: Power flow for 80% wind power and 20% infeed.

Power Flow - 70% Wind Power, 30% Infeed						
Measuring point	BB66	BB132	BB3	BB2	BB1	Infeed
P [MW]	307.267	306.457	432.888	430.653	428.475	128.278
Q [MVAr]	-0.240	-38.075	-85.321	-68.537	-44.025	-17.398
S [MVA]	307.267	308.813	441.216	436.073	430.731	129.452

Table 13: Power flow for 70% wind power and 30% infeed.

Power Flow - 60% Wind Power, 40% Infeed						
Measuring point	BB66	BB132	BB3	BB2	BB1	Infeed
P [MW]	263.449	262.788	432.605	430.382	428.219	170.347
Q [MVAr]	-0.208	-30.061	-78.845	-61.706	-36.83	-25.481
S [MVA]	263.449	264.502	439.731	434.783	429.800	172.242

Table 14: Power flow for 60% wind power and 40% infeed.

Power Flow - 50% Wind Power, 50% Infeed						
Measuring point	BB66	BB132	BB3	BB2	BB1	Infeed
P [MW]	219.532	219.075	432.304	430.089	427.936	213.651
Q [MVAr]	-0.175	-23.441	-74.938	-57.579	-32.477	-33.591
S [MVA]	219.532	220.326	438.751	433.926	429.167	216.276

Table 15: Power flow for 50% wind power and 50% infeed.

B Results on Fault Resistance

These figures show the impact of fault resistance on DR23 for all penetration levels of wind power. See table 9 for coloring description of trip times.

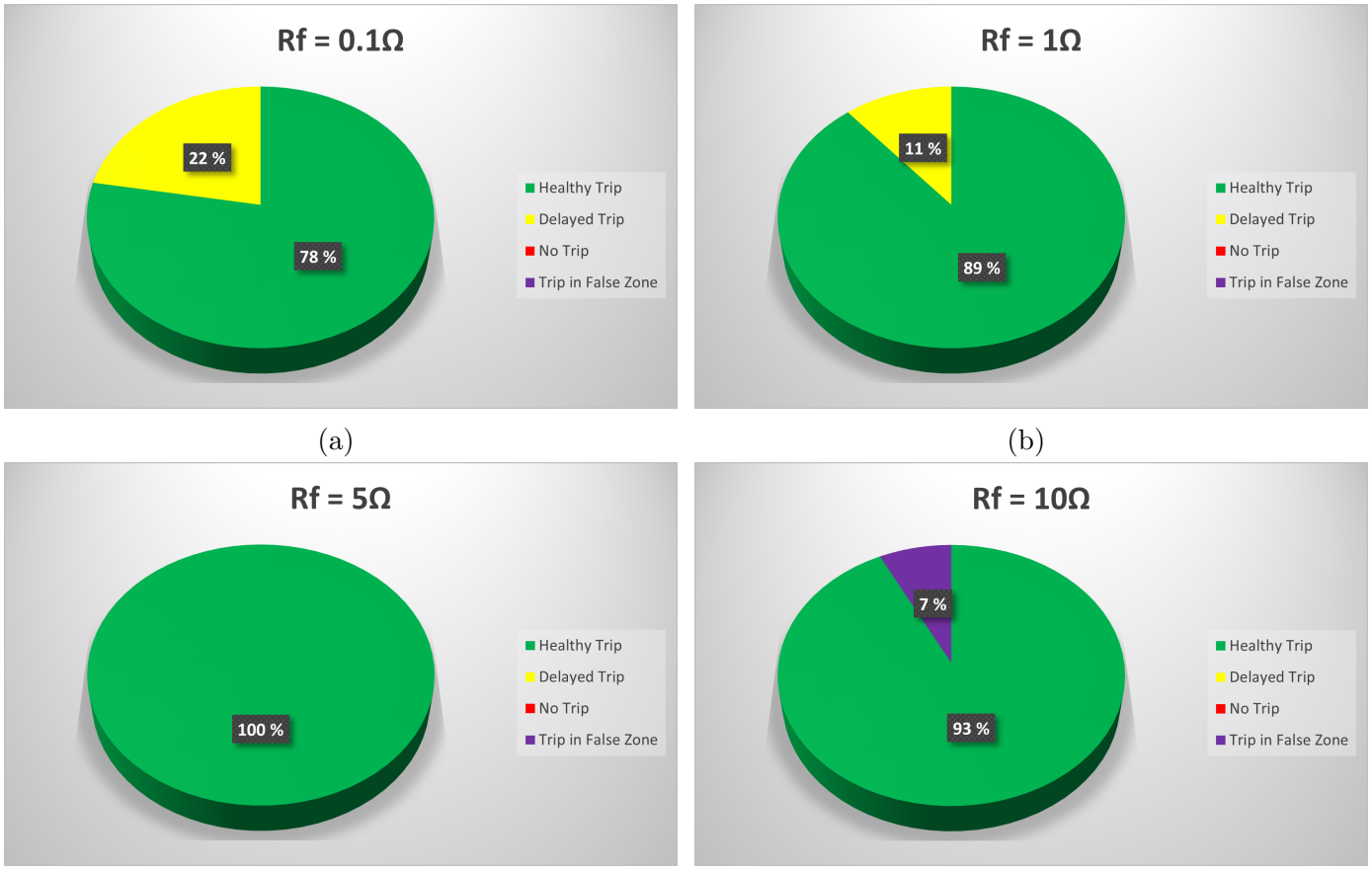

(a) (b)

(c) (d)

Figure 31: Impact of fault resistance on DR23 for all fault types, penetration levels, fault distances and control strategies. a) $Rf = 0.1\Omega$, b) $Rf = 1\Omega$, c) $Rf = 5\Omega$ and d) $Rf = 10\Omega$

In figure 32, the results for all penetration levels are combined. They show a increase to "trip in false zone" and "no trip" as the fault resistance increases.

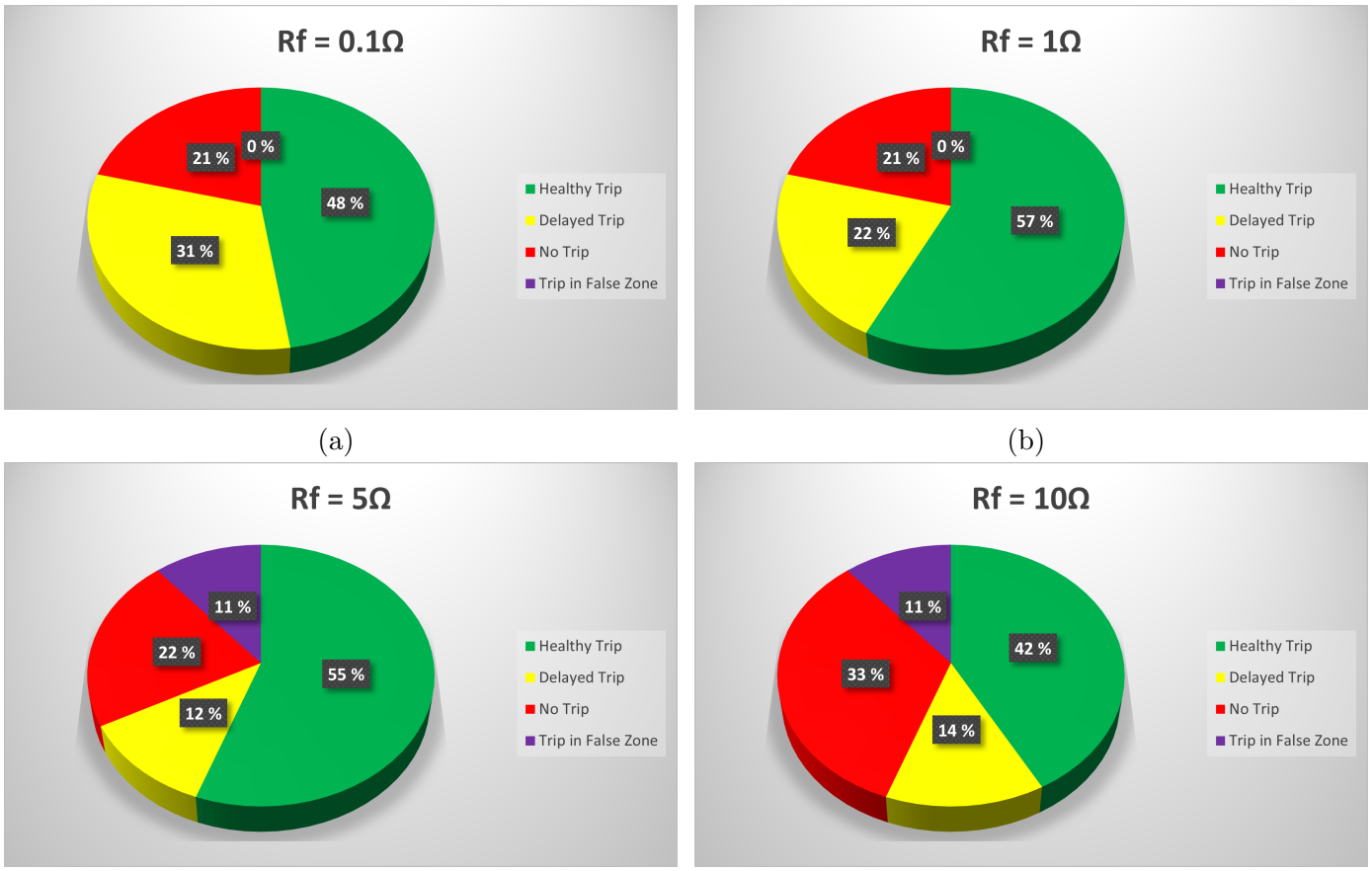

(a) (b)

(c) (d)

Figure 32: Impact of different fault resistance, where all penetration levels are included. a) $Rf = 0.1\Omega$, b) $Rf = 1\Omega$, c) $Rf = 5\Omega$ and d) $Rf = 10\Omega$

C DR21 Overreach

In figure 33, the RX-diagram with impedance calculation for DR21 is depicted, showing measurements for a BG fault entering zone 1, which resulted in a trip.

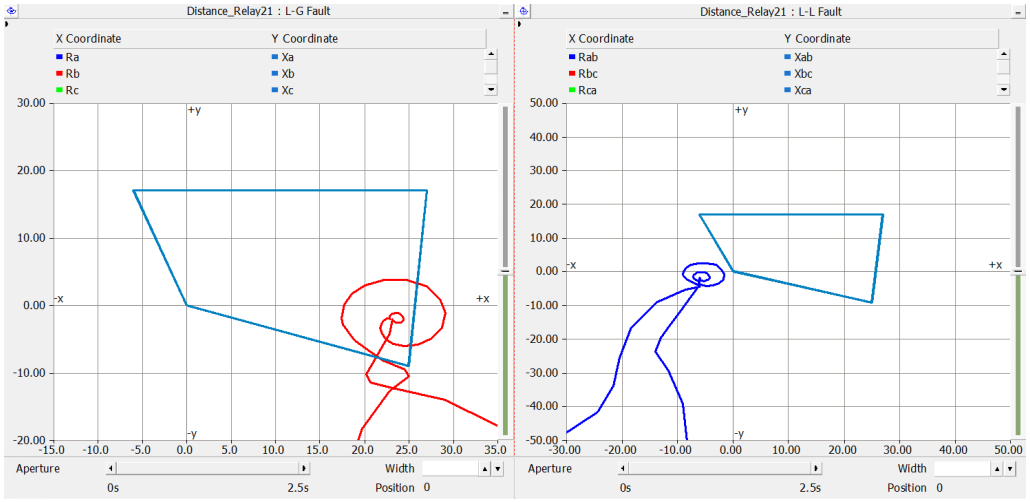

Figure 33: DR21 trip incident, where the trip was initiated by the BG fault impedance measurement.

D Result of wind farm synchronization issue

The same RX-diagrams showing how DR32 calculates the impedance before and after DR23 breaker trips, in figure 34a and 34b respectively.

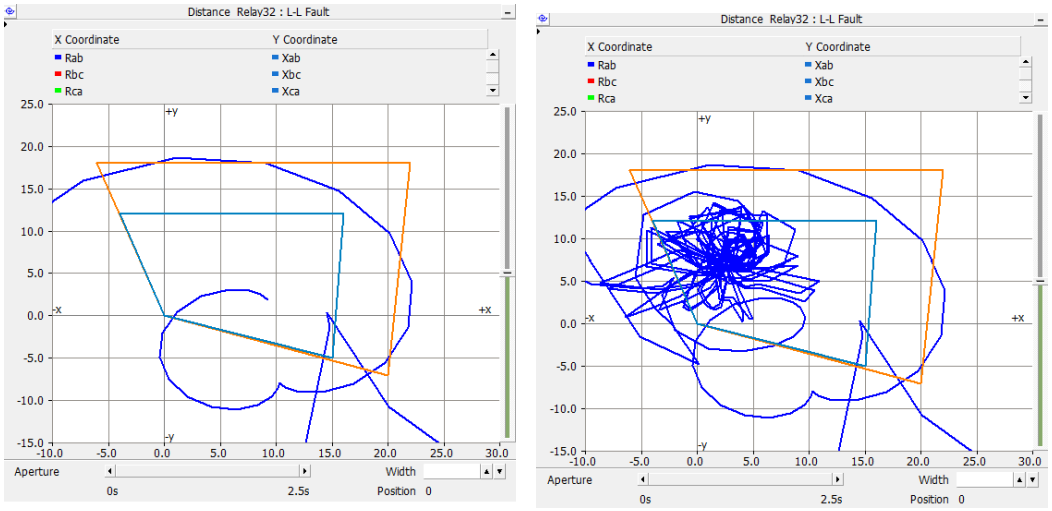

(a) (b)

Figure 34: DR32 RX-Diagram showing two different time incidents, a) before DR23 trip and b) after DR23 trip.

Since the wind turbine model is mainly intended for unsymmetrical faults only, a comparison on distance relay performance is added with results for unsymmetrical faults only and all fault types. From figure 35, they are shown side by side with unsymmetrical fault only are shown in the left column and for all faults in the right column.

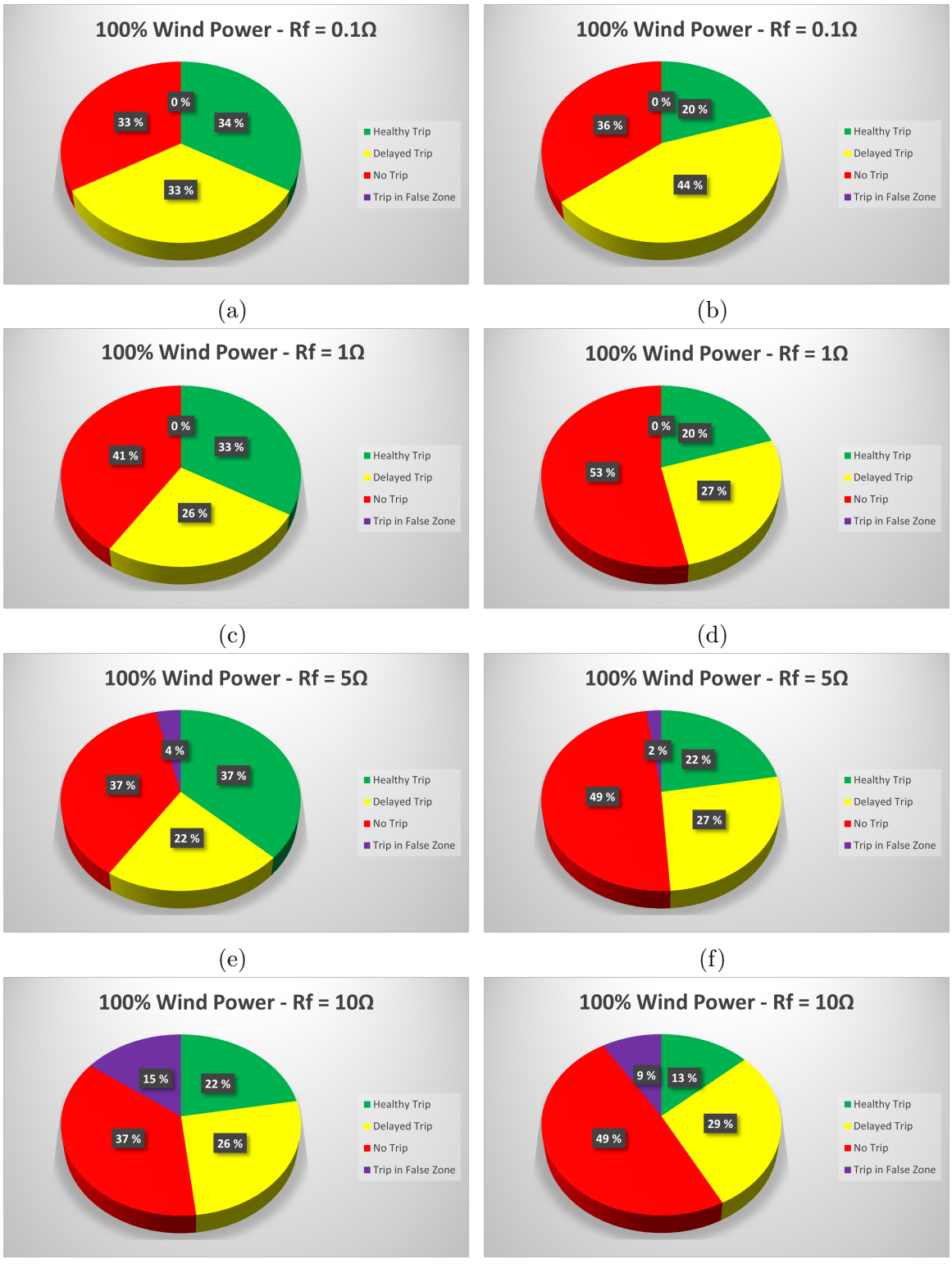

Figure 35: Impact of fault resistance on DR32 with 100% wind power penetration, where simulations for all control strategies are included. For a), c), e) and g) (left side) only unsymmetrical faults are included, while for b), d), f) and h) (right side) all faults are included.

E Complete List of Results - Trip times

The following pages includes the trip times for DR32 and DR23. See table 9 for coloring description of trip times. "WF 100%, Infeed 0% - Distance 10%" is the title for the first page meaning the wind farm is producing full power and the fault is located 10% out on the line from Bus 3. As mentioned earlier in the thesis, $K_p = -1$ refers to constant active power control, $K_p = 1$ refers to constant reactive power control, and $K_p = 0$ refers to balanced currents control.

WF 100%, Infeed 0% - Distance 10%						
Fault	Rf [Ω]	k_p	DR32_Z1	DR32_Z2	DR23_Z1	DR23_Z2
AG	0.1	-1	0.11	No Trip	No Trip	0.38625
	1	-1	0.10625	No Trip	No Trip	0.36875
	5	-1	7.50E-02	No Trip	No Trip	0.36875
	10	-1	9.75E-02	No Trip	No Trip	0.39125
ABG	0.1	-1	7.50E-02	No Trip	No Trip	0.3675
	1	-1	7.38E-02	No Trip	No Trip	0.3675
	5	-1	6.38E-02	No Trip	No Trip	0.36875
	10	-1	No Trip	0.37375	No Trip	0.370005
AB	0.1	-1	0.16	No Trip	No Trip	0.3675
	1	-1	No Trip	No Trip	No Trip	0.3675
	5	-1	No Trip	No Trip	No Trip	0.36875
	10	-1	No Trip	No Trip	No Trip	0.36875
ABCG	0.1	-1	No Trip	No Trip	No Trip	0.3675
	1	-1	No Trip	No Trip	No Trip	0.3675
	5	-1	No Trip	No Trip	No Trip	0.36875
	10	-1	No Trip	No Trip	No Trip	0.370005
ABC	0.1	-1	No Trip	No Trip	No Trip	0.3675
	1	-1	No Trip	No Trip	No Trip	0.3675
	5	-1	No Trip	No Trip	No Trip	0.3675
	10	-1	No Trip	No Trip	No Trip	0.36875
AG	0.1	0	0.13625	No Trip	No Trip	0.38625
	1	0	0.1075	No Trip	No Trip	0.36875
	5	0	7.63E-02	No Trip	No Trip	0.36875
	10	0	0.1575	No Trip	No Trip	0.39125
ABG	0.1	0	7.38E-02	No Trip	No Trip	0.3675
	1	0	5.50E-02	No Trip	No Trip	0.3675
	5	0	5.63E-02	No Trip	No Trip	0.36875
	10	0	0.115	No Trip	0.175	No Trip
AB	0.1	0	0.41	No Trip	No Trip	0.3675
	1	0	No Trip	No Trip	No Trip	0.3675
	5	0	No Trip	No Trip	No Trip	0.36875
	10	0	No Trip	No Trip	No Trip	0.36875
ABCG	0.1	0	0.1525	No Trip	No Trip	0.3675
	1	0	No Trip	No Trip	No Trip	0.3675
	5	0	No Trip	No Trip	No Trip	0.36875
	10	0	No Trip	No Trip	No Trip	0.36875
ABC	0.1	0	0.12625	No Trip	No Trip	0.3675
	1	0	No Trip	No Trip	No Trip	0.3675
	5	0	No Trip	No Trip	No Trip	0.3675
	10	0	No Trip	No Trip	No Trip	0.36875
AG	0.1	1	0.111255	No Trip	No Trip	0.38625
	1	1	0.1075	No Trip	No Trip	0.36875
	5	1	7.63E-02	No Trip	No Trip	0.36875
	10	1	9.88E-02	No Trip	No Trip	0.370005
ABG	0.1	1	7.50E-02	No Trip	No Trip	0.3675
	1	1	5.63E-02	No Trip	No Trip	0.3675
	5	1	5.63E-02	No Trip	No Trip	0.36875
	10	1	9.75E-02	No Trip	0.15625	No Trip
AB	0.1	1	0.64	No Trip	No Trip	0.3675
	1	1	0.57125	No Trip	No Trip	0.3675
	5	1	0.557505	No Trip	No Trip	0.36875
	10	1	No Trip	No Trip	No Trip	0.36875
ABCG	0.1	1	0.125	No Trip	No Trip	0.3675
	1	1	No Trip	No Trip	No Trip	0.3675
	5	1	No Trip	No Trip	No Trip	0.36875
	10	1	No Trip	No Trip	No Trip	0.36875
ABC	0.1	1	0.125	No Trip	No Trip	0.3675
	1	1	No Trip	No Trip	No Trip	0.3675
	5	1	No Trip	No Trip	No Trip	0.3675
	10	1	No Trip	No Trip	No Trip	0.36875

WF 100%, Infeed 0% - Distance 50%						
Fault	Rf [Ω]	k_p	DR32_Z1	DR32_Z2	DR23_Z1	DR23_Z2
AG	0.1	-1	8.25E-02	No Trip	7.88E-02	No Trip
	1	-1	8.13E-02	No Trip	7.75E-02	No Trip
	5	-1	6.00E-02	No Trip	5.88E-02	No Trip
	10	-1	No Trip	0.37125	6.13E-02	No Trip
ABG	0.1	-1	5.88E-02	No Trip	5.75E-02	No Trip
	1	-1	5.88E-02	No Trip	5.75E-02	No Trip
	5	-1	5.88E-02	No Trip	5.88E-02	No Trip
	10	-1	6.63E-02	No Trip	6.13E-02	No Trip
AB	0.1	-1	No Trip	No Trip	7.63E-02	No Trip
	1	-1	No Trip	No Trip	7.63E-02	No Trip
	5	-1	No Trip	No Trip	5.75E-02	No Trip
	10	-1	No Trip	No Trip	5.88E-02	No Trip
ABCG	0.1	-1	0.2075	No Trip	5.75E-02	No Trip
	1	-1	0.22875	No Trip	5.75E-02	No Trip
	5	-1	0.26125	No Trip	5.88E-02	No Trip
	10	-1	0.26875	No Trip	6.00E-02	No Trip
ABC	0.1	-1	0.2075	No Trip	5.75E-02	No Trip
	1	-1	0.21375	No Trip	5.75E-02	No Trip
	5	-1	0.22875	No Trip	5.75E-02	No Trip
	10	-1	0.236255	No Trip	5.75E-02	No Trip
AG	0.1	0	8.38E-02	No Trip	7.88E-02	No Trip
	1	0	8.25E-02	No Trip	7.75E-02	No Trip
	5	0	0.12125	No Trip	5.88E-02	No Trip
	10	0	0.13375	No Trip	6.00E-02	No Trip
ABG	0.1	0	5.88E-02	No Trip	5.75E-02	No Trip
	1	0	6.00E-02	No Trip	5.75E-02	No Trip
	5	0	5.75E-02	No Trip	5.88E-02	No Trip
	10	0	6.88E-02	No Trip	6.00E-02	No Trip
AB	0.1	0	0.14625	No Trip	7.63E-02	No Trip
	1	0	0.14625	No Trip	7.63E-02	No Trip
	5	0	0.13375	No Trip	5.75E-02	No Trip
	10	0	0.135	No Trip	5.88E-02	No Trip
ABCG	0.1	0	0.14	No Trip	5.75E-02	No Trip
	1	0	0.14	No Trip	5.75E-02	No Trip
	5	0	0.14875	No Trip	5.88E-02	No Trip
	10	0	0.17	No Trip	6.00E-02	No Trip
ABC	0.1	0	0.14	No Trip	5.75E-02	No Trip
	1	0	0.14	No Trip	5.75E-02	No Trip
	5	0	0.14	No Trip	5.75E-02	No Trip
	10	0	0.1475	No Trip	5.75E-02	No Trip
AG	0.1	1	8.25E-02	No Trip	7.88E-02	No Trip
	1	1	8.25E-02	No Trip	7.75E-02	No Trip
	5	1	0.34875	No Trip	5.88E-02	No Trip
	10	1	0.371255	No Trip	6.13E-02	No Trip
ABG	0.1	1	6.00E-02	No Trip	5.75E-02	No Trip
	1	1	6.00E-02	No Trip	5.75E-02	No Trip
	5	1	6.63E-02	No Trip	5.75E-02	No Trip
	10	1	7.00E-02	No Trip	5.88E-02	No Trip
AB	0.1	1	0.1675	No Trip	7.63E-02	No Trip
	1	1	0.21125	No Trip	7.63E-02	No Trip
	5	1	0.23875	No Trip	5.75E-02	No Trip
	10	1	0.24125	No Trip	5.75E-02	No Trip
ABCG	0.1	1	0.14125	No Trip	5.75E-02	No Trip
	1	1	0.13875	No Trip	5.75E-02	No Trip
	5	1	0.14625	No Trip	5.75E-02	No Trip
	10	1	0.1725	No Trip	5.88E-02	No Trip
ABC	0.1	1	0.14125	No Trip	5.75E-02	No Trip
	1	1	0.14125	No Trip	5.75E-02	No Trip
	5	1	0.145	No Trip	5.75E-02	No Trip
	10	1	0.14625	No Trip	5.75E-02	No Trip

WF 100%, Infeed 0% - Distance 90%						
Fault	Rf [Ω]	k_p	DR32_Z1	DR32_Z2	DR23_Z1	DR23_Z2
AG	0.1	-1	No Trip	No Trip	0.10875	No Trip
	1	-1	No Trip	No Trip	8.00E-02	No Trip
	5	-1	No Trip	No Trip	7.50E-02	No Trip
	10	-1	No Trip	No Trip	6.00E-02	No Trip
ABG	0.1	-1	No Trip	No Trip	7.63E-02	No Trip
	1	-1	No Trip	No Trip	7.50E-02	No Trip
	5	-1	6.00E-02	No Trip	5.63E-02	No Trip
	10	-1	6.13E-02	No Trip	5.75E-02	No Trip
AB	0.1	-1	No Trip	No Trip	0.1075	No Trip
	1	-1	No Trip	No Trip	0.10625	No Trip
	5	-1	No Trip	No Trip	7.63E-02	No Trip
	10	-1	No Trip	No Trip	7.25E-02	No Trip
ABCG	0.1	-1	No Trip	No Trip	7.75E-02	No Trip
	1	-1	No Trip	No Trip	5.63E-02	No Trip
	5	-1	No Trip	No Trip	5.63E-02	No Trip
	10	-1	No Trip	No Trip	5.75E-02	No Trip
ABC	0.1	-1	No Trip	No Trip	7.75E-02	No Trip
	1	-1	No Trip	No Trip	5.63E-02	No Trip
	5	-1	No Trip	No Trip	5.63E-02	No Trip
	10	-1	No Trip	No Trip	5.63E-02	No Trip
AG	0.1	0	No Trip	No Trip	0.11	No Trip
	1	0	No Trip	No Trip	8.00E-02	No Trip
	5	0	No Trip	No Trip	7.50E-02	No Trip
	10	0	No Trip	No Trip	6.00E-02	No Trip
ABG	0.1	0	No Trip	No Trip	7.63E-02	No Trip
	1	0	No Trip	No Trip	7.50E-02	No Trip
	5	0	No Trip	No Trip	5.63E-02	No Trip
	10	0	6.63E-02	No Trip	5.75E-02	No Trip
AB	0.1	0	No Trip	No Trip	0.1075	No Trip
	1	0	No Trip	No Trip	0.10625	No Trip
	5	0	No Trip	No Trip	7.63E-02	No Trip
	10	0	No Trip	No Trip	7.38E-02	No Trip
ABCG	0.1	0	No Trip	No Trip	7.75E-02	No Trip
	1	0	No Trip	No Trip	5.63E-02	No Trip
	5	0	No Trip	No Trip	5.63E-02	No Trip
	10	0	No Trip	No Trip	5.75E-02	No Trip
ABC	0.1	0	No Trip	No Trip	7.75E-02	No Trip
	1	0	No Trip	No Trip	5.63E-02	No Trip
	5	0	No Trip	No Trip	5.63E-02	No Trip
	10	0	No Trip	No Trip	5.63E-02	No Trip
AG	0.1	1	No Trip	0.68125	0.11	No Trip
	1	1	No Trip	0.625	8.00E-02	No Trip
	5	1	No Trip	0.6425	7.50E-02	No Trip
	10	1	No Trip	0.74125	6.00E-02	No Trip
ABG	0.1	1	No Trip	No Trip	7.63E-02	No Trip
	1	1	No Trip	No Trip	7.50E-02	No Trip
	5	1	No Trip	No Trip	5.63E-02	No Trip
	10	1	No Trip	No Trip	5.75E-02	No Trip
AB	0.1	1	No Trip	No Trip	0.1075	No Trip
	1	1	No Trip	No Trip	0.10625	No Trip
	5	1	No Trip	No Trip	7.63E-02	No Trip
	10	1	No Trip	No Trip	7.38E-02	No Trip
ABCG	0.1	1	No Trip	No Trip	7.75E-02	No Trip
	1	1	No Trip	No Trip	5.63E-02	No Trip
	5	1	No Trip	No Trip	5.63E-02	No Trip
	10	1	No Trip	No Trip	5.75E-02	No Trip
ABC	0.1	1	No Trip	No Trip	7.75E-02	No Trip
	1	1	No Trip	No Trip	5.63E-02	No Trip
	5	1	No Trip	No Trip	5.63E-02	No Trip
	10	1	No Trip	No Trip	5.63E-02	No Trip

WF 90%, Infeed 10% - Distance 10%						
Fault	Rf [Ω]	k_p	DR32_Z1	DR32_Z2	DR23_Z1	DR23_Z2
AG	0.1	-1	0.10875	No Trip	No Trip	0.38625
	1	-1	0.10625	No Trip	No Trip	0.36875
	5	-1	7.50E-02	No Trip	No Trip	0.36875
	10	-1	7.00E-02	No Trip	No Trip	0.39125
ABG	0.1	-1	7.50E-02	No Trip	No Trip	0.3675
	1	-1	7.38E-02	No Trip	No Trip	0.3675
	5	-1	5.50E-02	No Trip	No Trip	0.36875
	10	-1	0.1275	No Trip	0.185005	No Trip
AB	0.1	-1	0.13375	No Trip	No Trip	0.3675
	1	-1	No Trip	No Trip	No Trip	0.3675
	5	-1	No Trip	No Trip	No Trip	0.36875
	10	-1	No Trip	No Trip	No Trip	0.36875
ABCG	0.1	-1	0.13375	No Trip	No Trip	0.3675
	1	-1	0.22125	No Trip	No Trip	0.3675
	5	-1	No Trip	No Trip	No Trip	0.36875
	10	-1	No Trip	No Trip	No Trip	0.370005
ABC	0.1	-1	0.135	No Trip	No Trip	0.3675
	1	-1	0.16	No Trip	No Trip	0.3675
	5	-1	No Trip	No Trip	No Trip	0.36875
	10	-1	No Trip	No Trip	No Trip	0.36875
AG	0.1	0	0.11	No Trip	No Trip	0.38625
	1	0	0.1075	No Trip	No Trip	0.36875
	5	0	7.63E-02	No Trip	No Trip	0.36875
	10	0	9.88E-02	No Trip	No Trip	0.39125
ABG	0.1	0	7.38E-02	No Trip	No Trip	0.3675
	1	0	5.50E-02	No Trip	No Trip	0.3675
	5	0	5.63E-02	No Trip	No Trip	0.36875
	10	0	9.75E-02	No Trip	0.153755	No Trip
AB	0.1	0	0.16	No Trip	No Trip	0.3675
	1	0	No Trip	No Trip	No Trip	0.3675
	5	0	No Trip	No Trip	No Trip	0.36875
	10	0	No Trip	No Trip	No Trip	0.36875
ABCG	0.1	0	0.18375	No Trip	No Trip	0.3675
	1	0	No Trip	No Trip	No Trip	0.3675
	5	0	No Trip	No Trip	No Trip	0.36875
	10	0	No Trip	No Trip	No Trip	0.370005
ABC	0.1	0	0.185005	No Trip	No Trip	0.3675
	1	0	No Trip	No Trip	No Trip	0.3675
	5	0	No Trip	No Trip	No Trip	0.3675
	10	0	No Trip	No Trip	No Trip	0.36875
AG	0.1	1	0.11	No Trip	No Trip	0.38625
	1	1	0.10625	No Trip	No Trip	0.36875
	5	1	7.50E-02	No Trip	No Trip	0.36875
	10	1	7.00E-02	No Trip	No Trip	0.370005
ABG	0.1	1	7.50E-02	No Trip	No Trip	0.3675
	1	1	5.50E-02	No Trip	No Trip	0.3675
	5	1	5.63E-02	No Trip	No Trip	0.36875
	10	1	9.75E-02	No Trip	0.155	No Trip
AB	0.1	1	0.16625	No Trip	No Trip	0.3675
	1	1	0.16125	No Trip	No Trip	0.3675
	5	1	No Trip	No Trip	No Trip	0.36875
	10	1	No Trip	No Trip	No Trip	0.36875
ABCG	0.1	1	0.13625	No Trip	No Trip	0.3675
	1	1	0.13375	No Trip	No Trip	0.3675
	5	1	No Trip	No Trip	No Trip	0.36875
	10	1	No Trip	No Trip	No Trip	0.370005
ABC	0.1	1	0.13625	No Trip	No Trip	0.3675
	1	1	0.135	No Trip	No Trip	0.3675
	5	1	No Trip	No Trip	No Trip	0.3675
	10	1	No Trip	No Trip	No Trip	0.36875

WF 90%, Infeed 10% - Distance 50%						
Fault	Rf [Ω]	k_p	DR32_Z1	DR32_Z2	DR23_Z1	DR23_Z2
AG	0.1	-1	8.13E-02	No Trip	7.88E-02	No Trip
	1	-1	8.13E-02	No Trip	7.75E-02	No Trip
	5	-1	6.00E-02	No Trip	5.88E-02	No Trip
	10	-1	No Trip	No Trip	6.13E-02	No Trip
ABG	0.1	-1	5.75E-02	No Trip	5.75E-02	No Trip
	1	-1	5.88E-02	No Trip	5.75E-02	No Trip
	5	-1	5.88E-02	No Trip	5.88E-02	No Trip
	10	-1	6.38E-02	No Trip	6.13E-02	No Trip
AB	0.1	-1	No Trip	No Trip	7.63E-02	No Trip
	1	-1	No Trip	No Trip	7.63E-02	No Trip
	5	-1	No Trip	No Trip	5.75E-02	No Trip
	10	-1	No Trip	No Trip	5.88E-02	No Trip
ABCG	0.1	-1	0.13375	No Trip	5.75E-02	No Trip
	1	-1	0.13125	No Trip	5.75E-02	No Trip
	5	-1	0.11875	No Trip	5.88E-02	No Trip
	10	-1	0.143755	No Trip	6.00E-02	No Trip
ABC	0.1	-1	0.13375	No Trip	5.75E-02	No Trip
	1	-1	0.135	No Trip	5.75E-02	No Trip
	5	-1	0.13125	No Trip	5.75E-02	No Trip
	10	-1	0.132505	No Trip	5.75E-02	No Trip
AG	0.1	0	8.25E-02	No Trip	7.88E-02	No Trip
	1	0	8.25E-02	No Trip	7.75E-02	No Trip
	5	0	6.00E-02	No Trip	5.88E-02	No Trip
	10	0	0.15125	No Trip	6.13E-02	No Trip
ABG	0.1	0	5.88E-02	No Trip	5.75E-02	No Trip
	1	0	5.88E-02	No Trip	5.75E-02	No Trip
	5	0	5.63E-02	No Trip	5.88E-02	No Trip
	10	0	6.88E-02	No Trip	6.13E-02	No Trip
AB	0.1	0	No Trip	No Trip	7.63E-02	No Trip
	1	0	No Trip	No Trip	7.63E-02	No Trip
	5	0	No Trip	No Trip	5.75E-02	No Trip
	10	0	No Trip	No Trip	5.88E-02	No Trip
ABCG	0.1	0	0.2025	No Trip	5.75E-02	No Trip
	1	0	0.1525	No Trip	5.75E-02	No Trip
	5	0	0.20375	No Trip	5.88E-02	No Trip
	10	0	0.17	No Trip	6.00E-02	No Trip
ABC	0.1	0	0.2025	No Trip	5.75E-02	No Trip
	1	0	0.2025	No Trip	5.75E-02	No Trip
	5	0	0.1525	No Trip	5.75E-02	No Trip
	10	0	0.16625	No Trip	5.75E-02	No Trip
AG	0.1	1	7.88E-02	No Trip	7.88E-02	No Trip
	1	1	8.13E-02	No Trip	7.75E-02	No Trip
	5	1	6.00E-02	No Trip	5.88E-02	No Trip
	10	1	0.145	No Trip	6.13E-02	No Trip
ABG	0.1	1	6.00E-02	No Trip	5.75E-02	No Trip
	1	1	6.00E-02	No Trip	5.75E-02	No Trip
	5	1	6.63E-02	No Trip	5.88E-02	No Trip
	10	1	6.88E-02	No Trip	6.00E-02	No Trip
AB	0.1	1	0.14	No Trip	7.63E-02	No Trip
	1	1	0.11625	No Trip	7.63E-02	No Trip
	5	1	0.142505	No Trip	5.75E-02	No Trip
	10	1	0.143755	No Trip	5.88E-02	No Trip
ABCG	0.1	1	No Trip	No Trip	5.75E-02	No Trip
	1	1	No Trip	No Trip	5.75E-02	No Trip
	5	1	No Trip	No Trip	5.88E-02	No Trip
	10	1	No Trip	No Trip	6.00E-02	No Trip
ABC	0.1	1	No Trip	No Trip	5.75E-02	No Trip
	1	1	No Trip	No Trip	5.75E-02	No Trip
	5	1	No Trip	No Trip	5.75E-02	No Trip
	10	1	No Trip	No Trip	5.75E-02	No Trip

WF 90%, Infeed 10% - Distance 90%						
Fault	Rf [Ω]	k_p	DR32_Z1	DR32_Z2	DR23_Z1	DR23_Z2
AG	0.1	-1	No Trip	No Trip	0.10875	No Trip
	1	-1	No Trip	No Trip	8.00E-02	No Trip
	5	-1	No Trip	No Trip	7.38E-02	No Trip
	10	-1	No Trip	No Trip	6.00E-02	No Trip
ABG	0.1	-1	No Trip	No Trip	7.63E-02	No Trip
	1	-1	No Trip	No Trip	7.50E-02	No Trip
	5	-1	6.13E-02	No Trip	5.63E-02	No Trip
	10	-1	6.13E-02	No Trip	5.75E-02	No Trip
AB	0.1	-1	No Trip	No Trip	0.1075	No Trip
	1	-1	No Trip	No Trip	0.10625	No Trip
	5	-1	No Trip	No Trip	7.63E-02	No Trip
	10	-1	No Trip	No Trip	7.25E-02	No Trip
ABCG	0.1	-1	No Trip	No Trip	7.75E-02	No Trip
	1	-1	No Trip	No Trip	5.63E-02	No Trip
	5	-1	No Trip	No Trip	5.63E-02	No Trip
	10	-1	No Trip	No Trip	5.75E-02	No Trip
ABC	0.1	-1	No Trip	No Trip	7.75E-02	No Trip
	1	-1	No Trip	No Trip	5.63E-02	No Trip
	5	-1	No Trip	No Trip	5.63E-02	No Trip
	10	-1	No Trip	No Trip	5.63E-02	No Trip
AG	0.1	0	No Trip	No Trip	0.10875	No Trip
	1	0	No Trip	No Trip	8.00E-02	No Trip
	5	0	No Trip	No Trip	7.50E-02	No Trip
	10	0	No Trip	No Trip	6.00E-02	No Trip
ABG	0.1	0	No Trip	No Trip	7.63E-02	No Trip
	1	0	No Trip	No Trip	7.50E-02	No Trip
	5	0	No Trip	No Trip	5.63E-02	No Trip
	10	0	6.13E-02	No Trip	5.75E-02	No Trip
AB	0.1	0	No Trip	No Trip	0.1075	No Trip
	1	0	No Trip	No Trip	0.10625	No Trip
	5	0	No Trip	No Trip	7.63E-02	No Trip
	10	0	No Trip	No Trip	7.25E-02	No Trip
ABCG	0.1	0	No Trip	No Trip	7.75E-02	No Trip
	1	0	No Trip	No Trip	5.63E-02	No Trip
	5	0	No Trip	No Trip	5.63E-02	No Trip
	10	0	No Trip	No Trip	5.75E-02	No Trip
ABC	0.1	0	No Trip	No Trip	7.75E-02	No Trip
	1	0	No Trip	No Trip	5.63E-02	No Trip
	5	0	No Trip	No Trip	5.63E-02	No Trip
	10	0	No Trip	No Trip	5.63E-02	No Trip
AG	0.1	1	No Trip	No Trip	0.11	No Trip
	1	1	No Trip	No Trip	8.00E-02	No Trip
	5	1	No Trip	0.370005	7.50E-02	No Trip
	10	1	No Trip	No Trip	6.00E-02	No Trip
ABG	0.1	1	No Trip	No Trip	7.63E-02	No Trip
	1	1	No Trip	No Trip	7.50E-02	No Trip
	5	1	No Trip	No Trip	5.63E-02	No Trip
	10	1	No Trip	No Trip	5.75E-02	No Trip
AB	0.1	1	No Trip	No Trip	0.1075	No Trip
	1	1	No Trip	No Trip	0.10625	No Trip
	5	1	No Trip	No Trip	7.63E-02	No Trip
	10	1	No Trip	No Trip	7.38E-02	No Trip
ABCG	0.1	1	No Trip	No Trip	7.75E-02	No Trip
	1	1	No Trip	No Trip	5.63E-02	No Trip
	5	1	No Trip	No Trip	5.63E-02	No Trip
	10	1	No Trip	No Trip	5.75E-02	No Trip
ABC	0.1	1	No Trip	No Trip	7.75E-02	No Trip
	1	1	No Trip	No Trip	5.63E-02	No Trip
	5	1	No Trip	No Trip	5.63E-02	No Trip
	10	1	No Trip	No Trip	5.63E-02	No Trip

Wf 80%, Infeed 20% - Distance 10%						
Fault	Rf [Ω]	k_p	DR32_Z1	DR32_Z2	DR23_Z1	DR23_Z2
AG	0.1	-1	0.10875	No Trip	No Trip	0.38625
	1	-1	7.88E-02	No Trip	No Trip	0.36875
	5	-1	7.50E-02	No Trip	No Trip	0.36875
	10	-1	6.88E-02	No Trip	No Trip	0.392505
ABG	0.1	-1	7.50E-02	No Trip	No Trip	0.3675
	1	-1	7.38E-02	No Trip	No Trip	0.3675
	5	-1	5.50E-02	No Trip	No Trip	0.36875
	10	-1	9.75E-02	No Trip	0.155	No Trip
AB	0.1	-1	0.135	No Trip	No Trip	0.3675
	1	-1	0.15875	No Trip	No Trip	0.3675
	5	-1	No Trip	No Trip	No Trip	0.36875
	10	-1	No Trip	No Trip	No Trip	0.36875
ABCG	0.1	-1	0.10625	No Trip	No Trip	0.3675
	1	-1	0.12875	No Trip	No Trip	0.3675
	5	-1	No Trip	No Trip	No Trip	0.36875
	10	-1	No Trip	No Trip	No Trip	0.370005
ABC	0.1	-1	0.10625	No Trip	No Trip	0.3675
	1	-1	0.13	No Trip	No Trip	0.3675
	5	-1	0.12875	No Trip	No Trip	0.36875
	10	-1	No Trip	No Trip	No Trip	0.36875
AG	0.1	0	0.11	No Trip	No Trip	0.38625
	1	0	0.10625	No Trip	No Trip	0.36875
	5	0	7.50E-02	No Trip	No Trip	0.36875
	10	0	6.88E-02	No Trip	No Trip	0.392505
ABG	0.1	0	7.38E-02	No Trip	No Trip	0.3675
	1	0	7.38E-02	No Trip	No Trip	0.3675
	5	0	5.50E-02	No Trip	No Trip	0.36875
	10	0	9.63E-02	No Trip	0.1775	No Trip
AB	0.1	0	0.16125	No Trip	No Trip	0.3675
	1	0	No Trip	No Trip	No Trip	0.3675
	5	0	No Trip	No Trip	No Trip	0.36875
	10	0	No Trip	No Trip	No Trip	0.36875
ABCG	0.1	0	0.132505	No Trip	No Trip	0.3675
	1	0	0.132505	No Trip	No Trip	0.3675
	5	0	No Trip	No Trip	No Trip	0.36875
	10	0	No Trip	No Trip	No Trip	0.370005
ABC	0.1	0	0.165	No Trip	No Trip	0.3675
	1	0	0.132505	No Trip	No Trip	0.3675
	5	0	0.132505	No Trip	No Trip	0.36875
	10	0	No Trip	No Trip	No Trip	0.36875
AG	0.1	1	0.11	No Trip	No Trip	0.38625
	1	1	8.00E-02	No Trip	No Trip	0.36875
	5	1	7.50E-02	No Trip	No Trip	0.36875
	10	1	6.88E-02	No Trip	No Trip	0.370005
ABG	0.1	1	7.50E-02	No Trip	No Trip	0.3675
	1	1	7.38E-02	No Trip	No Trip	0.3675
	5	1	5.50E-02	No Trip	No Trip	0.36875
	10	1	9.50E-02	No Trip	0.155	No Trip
AB	0.1	1	0.163755	No Trip	No Trip	0.3675
	1	1	0.132505	No Trip	No Trip	0.3675
	5	1	No Trip	No Trip	No Trip	0.36875
	10	1	No Trip	No Trip	No Trip	0.36875
ABCG	0.1	1	0.13125	No Trip	No Trip	0.3675
	1	1	0.13125	No Trip	No Trip	0.3675
	5	1	No Trip	No Trip	No Trip	0.36875
	10	1	No Trip	No Trip	No Trip	0.370005
ABC	0.1	1	0.163755	No Trip	No Trip	0.3675
	1	1	0.13125	No Trip	No Trip	0.3675
	5	1	0.13125	No Trip	No Trip	0.3675
	10	1	No Trip	No Trip	No Trip	0.36875

Wf 80%, Infeed 20% - Distance 50%						
Fault	Rf [Ω]	k_p	DR32_Z1	DR32_Z2	DR23_Z1	DR23_Z2
AG	0.1	-1	7.88E-02	No Trip	7.88E-02	No Trip
	1	-1	7.75E-02	No Trip	7.75E-02	No Trip
	5	-1	6.00E-02	No Trip	5.88E-02	No Trip
	10	-1	9.75E-02	No Trip	8.13E-02	No Trip
ABG	0.1	-1	5.75E-02	No Trip	5.75E-02	No Trip
	1	-1	5.88E-02	No Trip	5.75E-02	No Trip
	5	-1	5.63E-02	No Trip	5.88E-02	No Trip
	10	-1	6.13E-02	No Trip	6.13E-02	No Trip
AB	0.1	-1	0.10875	No Trip	7.63E-02	No Trip
	1	-1	0.10375	No Trip	7.63E-02	No Trip
	5	-1	0.1025	No Trip	5.75E-02	No Trip
	10	-1	0.1375	No Trip	5.88E-02	No Trip
ABCG	0.1	-1	8.38E-02	No Trip	5.75E-02	No Trip
	1	-1	8.00E-02	No Trip	5.75E-02	No Trip
	5	-1	0.1175	No Trip	5.88E-02	No Trip
	10	-1	0.122505	No Trip	6.13E-02	No Trip
ABC	0.1	-1	0.112505	No Trip	5.75E-02	No Trip
	1	-1	8.13E-02	No Trip	5.75E-02	No Trip
	5	-1	9.63E-02	No Trip	5.75E-02	No Trip
	10	-1	0.10625	No Trip	5.75E-02	No Trip
AG	0.1	0	8.13E-02	No Trip	7.88E-02	No Trip
	1	0	8.13E-02	No Trip	7.75E-02	No Trip
	5	0	6.00E-02	No Trip	5.88E-02	No Trip
	10	0	No Trip	No Trip	6.38E-02	No Trip
ABG	0.1	0	5.88E-02	No Trip	5.75E-02	No Trip
	1	0	5.88E-02	No Trip	5.75E-02	No Trip
	5	0	5.63E-02	No Trip	5.88E-02	No Trip
	10	0	6.88E-02	No Trip	6.13E-02	No Trip
AB	0.1	0	No Trip	No Trip	7.63E-02	No Trip
	1	0	No Trip	No Trip	7.63E-02	No Trip
	5	0	No Trip	No Trip	5.75E-02	No Trip
	10	0	No Trip	No Trip	5.88E-02	No Trip
ABCG	0.1	0	0.135	No Trip	5.75E-02	No Trip
	1	0	0.101255	No Trip	5.75E-02	No Trip
	5	0	0.11875	No Trip	5.88E-02	No Trip
	10	0	0.142505	No Trip	6.00E-02	No Trip
ABC	0.1	0	0.135	No Trip	5.75E-02	No Trip
	1	0	0.135	No Trip	5.75E-02	No Trip
	5	0	0.101255	No Trip	5.75E-02	No Trip
	10	0	0.105	No Trip	5.75E-02	No Trip
AG	0.1	1	7.88E-02	No Trip	7.88E-02	No Trip
	1	1	7.75E-02	No Trip	7.75E-02	No Trip
	5	1	6.00E-02	No Trip	5.88E-02	No Trip
	10	1	0.1275	No Trip	6.50E-02	No Trip
ABG	0.1	1	6.00E-02	No Trip	5.75E-02	No Trip
	1	1	5.88E-02	No Trip	5.75E-02	No Trip
	5	1	6.38E-02	No Trip	5.88E-02	No Trip
	10	1	6.88E-02	No Trip	6.00E-02	No Trip
AB	0.1	1	0.13375	No Trip	7.63E-02	No Trip
	1	1	0.112505	No Trip	7.63E-02	No Trip
	5	1	0.11625	No Trip	5.75E-02	No Trip
	10	1	0.14125	No Trip	5.88E-02	No Trip
ABCG	0.1	1	0.13375	No Trip	5.75E-02	No Trip
	1	1	0.1	No Trip	5.75E-02	No Trip
	5	1	0.11625	No Trip	5.88E-02	No Trip
	10	1	0.14125	No Trip	6.00E-02	No Trip
ABC	0.1	1	0.13375	No Trip	5.75E-02	No Trip
	1	1	0.13375	No Trip	5.75E-02	No Trip
	5	1	0.1	No Trip	5.75E-02	No Trip
	10	1	0.101255	No Trip	5.75E-02	No Trip

Wf 80%, Infeed 20% - Distance 90%						
Fault	Rf [Ω]	k_p	DR32_Z1	DR32_Z2	DR23_Z1	DR23_Z2
AG	0.1	-1	No Trip	No Trip	0.10875	No Trip
	1	-1	No Trip	No Trip	8.00E-02	No Trip
	5	-1	No Trip	No Trip	7.38E-02	No Trip
	10	-1	No Trip	No Trip	6.00E-02	No Trip
ABG	0.1	-1	No Trip	0.365	7.63E-02	No Trip
	1	-1	No Trip	0.365	7.50E-02	No Trip
	5	-1	6.13E-02	No Trip	5.63E-02	No Trip
	10	-1	6.13E-02	No Trip	5.75E-02	No Trip
AB	0.1	-1	No Trip	No Trip	0.1075	No Trip
	1	-1	No Trip	No Trip	0.10625	No Trip
	5	-1	8.63E-02	No Trip	7.63E-02	No Trip
	10	-1	No Trip	No Trip	7.25E-02	No Trip
ABCG	0.1	-1	No Trip	0.39375	7.75E-02	No Trip
	1	-1	No Trip	0.39	5.63E-02	No Trip
	5	-1	No Trip	No Trip	5.63E-02	No Trip
	10	-1	No Trip	No Trip	5.75E-02	No Trip
ABC	0.1	-1	No Trip	0.39375	7.75E-02	No Trip
	1	-1	No Trip	0.392505	5.63E-02	No Trip
	5	-1	No Trip	0.4025	5.63E-02	No Trip
	10	-1	No Trip	No Trip	5.63E-02	No Trip
AG	0.1	0	No Trip	No Trip	0.10875	No Trip
	1	0	No Trip	No Trip	8.00E-02	No Trip
	5	0	No Trip	No Trip	7.50E-02	No Trip
	10	0	No Trip	No Trip	6.00E-02	No Trip
ABG	0.1	0	No Trip	0.36875	7.63E-02	No Trip
	1	0	No Trip	0.36875	7.50E-02	No Trip
	5	0	6.00E-02	No Trip	5.63E-02	No Trip
	10	0	6.13E-02	No Trip	5.75E-02	No Trip
AB	0.1	0	No Trip	No Trip	0.1075	No Trip
	1	0	No Trip	No Trip	0.10625	No Trip
	5	0	No Trip	No Trip	7.63E-02	No Trip
	10	0	No Trip	No Trip	7.25E-02	No Trip
ABCG	0.1	0	No Trip	No Trip	7.75E-02	No Trip
	1	0	No Trip	0.401255	5.63E-02	No Trip
	5	0	No Trip	No Trip	5.63E-02	No Trip
	10	0	No Trip	No Trip	5.75E-02	No Trip
ABC	0.1	0	No Trip	No Trip	7.75E-02	No Trip
	1	0	No Trip	No Trip	5.63E-02	No Trip
	5	0	No Trip	No Trip	5.63E-02	No Trip
	10	0	No Trip	No Trip	5.63E-02	No Trip
AG	0.1	1	No Trip	No Trip	0.10875	No Trip
	1	1	No Trip	0.36875	8.00E-02	No Trip
	5	1	No Trip	0.36875	7.50E-02	No Trip
	10	1	No Trip	No Trip	6.00E-02	No Trip
ABG	0.1	1	No Trip	0.370005	7.63E-02	No Trip
	1	1	No Trip	0.36875	7.50E-02	No Trip
	5	1	6.00E-02	No Trip	5.63E-02	No Trip
	10	1	6.38E-02	No Trip	5.75E-02	No Trip
AB	0.1	1	No Trip	No Trip	0.1075	No Trip
	1	1	No Trip	No Trip	0.10625	No Trip
	5	1	No Trip	No Trip	7.63E-02	No Trip
	10	1	No Trip	No Trip	7.25E-02	No Trip
ABCG	0.1	1	No Trip	No Trip	7.75E-02	No Trip
	1	1	No Trip	No Trip	5.63E-02	No Trip
	5	1	No Trip	No Trip	5.63E-02	No Trip
	10	1	No Trip	No Trip	5.75E-02	No Trip
ABC	0.1	1	No Trip	No Trip	7.75E-02	No Trip
	1	1	No Trip	No Trip	5.63E-02	No Trip
	5	1	No Trip	No Trip	5.63E-02	No Trip
	10	1	No Trip	No Trip	5.63E-02	No Trip

WF 70%, Infeed 30% - Distance 10%						
Fault	Rf [Ω]	k_p	DR32_Z1	DR32_Z2	DR23_Z1	DR23_Z2
AG	0.1	-1	0.10875	No Trip	No Trip	0.38625
	1	-1	7.88E-02	No Trip	No Trip	0.36875
	5	-1	7.50E-02	No Trip	No Trip	0.36875
	10	-1	6.00E-02	No Trip	No Trip	0.392505
ABG	0.1	-1	7.38E-02	No Trip	No Trip	0.3675
	1	-1	5.50E-02	No Trip	No Trip	0.3675
	5	-1	5.50E-02	No Trip	No Trip	0.36875
	10	-1	9.50E-02	No Trip	0.17875	No Trip
AB	0.1	-1	0.135	No Trip	No Trip	0.3675
	1	-1	0.13125	No Trip	No Trip	0.3675
	5	-1	No Trip	No Trip	No Trip	0.36875
	10	-1	No Trip	No Trip	No Trip	0.370005
ABCG	0.1	-1	0.10625	No Trip	No Trip	0.3675
	1	-1	0.1025	No Trip	No Trip	0.3675
	5	-1	No Trip	No Trip	No Trip	0.36875
	10	-1	No Trip	No Trip	No Trip	0.370005
ABC	0.1	-1	0.10625	No Trip	No Trip	0.3675
	1	-1	0.105	No Trip	No Trip	0.3675
	5	-1	0.1025	No Trip	No Trip	0.36875
	10	-1	No Trip	No Trip	No Trip	0.36875
AG	0.1	0	0.10875	No Trip	No Trip	0.38625
	1	0	7.88E-02	No Trip	No Trip	0.36875
	5	0	7.50E-02	No Trip	No Trip	0.36875
	10	0	6.75E-02	No Trip	No Trip	0.392505
ABG	0.1	0	7.38E-02	No Trip	No Trip	0.3675
	1	0	7.38E-02	No Trip	No Trip	0.3675
	5	0	5.50E-02	No Trip	No Trip	0.36875
	10	0	9.50E-02	No Trip	0.17875	No Trip
AB	0.1	0	0.135	No Trip	No Trip	0.3675
	1	0	0.16	No Trip	No Trip	0.3675
	5	0	No Trip	No Trip	No Trip	0.36875
	10	0	No Trip	No Trip	No Trip	0.370005
ABCG	0.1	0	0.10625	No Trip	No Trip	0.3675
	1	0	0.1	No Trip	No Trip	0.3675
	5	0	No Trip	No Trip	No Trip	0.36875
	10	0	No Trip	No Trip	No Trip	0.370005
ABC	0.1	0	0.10625	No Trip	No Trip	0.3675
	1	0	0.105	No Trip	No Trip	0.3675
	5	0	0.1	No Trip	No Trip	0.36875
	10	0	No Trip	No Trip	No Trip	0.36875
AG	0.1	1	0.11	No Trip	No Trip	0.38625
	1	1	8.00E-02	No Trip	No Trip	0.36875
	5	1	7.50E-02	No Trip	No Trip	0.36875
	10	1	6.75E-02	No Trip	No Trip	0.37125
ABG	0.1	1	7.50E-02	No Trip	No Trip	0.3675
	1	1	7.38E-02	No Trip	No Trip	0.3675
	5	1	5.50E-02	No Trip	No Trip	0.36875
	10	1	6.38E-02	No Trip	0.12375	No Trip
AB	0.1	1	0.13625	No Trip	No Trip	0.3675
	1	1	0.13125	No Trip	No Trip	0.3675
	5	1	0.1175	No Trip	No Trip	0.36875
	10	1	No Trip	No Trip	No Trip	0.36875
ABCG	0.1	1	0.10625	No Trip	No Trip	0.3675
	1	1	0.1	No Trip	No Trip	0.3675
	5	1	No Trip	No Trip	No Trip	0.36875
	10	1	No Trip	No Trip	No Trip	0.370005
ABC	0.1	1	0.10625	No Trip	No Trip	0.3675
	1	1	0.105	No Trip	No Trip	0.3675
	5	1	7.50E-02	No Trip	No Trip	0.36875
	10	1	0.41625	0.405	No Trip	0.36875

WF 70%, Infeed 30% - Distance 50%						
Fault	Rf [Ω]	k_p	DR32_Z1	DR32_Z2	DR23_Z1	DR23_Z2
AG	0.1	-1	7.75E-02	No Trip	7.88E-02	No Trip
	1	-1	7.75E-02	No Trip	7.75E-02	No Trip
	5	-1	5.88E-02	No Trip	5.88E-02	No Trip
	10	-1	6.88E-02	No Trip	8.13E-02	No Trip
ABG	0.1	-1	5.75E-02	No Trip	5.75E-02	No Trip
	1	-1	5.88E-02	No Trip	5.75E-02	No Trip
	5	-1	5.63E-02	No Trip	5.88E-02	No Trip
	10	-1	6.13E-02	No Trip	6.13E-02	No Trip
AB	0.1	-1	0.10875	No Trip	7.63E-02	No Trip
	1	-1	0.10375	No Trip	7.63E-02	No Trip
	5	-1	0.101255	No Trip	5.75E-02	No Trip
	10	-1	0.11	No Trip	5.88E-02	No Trip
ABCG	0.1	-1	8.00E-02	No Trip	5.75E-02	No Trip
	1	-1	7.88E-02	No Trip	5.75E-02	No Trip
	5	-1	0.115	No Trip	5.88E-02	No Trip
	10	-1	0.125	No Trip	6.50E-02	No Trip
ABC	0.1	-1	8.13E-02	No Trip	5.75E-02	No Trip
	1	-1	8.00E-02	No Trip	5.75E-02	No Trip
	5	-1	7.00E-02	No Trip	5.75E-02	No Trip
	10	-1	0.1	No Trip	5.88E-02	No Trip
AG	0.1	0	7.75E-02	No Trip	7.88E-02	No Trip
	1	0	7.75E-02	No Trip	7.75E-02	No Trip
	5	0	5.88E-02	No Trip	5.88E-02	No Trip
	10	0	9.75E-02	No Trip	8.13E-02	No Trip
ABG	0.1	0	5.88E-02	No Trip	5.75E-02	No Trip
	1	0	5.88E-02	No Trip	5.75E-02	No Trip
	5	0	5.63E-02	No Trip	5.88E-02	No Trip
	10	0	6.63E-02	No Trip	6.13E-02	No Trip
AB	0.1	0	0.11	No Trip	7.63E-02	No Trip
	1	0	0.10375	No Trip	7.63E-02	No Trip
	5	0	0.1025	No Trip	5.75E-02	No Trip
	10	0	0.122505	No Trip	5.88E-02	No Trip
ABCG	0.1	0	8.13E-02	No Trip	5.75E-02	No Trip
	1	0	7.88E-02	No Trip	5.75E-02	No Trip
	5	0	0.11625	No Trip	5.88E-02	No Trip
	10	0	0.122505	No Trip	6.13E-02	No Trip
ABC	0.1	0	8.25E-02	No Trip	5.75E-02	No Trip
	1	0	8.00E-02	No Trip	5.75E-02	No Trip
	5	0	9.13E-02	No Trip	5.75E-02	No Trip
	10	0	0.1	No Trip	5.75E-02	No Trip
AG	0.1	1	7.88E-02	No Trip	7.88E-02	No Trip
	1	1	7.75E-02	No Trip	7.75E-02	No Trip
	5	1	5.88E-02	No Trip	5.88E-02	No Trip
	10	1	6.88E-02	No Trip	6.75E-02	No Trip
ABG	0.1	1	6.00E-02	No Trip	5.75E-02	No Trip
	1	1	5.88E-02	No Trip	5.75E-02	No Trip
	5	1	5.63E-02	No Trip	5.88E-02	No Trip
	10	1	6.75E-02	No Trip	6.00E-02	No Trip
AB	0.1	1	0.111255	No Trip	7.63E-02	No Trip
	1	1	0.111255	No Trip	7.63E-02	No Trip
	5	1	0.101255	No Trip	5.75E-02	No Trip
	10	1	0.11875	No Trip	5.88E-02	No Trip
ABCG	0.1	1	8.13E-02	No Trip	5.75E-02	No Trip
	1	1	8.00E-02	No Trip	5.75E-02	No Trip
	5	1	0.115	No Trip	5.88E-02	No Trip
	10	1	0.12	No Trip	6.00E-02	No Trip
ABC	0.1	1	8.13E-02	No Trip	5.75E-02	No Trip
	1	1	8.13E-02	No Trip	5.75E-02	No Trip
	5	1	7.63E-02	No Trip	5.75E-02	No Trip
	10	1	0.1	No Trip	5.75E-02	No Trip

WF 70%, Infeed 30% - Distance 90%						
Fault	Rf [Ω]	k_p	DR32_Z1	DR32_Z2	DR23_Z1	DR23_Z2
AG	0.1	-1	No Trip	No Trip	0.10875	No Trip
	1	-1	No Trip	0.3675	8.00E-02	No Trip
	5	-1	No Trip	0.36875	7.38E-02	No Trip
	10	-1	No Trip	0.37125	6.00E-02	No Trip
ABG	0.1	-1	No Trip	0.365	7.63E-02	No Trip
	1	-1	No Trip	0.365	7.38E-02	No Trip
	5	-1	6.13E-02	No Trip	5.63E-02	No Trip
	10	-1	6.13E-02	No Trip	5.75E-02	No Trip
AB	0.1	-1	No Trip	No Trip	0.1075	No Trip
	1	-1	No Trip	0.39125	0.10625	No Trip
	5	-1	8.50E-02	No Trip	7.63E-02	No Trip
	10	-1	No Trip	No Trip	7.25E-02	No Trip
ABCG	0.1	-1	No Trip	0.39	7.75E-02	No Trip
	1	-1	No Trip	0.3675	5.63E-02	No Trip
	5	-1	No Trip	No Trip	5.63E-02	No Trip
	10	-1	No Trip	No Trip	5.88E-02	No Trip
ABC	0.1	-1	No Trip	0.39	7.75E-02	No Trip
	1	-1	No Trip	0.39	5.63E-02	No Trip
	5	-1	8.25E-02	No Trip	5.63E-02	No Trip
	10	-1	No Trip	0.4075	5.63E-02	No Trip
AG	0.1	0	No Trip	No Trip	0.10875	No Trip
	1	0	No Trip	No Trip	8.00E-02	No Trip
	5	0	No Trip	No Trip	7.38E-02	No Trip
	10	0	No Trip	No Trip	6.00E-02	No Trip
ABG	0.1	0	No Trip	0.365	7.63E-02	No Trip
	1	0	No Trip	0.365	7.50E-02	No Trip
	5	0	6.13E-02	No Trip	5.63E-02	No Trip
	10	0	6.13E-02	No Trip	5.75E-02	No Trip
AB	0.1	0	No Trip	No Trip	0.1075	No Trip
	1	0	No Trip	No Trip	0.10625	No Trip
	5	0	9.88E-02	No Trip	7.63E-02	No Trip
	10	0	No Trip	No Trip	7.25E-02	No Trip
ABCG	0.1	0	No Trip	0.39375	7.75E-02	No Trip
	1	0	No Trip	0.37625	5.63E-02	No Trip
	5	0	No Trip	No Trip	5.63E-02	No Trip
	10	0	No Trip	No Trip	5.75E-02	No Trip
ABC	0.1	0	No Trip	0.39375	7.75E-02	No Trip
	1	0	No Trip	0.39375	5.63E-02	No Trip
	5	0	9.38E-02	No Trip	5.63E-02	No Trip
	10	0	No Trip	0.40625	5.63E-02	No Trip
AG	0.1	1	No Trip	0.38625	0.10875	No Trip
	1	1	No Trip	0.36875	8.00E-02	No Trip
	5	1	No Trip	0.36875	7.50E-02	No Trip
	10	1	No Trip	0.3725	6.00E-02	No Trip
ABG	0.1	1	No Trip	0.365	7.63E-02	No Trip
	1	1	No Trip	0.36875	7.50E-02	No Trip
	5	1	6.00E-02	No Trip	5.63E-02	No Trip
	10	1	6.13E-02	No Trip	5.75E-02	No Trip
AB	0.1	1	No Trip	No Trip	0.1075	No Trip
	1	1	No Trip	No Trip	0.10625	No Trip
	5	1	No Trip	No Trip	7.63E-02	No Trip
	10	1	No Trip	No Trip	7.25E-02	No Trip
ABCG	0.1	1	No Trip	0.39125	7.75E-02	No Trip
	1	1	No Trip	0.36875	5.63E-02	No Trip
	5	1	No Trip	No Trip	5.63E-02	No Trip
	10	1	No Trip	No Trip	5.75E-02	No Trip
ABC	0.1	1	No Trip	0.392505	7.75E-02	No Trip
	1	1	No Trip	0.39125	5.63E-02	No Trip
	5	1	8.88E-02	No Trip	5.63E-02	No Trip
	10	1	No Trip	0.40875	5.63E-02	No Trip

WF 60%, Infeed 40% - Distance 10%						
Fault	Rf [Ω]	k_p	DR32_Z1	DR32_Z2	DR23_Z1	DR23_Z2
AG	0.1	-1	0.10875	No Trip	No Trip	0.38625
	1	-1	7.88E-02	No Trip	No Trip	0.36875
	5	-1	7.50E-02	No Trip	No Trip	0.36875
	10	-1	6.00E-02	No Trip	No Trip	0.4025
ABG	0.1	-1	7.38E-02	No Trip	No Trip	0.3675
	1	-1	5.50E-02	No Trip	No Trip	0.3675
	5	-1	5.50E-02	No Trip	No Trip	0.36875
	10	-1	6.50E-02	No Trip	0.14875	No Trip
AB	0.1	-1	0.135	No Trip	No Trip	0.3675
	1	-1	0.10625	No Trip	No Trip	0.3675
	5	-1	0.24	No Trip	No Trip	0.36875
	10	-1	No Trip	No Trip	No Trip	0.370005
ABCG	0.1	-1	0.10625	No Trip	No Trip	0.3675
	1	-1	7.50E-02	No Trip	No Trip	0.3675
	5	-1	0.4175	0.405	No Trip	0.36875
	10	-1	No Trip	No Trip	No Trip	0.37125
ABC	0.1	-1	0.10625	No Trip	No Trip	0.3675
	1	-1	0.1	No Trip	No Trip	0.3675
	5	-1	7.38E-02	No Trip	No Trip	0.36875
	10	-1	9.50E-02	No Trip	No Trip	0.36875
AG	0.1	0	0.10875	No Trip	No Trip	0.38625
	1	0	7.88E-02	No Trip	No Trip	0.36875
	5	0	7.50E-02	No Trip	No Trip	0.36875
	10	0	6.00E-02	No Trip	No Trip	0.4025
ABG	0.1	0	7.38E-02	No Trip	No Trip	0.3675
	1	0	7.38E-02	No Trip	No Trip	0.3675
	5	0	5.50E-02	No Trip	No Trip	0.36875
	10	0	6.38E-02	No Trip	0.14875	No Trip
AB	0.1	0	0.135	No Trip	No Trip	0.3675
	1	0	0.13125	No Trip	No Trip	0.3675
	5	0	No Trip	No Trip	No Trip	0.36875
	10	0	No Trip	No Trip	No Trip	0.370005
ABCG	0.1	0	0.101255	No Trip	No Trip	0.3675
	1	0	7.50E-02	No Trip	No Trip	0.3675
	5	0	No Trip	No Trip	No Trip	0.36875
	10	0	No Trip	No Trip	No Trip	0.37125
ABC	0.1	0	0.10625	No Trip	No Trip	0.3675
	1	0	0.1	No Trip	No Trip	0.3675
	5	0	7.38E-02	No Trip	No Trip	0.36875
	10	0	9.63E-02	No Trip	No Trip	0.36875
AG	0.1	1	0.11	No Trip	No Trip	0.38625
	1	1	8.00E-02	No Trip	No Trip	0.36875
	5	1	7.50E-02	No Trip	No Trip	0.36875
	10	1	6.00E-02	No Trip	No Trip	0.37125
ABG	0.1	1	7.38E-02	No Trip	No Trip	0.3675
	1	1	5.50E-02	No Trip	No Trip	0.3675
	5	1	5.50E-02	No Trip	No Trip	0.36875
	10	1	6.25E-02	No Trip	0.14875	No Trip
AB	0.1	1	0.13625	No Trip	No Trip	0.3675
	1	1	0.10625	No Trip	No Trip	0.3675
	5	1	0.10375	No Trip	No Trip	0.36875
	10	1	No Trip	No Trip	No Trip	0.36875
ABCG	0.1	1	0.10625	No Trip	No Trip	0.3675
	1	1	7.50E-02	No Trip	No Trip	0.3675
	5	1	No Trip	No Trip	No Trip	0.36875
	10	1	No Trip	No Trip	No Trip	0.370005
ABC	0.1	1	0.10625	No Trip	No Trip	0.3675
	1	1	0.1	No Trip	No Trip	0.3675
	5	1	7.38E-02	No Trip	No Trip	0.36875
	10	1	9.75E-02	No Trip	No Trip	0.36875

WF 60%, Infeed 40% - Distance 50%						
Fault	Rf [Ω]	k_p	DR32_Z1	DR32_Z2	DR23_Z1	DR23_Z2
AG	0.1	-1	7.75E-02	No Trip	7.88E-02	No Trip
	1	-1	7.63E-02	No Trip	7.75E-02	No Trip
	5	-1	5.88E-02	No Trip	5.88E-02	No Trip
	10	-1	6.75E-02	No Trip	8.13E-02	No Trip
ABG	0.1	-1	5.75E-02	No Trip	5.75E-02	No Trip
	1	-1	5.50E-02	No Trip	5.75E-02	No Trip
	5	-1	5.63E-02	No Trip	5.88E-02	No Trip
	10	-1	6.13E-02	No Trip	6.13E-02	No Trip
AB	0.1	-1	0.105	No Trip	7.63E-02	No Trip
	1	-1	0.10375	No Trip	7.63E-02	No Trip
	5	-1	8.00E-02	No Trip	5.75E-02	No Trip
	10	-1	0.101255	No Trip	5.88E-02	No Trip
ABCG	0.1	-1	8.00E-02	No Trip	5.75E-02	No Trip
	1	-1	5.88E-02	No Trip	5.75E-02	No Trip
	5	-1	0.1025	No Trip	5.88E-02	No Trip
	10	-1	0.125	No Trip	6.50E-02	No Trip
ABC	0.1	-1	8.00E-02	No Trip	5.75E-02	No Trip
	1	-1	8.00E-02	No Trip	5.75E-02	No Trip
	5	-1	6.50E-02	No Trip	5.75E-02	No Trip
	10	-1	9.63E-02	No Trip	5.88E-02	No Trip
AG	0.1	0	7.75E-02	No Trip	7.88E-02	No Trip
	1	0	7.75E-02	No Trip	7.75E-02	No Trip
	5	0	5.88E-02	No Trip	5.88E-02	No Trip
	10	0	6.75E-02	No Trip	8.13E-02	No Trip
ABG	0.1	0	5.75E-02	No Trip	5.75E-02	No Trip
	1	0	5.88E-02	No Trip	5.75E-02	No Trip
	5	0	5.63E-02	No Trip	5.88E-02	No Trip
	10	0	6.00E-02	No Trip	6.13E-02	No Trip
AB	0.1	0	0.10875	No Trip	7.63E-02	No Trip
	1	0	0.10375	No Trip	7.63E-02	No Trip
	5	0	0.101255	No Trip	5.75E-02	No Trip
	10	0	0.10875	No Trip	5.88E-02	No Trip
ABCG	0.1	0	8.00E-02	No Trip	5.75E-02	No Trip
	1	0	6.50E-02	No Trip	5.75E-02	No Trip
	5	0	0.11	No Trip	5.88E-02	No Trip
	10	0	0.125	No Trip	6.50E-02	No Trip
ABC	0.1	0	8.00E-02	No Trip	5.75E-02	No Trip
	1	0	8.00E-02	No Trip	5.75E-02	No Trip
	5	0	6.50E-02	No Trip	5.75E-02	No Trip
	10	0	9.75E-02	No Trip	5.88E-02	No Trip
AG	0.1	1	7.88E-02	No Trip	7.88E-02	No Trip
	1	1	7.75E-02	No Trip	7.75E-02	No Trip
	5	1	5.88E-02	No Trip	5.88E-02	No Trip
	10	1	6.88E-02	No Trip	6.75E-02	No Trip
ABG	0.1	1	5.75E-02	No Trip	5.75E-02	No Trip
	1	1	5.88E-02	No Trip	5.75E-02	No Trip
	5	1	5.63E-02	No Trip	5.88E-02	No Trip
	10	1	6.63E-02	No Trip	6.00E-02	No Trip
AB	0.1	1	0.11	No Trip	7.63E-02	No Trip
	1	1	0.105	No Trip	7.63E-02	No Trip
	5	1	9.63E-02	No Trip	5.75E-02	No Trip
	10	1	0.11625	No Trip	5.88E-02	No Trip
ABCG	0.1	1	8.00E-02	No Trip	5.75E-02	No Trip
	1	1	5.88E-02	No Trip	5.75E-02	No Trip
	5	1	0.11	No Trip	5.88E-02	No Trip
	10	1	0.125	No Trip	6.50E-02	No Trip
ABC	0.1	1	8.00E-02	No Trip	5.75E-02	No Trip
	1	1	7.88E-02	No Trip	5.75E-02	No Trip
	5	1	6.50E-02	No Trip	5.75E-02	No Trip
	10	1	9.75E-02	No Trip	5.75E-02	No Trip

WF 60%, Infeed 40% - Distance 90%						
Fault	Rf [Ω]	k_p	DR32_Z1	DR32_Z2	DR23_Z1	DR23_Z2
AG	0.1	-1	No Trip	0.38625	0.10875	No Trip
	1	-1	No Trip	0.3675	8.00E-02	No Trip
	5	-1	No Trip	0.36875	7.38E-02	No Trip
	10	-1	No Trip	0.370005	6.00E-02	No Trip
ABG	0.1	-1	No Trip	0.365	7.63E-02	No Trip
	1	-1	No Trip	0.365	7.38E-02	No Trip
	5	-1	6.13E-02	No Trip	5.63E-02	No Trip
	10	-1	6.13E-02	No Trip	5.88E-02	No Trip
AB	0.1	-1	No Trip	0.392505	0.1075	No Trip
	1	-1	No Trip	0.39125	0.105	No Trip
	5	-1	No Trip	0.39	7.63E-02	No Trip
	10	-1	No Trip	No Trip	7.13E-02	No Trip
ABCG	0.1	-1	No Trip	0.39	7.75E-02	No Trip
	1	-1	No Trip	0.3675	5.63E-02	No Trip
	5	-1	No Trip	0.4075	5.63E-02	No Trip
	10	-1	No Trip	No Trip	6.50E-02	No Trip
ABC	0.1	-1	No Trip	0.39	7.75E-02	No Trip
	1	-1	8.63E-02	0.39	5.63E-02	No Trip
	5	-1	8.38E-02	0.3675	5.63E-02	No Trip
	10	-1	No Trip	0.375	5.63E-02	No Trip
AG	0.1	0	No Trip	0.38625	0.10875	No Trip
	1	0	No Trip	0.3675	8.00E-02	No Trip
	5	0	No Trip	0.36875	7.38E-02	No Trip
	10	0	No Trip	No Trip	6.00E-02	No Trip
ABG	0.1	0	No Trip	0.365	7.63E-02	No Trip
	1	0	No Trip	0.365	7.50E-02	No Trip
	5	0	6.13E-02	No Trip	5.63E-02	No Trip
	10	0	6.13E-02	No Trip	5.88E-02	No Trip
AB	0.1	0	No Trip	No Trip	0.1075	No Trip
	1	0	No Trip	No Trip	0.10625	No Trip
	5	0	8.50E-02	No Trip	7.63E-02	No Trip
	10	0	No Trip	No Trip	7.25E-02	No Trip
ABCG	0.1	0	No Trip	0.39	7.75E-02	No Trip
	1	0	No Trip	0.36875	5.63E-02	No Trip
	5	0	No Trip	No Trip	5.63E-02	No Trip
	10	0	No Trip	No Trip	6.50E-02	No Trip
ABC	0.1	0	No Trip	0.39	7.75E-02	No Trip
	1	0	No Trip	0.39	5.63E-02	No Trip
	5	0	8.50E-02	No Trip	5.63E-02	No Trip
	10	0	No Trip	0.4025	5.63E-02	No Trip
AG	0.1	1	No Trip	0.38625	0.10875	No Trip
	1	1	No Trip	0.36875	8.00E-02	No Trip
	5	1	No Trip	0.36875	7.38E-02	No Trip
	10	1	No Trip	0.37125	6.00E-02	No Trip
ABG	0.1	1	No Trip	0.3675	7.63E-02	No Trip
	1	1	No Trip	0.365	7.50E-02	No Trip
	5	1	6.13E-02	No Trip	5.63E-02	No Trip
	10	1	6.13E-02	No Trip	5.88E-02	No Trip
AB	0.1	1	No Trip	No Trip	0.1075	No Trip
	1	1	No Trip	0.392505	0.10625	No Trip
	5	1	No Trip	0.39125	7.63E-02	No Trip
	10	1	No Trip	No Trip	7.25E-02	No Trip
ABCG	0.1	1	No Trip	0.39	7.75E-02	No Trip
	1	1	No Trip	0.3675	5.63E-02	No Trip
	5	1	No Trip	0.41125	5.63E-02	No Trip
	10	1	No Trip	No Trip	5.88E-02	No Trip
ABC	0.1	1	No Trip	0.39	7.75E-02	No Trip
	1	1	No Trip	0.39	5.63E-02	No Trip
	5	1	8.38E-02	No Trip	5.63E-02	No Trip
	10	1	No Trip	0.4025	5.63E-02	No Trip

WF 50%, Infeed 50% - Distance 10%						
Fault	Rf [Ω]	k_p	DR32_Z1	DR32_Z2	DR23_Z1	DR23_Z2
AG	0.1	-1	0.10875	No Trip	No Trip	0.38625
	1	-1	7.88E-02	No Trip	No Trip	0.36875
	5	-1	7.38E-02	No Trip	No Trip	0.36875
	10	-1	6.00E-02	No Trip	No Trip	0.40375
ABG	0.1	-1	7.38E-02	No Trip	No Trip	0.3675
	1	-1	5.50E-02	No Trip	No Trip	0.3675
	5	-1	5.50E-02	No Trip	No Trip	0.36875
	10	-1	6.38E-02	No Trip	0.15	No Trip
AB	0.1	-1	0.135	No Trip	No Trip	0.3675
	1	-1	0.10625	No Trip	No Trip	0.3675
	5	-1	0.13125	No Trip	No Trip	0.36875
	10	-1	No Trip	No Trip	No Trip	0.370005
ABCG	0.1	-1	0.10625	No Trip	No Trip	0.3675
	1	-1	7.50E-02	No Trip	No Trip	0.3675
	5	-1	No Trip	0.3825	No Trip	0.36875
	10	-1	No Trip	No Trip	No Trip	0.37125
ABC	0.1	-1	0.10625	No Trip	No Trip	0.3675
	1	-1	7.63E-02	No Trip	No Trip	0.3675
	5	-1	7.38E-02	No Trip	No Trip	0.36875
	10	-1	7.25E-02	No Trip	No Trip	0.36875
AG	0.1	0	0.10875	No Trip	No Trip	0.38625
	1	0	7.88E-02	No Trip	No Trip	0.36875
	5	0	7.50E-02	No Trip	No Trip	0.36875
	10	0	6.00E-02	No Trip	No Trip	0.40375
ABG	0.1	0	7.38E-02	No Trip	No Trip	0.3675
	1	0	5.50E-02	No Trip	No Trip	0.3675
	5	0	5.50E-02	No Trip	No Trip	0.36875
	10	0	6.25E-02	No Trip	0.15	No Trip
AB	0.1	0	0.135	No Trip	No Trip	0.3675
	1	0	0.10625	No Trip	No Trip	0.3675
	5	0	0.132505	No Trip	No Trip	0.36875
	10	0	No Trip	No Trip	No Trip	0.370005
ABCG	0.1	0	0.10625	No Trip	No Trip	0.3675
	1	0	7.50E-02	No Trip	No Trip	0.3675
	5	0	0.41625	0.4025	No Trip	0.36875
	10	0	No Trip	No Trip	No Trip	0.37125
ABC	0.1	0	0.10625	No Trip	No Trip	0.3675
	1	0	0.1	No Trip	No Trip	0.3675
	5	0	7.38E-02	No Trip	No Trip	0.36875
	10	0	7.25E-02	No Trip	No Trip	0.36875
AG	0.1	1	0.10875	No Trip	No Trip	0.38625
	1	1	7.88E-02	No Trip	No Trip	0.36875
	5	1	7.38E-02	No Trip	No Trip	0.36875
	10	1	6.00E-02	No Trip	No Trip	0.3725
ABG	0.1	1	7.38E-02	No Trip	No Trip	0.3675
	1	1	5.50E-02	No Trip	No Trip	0.3675
	5	1	5.50E-02	No Trip	No Trip	0.36875
	10	1	6.25E-02	No Trip	0.15	No Trip
AB	0.1	1	0.13625	No Trip	No Trip	0.3675
	1	1	0.10625	No Trip	No Trip	0.3675
	5	1	0.10375	No Trip	No Trip	0.36875
	10	1	No Trip	No Trip	No Trip	0.36875
ABCG	0.1	1	0.10375	No Trip	No Trip	0.3675
	1	1	7.50E-02	No Trip	No Trip	0.3675
	5	1	No Trip	0.3825	No Trip	0.36875
	10	1	No Trip	No Trip	No Trip	0.370005
ABC	0.1	1	0.10625	No Trip	No Trip	0.3675
	1	1	7.63E-02	No Trip	No Trip	0.3675
	5	1	7.38E-02	No Trip	No Trip	0.36875
	10	1	7.25E-02	No Trip	No Trip	0.36875

WF 50%, Infeed 50% - Distance 50%						
Fault	Rf [Ω]	k_p	DR32_Z1	DR32_Z2	DR23_Z1	DR23_Z2
AG	0.1	-1	7.75E-02	No Trip	7.88E-02	No Trip
	1	-1	7.63E-02	No Trip	7.75E-02	No Trip
	5	-1	5.88E-02	No Trip	5.88E-02	No Trip
	10	-1	6.50E-02	No Trip	8.13E-02	No Trip
ABG	0.1	-1	5.75E-02	No Trip	5.75E-02	No Trip
	1	-1	5.50E-02	No Trip	5.75E-02	No Trip
	5	-1	5.63E-02	No Trip	5.88E-02	No Trip
	10	-1	6.00E-02	No Trip	6.50E-02	No Trip
AB	0.1	-1	0.105	No Trip	7.63E-02	No Trip
	1	-1	8.13E-02	No Trip	7.63E-02	No Trip
	5	-1	8.00E-02	No Trip	5.75E-02	No Trip
	10	-1	9.88E-02	No Trip	5.88E-02	No Trip
ABCG	0.1	-1	7.88E-02	No Trip	5.75E-02	No Trip
	1	-1	5.75E-02	No Trip	5.75E-02	No Trip
	5	-1	0.1	No Trip	5.88E-02	No Trip
	10	-1	0.125	No Trip	6.63E-02	No Trip
ABC	0.1	-1	7.88E-02	No Trip	5.75E-02	No Trip
	1	-1	7.75E-02	No Trip	5.75E-02	No Trip
	5	-1	5.88E-02	No Trip	5.75E-02	No Trip
	10	-1	9.25E-02	No Trip	5.88E-02	No Trip
AG	0.1	0	7.75E-02	No Trip	7.88E-02	No Trip
	1	0	7.63E-02	No Trip	7.75E-02	No Trip
	5	0	5.88E-02	No Trip	5.88E-02	No Trip
	10	0	6.63E-02	No Trip	8.13E-02	No Trip
ABG	0.1	0	5.75E-02	No Trip	5.75E-02	No Trip
	1	0	5.50E-02	No Trip	5.75E-02	No Trip
	5	0	5.63E-02	No Trip	5.88E-02	No Trip
	10	0	6.00E-02	No Trip	6.50E-02	No Trip
AB	0.1	0	0.105	No Trip	7.63E-02	No Trip
	1	0	0.1025	No Trip	7.63E-02	No Trip
	5	0	8.00E-02	No Trip	5.75E-02	No Trip
	10	0	0.1	No Trip	5.88E-02	No Trip
ABCG	0.1	0	8.00E-02	No Trip	5.75E-02	No Trip
	1	0	5.75E-02	No Trip	5.75E-02	No Trip
	5	0	0.101255	No Trip	5.88E-02	No Trip
	10	0	0.125	No Trip	6.50E-02	No Trip
ABC	0.1	0	8.00E-02	No Trip	5.75E-02	No Trip
	1	0	7.88E-02	No Trip	5.75E-02	No Trip
	5	0	5.88E-02	No Trip	5.75E-02	No Trip
	10	0	9.63E-02	No Trip	5.88E-02	No Trip
AG	0.1	1	7.75E-02	No Trip	7.88E-02	No Trip
	1	1	7.63E-02	No Trip	7.75E-02	No Trip
	5	1	5.88E-02	No Trip	5.88E-02	No Trip
	10	1	6.63E-02	No Trip	6.88E-02	No Trip
ABG	0.1	1	5.75E-02	No Trip	5.75E-02	No Trip
	1	1	5.50E-02	No Trip	5.75E-02	No Trip
	5	1	5.63E-02	No Trip	5.88E-02	No Trip
	10	1	6.38E-02	No Trip	6.00E-02	No Trip
AB	0.1	1	0.105	No Trip	7.63E-02	No Trip
	1	1	0.10375	No Trip	7.63E-02	No Trip
	5	1	8.13E-02	No Trip	5.75E-02	No Trip
	10	1	0.11	No Trip	5.88E-02	No Trip
ABCG	0.1	1	7.88E-02	No Trip	5.75E-02	No Trip
	1	1	5.75E-02	No Trip	5.75E-02	No Trip
	5	1	0.1	No Trip	5.88E-02	No Trip
	10	1	0.125	No Trip	6.50E-02	No Trip
ABC	0.1	1	7.88E-02	No Trip	5.75E-02	No Trip
	1	1	5.75E-02	No Trip	5.75E-02	No Trip
	5	1	5.88E-02	No Trip	5.75E-02	No Trip
	10	1	9.63E-02	No Trip	5.88E-02	No Trip

WF 50%, Infeed 50% - Distance 90%						
Fault	Rf [Ω]	k_p	DR32_Z1	DR32_Z2	DR23_Z1	DR23_Z2
AG	0.1	-1	No Trip	0.385	0.10875	No Trip
	1	-1	No Trip	0.3675	8.00E-02	No Trip
	5	-1	No Trip	0.36875	7.38E-02	No Trip
	10	-1	No Trip	0.370005	6.00E-02	No Trip
ABG	0.1	-1	No Trip	0.365	7.63E-02	No Trip
	1	-1	No Trip	0.365	7.38E-02	No Trip
	5	-1	6.13E-02	No Trip	5.63E-02	No Trip
	10	-1	6.13E-02	No Trip	5.88E-02	No Trip
AB	0.1	-1	No Trip	0.392505	0.1075	No Trip
	1	-1	No Trip	0.39125	0.105	No Trip
	5	-1	No Trip	0.39	7.63E-02	No Trip
	10	-1	No Trip	No Trip	5.63E-02	No Trip
ABCG	0.1	-1	No Trip	0.3675	7.75E-02	No Trip
	1	-1	No Trip	0.3675	5.63E-02	No Trip
	5	-1	No Trip	0.405	5.63E-02	No Trip
	10	-1	No Trip	No Trip	6.50E-02	No Trip
ABC	0.1	-1	No Trip	0.38875	7.75E-02	No Trip
	1	-1	No Trip	0.3675	5.63E-02	No Trip
	5	-1	8.50E-02	No Trip	5.63E-02	No Trip
	10	-1	No Trip	0.36875	5.63E-02	No Trip
AG	0.1	0	No Trip	0.385	0.10875	No Trip
	1	0	No Trip	0.3675	8.00E-02	No Trip
	5	0	No Trip	0.36875	7.38E-02	No Trip
	10	0	No Trip	0.370005	6.00E-02	No Trip
ABG	0.1	0	No Trip	0.365	7.63E-02	No Trip
	1	0	No Trip	0.365	7.38E-02	No Trip
	5	0	6.13E-02	No Trip	5.63E-02	No Trip
	10	0	6.13E-02	No Trip	5.88E-02	No Trip
AB	0.1	0	No Trip	0.392505	0.1075	No Trip
	1	0	No Trip	0.39125	0.105	No Trip
	5	0	No Trip	0.38875	7.63E-02	No Trip
	10	0	No Trip	No Trip	7.13E-02	No Trip
ABCG	0.1	0	No Trip	0.38875	7.75E-02	No Trip
	1	0	No Trip	0.3675	5.63E-02	No Trip
	5	0	No Trip	No Trip	5.63E-02	No Trip
	10	0	No Trip	No Trip	6.50E-02	No Trip
ABC	0.1	0	No Trip	0.39	7.75E-02	No Trip
	1	0	No Trip	0.3675	5.63E-02	No Trip
	5	0	No Trip	0.3675	5.63E-02	No Trip
	10	0	No Trip	0.3725	5.63E-02	No Trip
AG	0.1	1	No Trip	0.3675	0.10875	No Trip
	1	1	No Trip	0.3675	8.00E-02	No Trip
	5	1	No Trip	0.36875	7.38E-02	No Trip
	10	1	No Trip	0.370005	6.00E-02	No Trip
ABG	0.1	1	No Trip	0.3675	7.63E-02	No Trip
	1	1	No Trip	0.365	7.50E-02	No Trip
	5	1	6.13E-02	No Trip	5.63E-02	No Trip
	10	1	6.13E-02	No Trip	5.88E-02	No Trip
AB	0.1	1	No Trip	0.392505	0.1075	No Trip
	1	1	No Trip	0.392505	0.105	No Trip
	5	1	No Trip	0.39125	7.63E-02	No Trip
	10	1	No Trip	No Trip	7.25E-02	No Trip
ABCG	0.1	1	No Trip	0.3675	7.75E-02	No Trip
	1	1	No Trip	0.3675	5.63E-02	No Trip
	5	1	No Trip	0.40875	5.63E-02	No Trip
	10	1	No Trip	No Trip	6.50E-02	No Trip
ABC	0.1	1	No Trip	0.3675	7.75E-02	No Trip
	1	1	No Trip	0.3675	5.63E-02	No Trip
	5	1	8.25E-02	No Trip	5.63E-02	No Trip
	10	1	No Trip	0.375	5.63E-02	No Trip

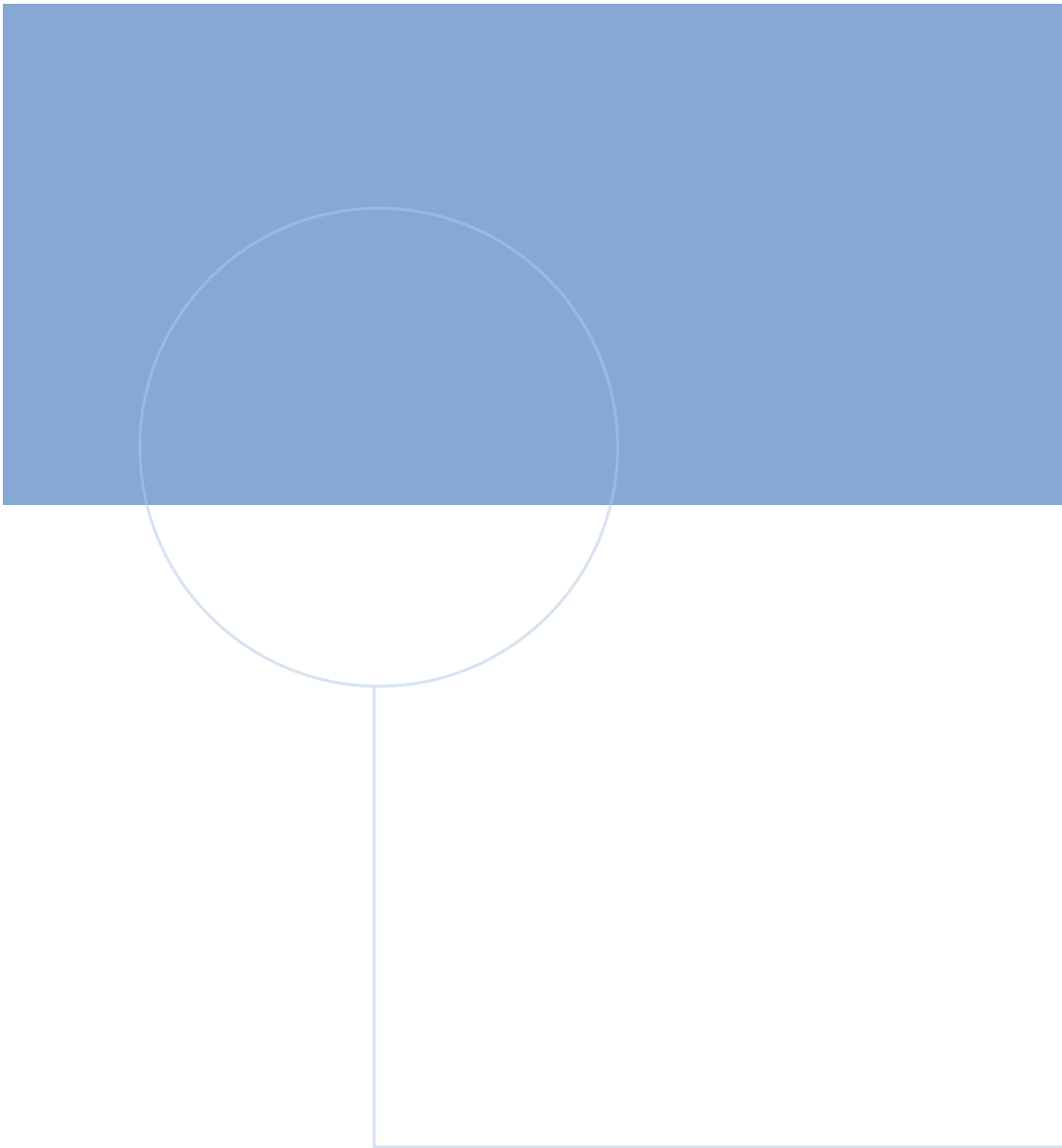

NTNU

Norwegian University of
Science and Technology